

**Investigations on the flooding behaviour of
a partially degraded reactor core**

Ailine J. Trometer



**Investigations on the flooding behaviour of
a partially degraded reactor core**

**Untersuchungen zum Flutverhalten eines
teilerstörten Reaktorkerns**

Von der Fakultät Energie-, Verfahrens- und Biotechnik
der Universität Stuttgart zur Erlangung der Würde eines
Doktor-Ingenieurs (Dr.-Ing.) genehmigte Abhandlung

Vorgelegt von

Ailine J. Trometer

geboren in Darmstadt

Hauptberichter: Prof. Dr.-Ing. Jörg Starflinger

Mitberichter: Prof. Dr.-Ing. Stefan Weihe

Tag der Einreichung: 07.10.2016

Tag der mündlichen Prüfung: 15.12.2016

ISSN 0173-6892

Dezember 2016 IKE 2-157



I humbly dedicate this work
to my beloved family.
Without your love and continued support,
none of this would have been possible.

„I think I am, therefore, I am. I think.“

from George Carlin

„Getting an education was a bit like a communicable sexual disease. It made you unsuitable for a lot of jobs and then you had the urge to pass it on.“

from Terry Pratchett's *Hogfather*

„And once the storm is over, you won't remember how you made it through, how you managed to survive. You won't even be sure, whether the storm is really over. But one thing is certain. When you come out of the storm, you won't be the same person who walked in. That's what this storm's all about.“

from Haruki Murakami's *Kafka on the Shore*

„Fact may not be truth, and truth may not be factual.“

from Haruki Murakami's *The Wind-Up Bird Chronicle*

„They were all in their early thirties. An age at which it is sometimes hard to admit that what you are living is your life.“

from Alice Munro's *The Moons of Jupiter*

Abstract

This work investigates a mid-sized break loss of coolant accident (MBLOCA) with a 200 cm^2 leak in the hot leg next to the pressurizer surge line in the most common reactor type which is the $1,300 \text{ MW}_{el}$ KONVOI class pressurized water reactor (PWR). The scope was to analyze different reflooding scenarios, where the reactor core has already started melting when the reflooding is initiated.

For this scenario a basic simulation called „BaseCase“ is conducted to get an overview of the accident progression and all the phenomena that occur. It also serves as a basis for all the following studies. In the MBLOCA scenario all active emergency core cooling systems are supposed to work correctly until the flooding pool is empty. Regularly, a switch to sump circulation would take place at that time, but in the simulation it is assumed to fail. So from then on no more water injection into the primary system takes place, which will eventually lead to complete core destruction.

In order to investigate whether stable and coolable core conditions can be reached by feeding water into the primary loops during core melting, a diverse set of reflooding scenarios were selected to be simulated based the findings of the BaseCase simulation. The feeding can be realized by turning on the high or low pressure injection pumps (HPI / LPI) in sump circulation mode for example, and it can take place at different locations. This leads to different reflooding scenarios, which are analyzed for differences and cooling potential.

From study A „Variation of the beginning of reflooding“ , it could be conducted that at least up to 40 t of melt can be cooled in the core, if the reflooding system has a sufficient injection rate. The results of study B „Variation of the reflooding system“ show that the reflooding via the LPI creates a self-blocking effect, which compromises the injection, thus preventing the core quenching for a time. This effect does not occur while using the HPI, leading to the question whether a middle pressure injection (MPI) system might be the optimum for the reflooding of a partially degraded PWR core, since it combines a higher mass flow rate than the HPI with a higher pressure head than the LPI.

The injection location varied in study C „Variation of the reflooding location“ does affect the simulations, but to a much lower extend than the used reflooding system. Nevertheless, a combined reflooding using both the hot and the cold legs seems to be the optimum. Study D „Variation of the number of available pumps“ revealed that at least two LPI pumps are necessary to perform a successful quenching of the core area. The simulation with only one pump did end with a core status that seems to be stable as well, but even after a simulation time twice as high as usual, the core could not be flooded with water and has to be cooled by steam.

Kurzfassung

Diese Arbeit untersucht einen Kühlmittelverluststörfall mit einem mittleren Leck des Querschnitts 200cm^2 im heißen Strang neben der Druckhalterzuleitung in einem 1.300MW_{el} Druckwasserreaktor vom Typ KONVOI. Das Ziel war es, verschiedene Flutszenarien zu analysieren, bei denen der Reaktorkern bereits begonnen hat zu schmelzen wenn das Fluten initiiert wird.

Es wurde zuerst ein Basisfall simuliert, um einen Überblick über den Unfallverlauf und die auftretenden Phänomene zu erhalten. Er diente als Grundlage für alle folgenden Studien. Im Fall des mittleren Lecks wurde angenommen, dass alle aktiven Wassereinspeisesysteme regulär funktionieren bis das Flutbecken leer ist. An dieser Stelle müsste ein Umschalten auf Sumpfbetrieb stattfinden, von dem für dieses Szenario angenommen wurde, dass es fehlschlägt und unbemerkt bleibt. Von diesem Zeitpunkt an wird also kein Wasser mehr in das Primärsystem eingespeist, sodass im Endeffekt das gesamte Kerninventar zerstört wird.

Auf der Grundlage des Basisfalls wurden Szenarien simuliert, in denen das Primärsystem während des Abschmelzvorgangs im Kern mit Wasser geflutet wird. Dabei sollte eine Antwort auf die Frage gefunden werden, ob sich so eine stabile, kühlbare Kernkonfiguration einstellen lässt. Der Flutvorgang kann initiiert werden, indem entweder die Hoch- oder die Niederdruckpumpen im Sumpfbetrieb eingeschaltet werden, und es kann in verschiedene Stellen der vier Stränge eingespeist werden. Daraus ergaben sich verschiedene Flutszenarien, die auf Unterschiede und Kühlpotential analysiert wurden.

Aus Studie A „Variation des Zeitpunkts zu dem das Fluten gestartet wird“ hat sich ergeben, dass zumindest 40 t Schmelze im Kernbereich gekühlt werden können, wenn das zum Fluten verwendete Einspeisesystem eine ausreichende Einspeiserate aufweist. Die Ergebnisse von Studie B „Variation des Pumpensystems“ zeigen, dass das Fluten mit dem Niederdruckeinspeisesystem zu einem Selbstblockadeeffekt führt, der eine weitere Einspeisung und damit ein schnelles Fluten des Kerns verhindert. Dieser Effekt tritt nicht auf, wenn das Hochdruckeinspeisesystem verwendet wird, was die Frage aufwirft, ob nicht ein Mitteldruckeinspeisesystem optimal wäre, da es eine höhere Einspeiserate als das Hochdruckeinspeisesystem mit einem höheren Förderdruck als das Niederdruckeinspeisesystem kombiniert.

Die Einspeisestelle, die in Studie C „Variation des Einspeiseorts“ variiert wurde, beeinflusst die Simulation zwar, aber zu einem deutlich niedrigeren Grad als das verwendete Einspeisesystem. Eine kombinierte Einspeisung in die kalten und heißen Stränge scheint hier das Optimum zu sein. In Studie D „Variation der Anzahl an verfügbaren Pumpen“ hat sich gezeigt, dass mindestens zwei Pumpen notwendig sind, um den

Kern erfolgreich zu quenchen. Die Simulation mit nur einer Pumpe ergab zwar ebenfalls einen Kernstatus, der stabil erschien, jedoch konnte der Druckbehälter selbst in der zweifachen Simulationszeit nicht geflutet werden, sodass die Wärme im oberen Kernbereich weiterhin nur durch Dampfkühlung abgeführt werden konnte.

Contents

List of Tables	XI
List of Figures	XIII
Symbols and Abbreviations	XVII
1 Introduction	1
1.1 Motivation	1
1.2 State of the art	3
1.2.1 The KONVOI type pressurized water reactor	3
1.2.2 Emergency core cooling systems in the design of a KONVOI type pressure water reactor	5
1.2.3 The German Risk Study, Phase B	7
1.2.4 Phenomenology of a core melt-down	8
1.2.5 The Severe Accident Mitigation Guidelines (SAMGs)	10
1.3 Objective of this work	12
2 The code system ATHLET-CD	15
2.1 Thermo fluid dynamics (TFD)	16
2.2 Heat conduction and heat transfer (HECU)	19
2.3 Time advancement procedure (FEBE)	21
2.4 General simulation control (GCSM)	22
2.5 Core degradation (ECORE)	22
2.5.1 Cladding oxidation	24
2.5.2 Melting and melt relocation	25
2.5.3 Effect of blockages on thermal hydraulics and melt relocation .	26
2.6 Behavior of melt in the lower plenum (AIDA)	27
2.7 State of the code validation	28
3 About the nuclear power plant	33
3.1 ATHLET-CD model of the reactors thermo fluid dynamic systems . . .	33
3.1.1 The primary system	33
3.1.2 Secondary systems	35
3.2 Emergency core cooling systems (ECCS)	35
3.2.1 Model parameters	36
3.3 Properties of the reactor core	37
3.3.1 Properties of the core materials	38
3.3.2 Model parameters	39
3.4 Use of the GCSM signals in the simulations	41

4	The reference case	45
4.1	The MBLOCA accident scenario	45
4.1.1	Thermal-hydraulic behavior during the accident evolution . . .	46
4.1.2	Accident evolution in the core	49
4.1.3	Accident evolution in the lower plenum	52
5	Reflooding	55
5.1	Implementation of the reflooding injection in the simulation model . .	55
5.2	Assumptions and boundary conditions	55
5.3	Reflooding configurations	56
5.4	Parametric studies	58
5.4.1	Study A: Variation of the beginning of reflooding	58
5.4.2	Study B: Variation of the reflooding system	59
5.4.3	Study C: Variation of the reflooding location	59
5.4.4	Study D: Variation of the number of available pumps	60
5.5	Overview of all conducted simulations	61
6	Discussion of the results	65
6.1	Coolability criteria	65
6.1.1	Criterion I: Vessel failure	65
6.1.2	Criterion II: Temperature criterion	66
6.1.3	Criterion III: Geometry criterion	66
6.1.4	Criterion IV: Heat removal criterion	67
6.2	Study A: Variation of the beginning of reflooding	68
6.3	Study B: Variation of the reflooding system	75
6.3.1	High and low pressure injection systems	76
6.3.2	Middle pressure injection systems WKTB and WKTR	77
6.3.3	Volume control and extra borating system	79
6.3.4	Results for reflooding after the formation of 40 t or 50 t of melt .	83
6.4	Study C: Variation of the reflooding location	85
6.4.1	Reflooding via the cold legs	85
6.4.2	Reflooding via the hot legs	86
6.5	Study D: Variation of the number of available pumps	88
7	Sensitivity and uncertainty considerations	95
7.1	The BLOCKAGE input parameters	95
7.2	The impact of the lower plenum modelling	100
8	Summary and Conclusions	103
	Appendix	107
A1	Input data for the AIDA module	108
A2	Input data for the GCSM signals used by the AIDA module	110
A3	Input data for the ECORE module	111
A4	GMCS input for the emergency cooling preparation signal (ECPS) . . .	114
A5	GCSM input for the reactor control systems observation values	115
A6	Input data for the GCSM signals used for the reflooding simulation . .	116
	Bibliography	123

List of Tables

- 2.1 Phenomena important for the degradation process and their occurrence temperatures 23
- 2.2 Porosity boundaries used in the blockage module 27

- 3.1 Simulation properties of the radial core sections in the ECOPE module 37
- 3.2 Simulation properties of the fuel rod structure 39
- 3.3 The four parts of the oxidation correlation 40
- 3.4 Overview of the most important values assumed in the simulation of rod relocation 41
- 3.5 Overview of the most important values assumed in the simulation of absorber and control rod behavior 42

- 4.1 Important points of the MBLOCA accident progression 47

- 5.1 Simulations conducted with varying reflooding starting times 58
- 5.2 Simulations conducted with varying reflooding systems 59
- 5.3 Simulations conducted with varying reflooding locations 60
- 5.4 Simulations conducted with reduced pump numbers 60
- 5.5 Reference table for all conducted simulations 61
- 5.6 Reference table for all conducted simulations, continued 62

- 6.1 Hydrogen produced and fraction of zirconium oxidized in the simulations of study A 74

- 7.1 BLOCKAGE values used in the BLOCKAGE study 96

List of Figures

- 1.1 Schematic of a KONVOI type pressure water reactors primary system [1] 3
- 1.2 Schematic of a reactor pressure vessel of a KONVOI type pressure water reactor [1] 4
- 1.3 Schematic of the different emergency core cooling systems in a KONVOI type pressure water reactor [2] 5
- 1.4 Schematic of the volume control system in a KONVOI type pressure water reactor [2] 6
- 1.5 Schematic of the extra borating system in a KONVOI type pressure water reactor [2] 7
- 1.6 Phenomenology of the fuel rod degradation process [3] 8
- 1.7 Schematic representation of the fuel rod degradation process as simulated by ATHLET-CD [3] 9

- 2.1 Overview of the modular code architecture of the ATHLET code system [3] 15
- 2.2 Schematic representation of two thermo fluid dynamic control volumes, connected by a junction 16
- 2.3 Schematic representation of the energy balance in an exemplified heat conduction layer 20

- 3.1 Graphical representation of the simulated reactor structure with an X indicating the location of the leak 34
- 3.2 Graphical representation of the simulated core structure as six concentric core rings 35
- 3.3 Pump characteristics of the low and high pressure injection pumps (HPI and LPI) 36
- 3.4 Structure of the simulated fuel rods (on the left) and schematic of the cross section of an 18x18-type fuel elements (on the right) [4] 37
- 3.5 Axial power profile (on the left) and decay heat (on the right), both generated from the ATHLET-CD input tables with linear interpolation between the values 38
- 3.6 Sub-division of the fuel rods (incl. upper and lower fuel rod plug) into 22 nodes 39
- 3.7 Cross section of a simulated fuel rod (on the left) and schematic of the smallest cell of the square fuel rod lattice (on the right) 40

- 4.1 MBLOCA: Comparison of pressure and void fraction near the leak with the injection and leak mass flow rates during the early accident phase . 48

4.2	MBLOCA: System pressure and injection rates of the pressurizer, accumulators as well as high and low pressure injection systems. Legend: SURGE - Injection of the pressurizer, ACCU - Injection of the accumulators, HPI - Injection of the high pressure injection system, LPI - Injection of the low pressure injection system	48
4.3	Water level evolution in the six core channels named CORE1 (innermost core channel) to CORE6 (outermost core channel)	49
4.4	Top: Highest material temperatures in the core (TB - Fuel temperature, TC - Cladding temperature, CRTA - Temperature of the absorber rod material, CRTC - Temperature of the absorber rod cladding, TL - Liquid temperature, TV - Vapor temperature), middle: ZrO_2 mass (AMIZO), Hydrogen mass (H2) and mass of molten corium (AMISUL), bottom: Comparison of Zirconium oxidation rate (Delta AMIZO), hydrogen production rate (Delta H2) and the heat released by oxidation (SQOXID)	50
4.5	Core status when the RPV fails at 21740 s in Node 12	51
4.6	MBLOCA: Wall and melt temperatures in the lower plenum, as well as the relocated melt and crust volume	52
5.1	Schematic of the reflooding implementation, linked to the usual ECCS representation	56
5.2	Flow paths of the water injected into the cold legs of the primary system	57
5.3	Flow paths of the water injected into the hot legs of the primary system	57
5.4	Pump curves of the different injection systems; compare with table 5.2	60
6.1	Mass of molten core material obtained in study A	68
6.2	Mass of melt present at each time during the accident in study A	69
6.3	Comparison of the core status at the time of the beginning of reflooding (left) and at the time of vessel failure (right) for simulation A3B1C3D4.	70
6.4	Porosity evolution in Rod 3 during simulation A3B1C3D4	70
6.5	Current amount of ceramic melt mass present in the nodes of rod 3 during simulation A3B1C3D4	71
6.6	Average temperature of ceramic melt mass present in the nodes of rod 3 during simulation A3B1C3D4	72
6.7	Power balance of the reactor for the simulations of study A	72
6.8	Mass of hydrogen produced in study A	73
6.9	Hydrogen production rate and exothermic heat release during oxidation (SQOXID) in study A	74
6.10	Comparison of the leak and injection mass flow rates with the pressure and void near the leak position for simulation A3B1C3D4 (30 t).	75
6.11	Comparison of the leak and injection mass flow rates with the pressure and void near the leak position for simulations A3B1C3D4 (LPI) and A3B2C3D4 (HPI)	76
6.12	Comparison of the core status after 5 minutes of reflooding for simulations A3B1C3D4 (LPI) and A3B2C3D4 (HPI)	77
6.13	Comparison of the leak and injection mass flow rates with the pressure and void near the leak position for simulations A3B6C3D4 (WKTR) and A3B7C3D4 (WKTB)	78
6.14	Comparison of the core status after 5 minutes of reflooding for simulations A3B6C3D4 (WKTR) and A3B7C3D4 (WKTB)	78

6.15	Mass of molten core material obtained in study B	79
6.16	Mass of hydrogen produced in study B	80
6.17	Comparison of the core status after 5 minutes of reflooding for simulations A3B3C3D4 (VCS) and A3B4C3D4 (EBS)	80
6.18	Comparison of the core status at the end of the simulation for simulations A3B3C3D4 (VCS) and A3B4C3D4 (EBS)	81
6.19	Mass relocated to the lower plenum in study B	82
6.20	Power balance of the reactor in study B for reflooding after 30 <i>t</i>	83
6.21	Power balance of the reactor in study B for reflooding after 40 <i>t</i>	84
6.22	Power balance of the reactor in study B for reflooding after 50 <i>t</i>	84
6.23	Comparison of the leak and injection mass flow rates with the pressure and void near the leak position for simulation A3B1C1D4 (CL)	85
6.24	Comparison of the core status after 5 minutes of reflooding and at the end of the simulation for simulation A3B1C1D4 (CL)	86
6.25	Comparison of the leak and injection mass flow rates with the pressure and void near the leak position for simulation A3B1C2D4 (HL)	87
6.26	Comparison of the core status after 5 minutes of reflooding and at the end of the simulation for simulation A3B1C2D4 (HL)	87
6.27	Comparison of the core status after 5 minutes of reflooding for the simulations of study D (top left:A3B1C3D4 - four pumps, top right: A3B1C3D3 - three pumps, bottom left: A3B1C3D2 - two pumps, bottom right: A3B1C3D1 - one pump)	89
6.28	Comparison of the core status at the end of the simulations of study D (top left:A3B1C3D4 - four pumps, top right: A3B1C3D3 - three pumps, bottom left: A3B1C3D2 - two pumps, bottom right: A3B1C3D1 - one pump)	90
6.29	Power balance of the reactor in study D for reflooding after 30 <i>t</i>	91
6.30	Comparison of the reflooding evolution for the simulations of study D (from top to bottom:A3B1C3D4 - four pumps, A3B1C3D3 - three pumps, A3B1C3D2 - two pumps and A3B1C3D1 - one pump)	92
6.31	Comparison of the core status at the original end of simulation A3B1C3D1 (one pump) and after an additional 30000 <i>s</i> of simulation time	93
6.32	Comparison of the leak and injection mass flow rates with the pressure and void near the leak position for simulation A3B1C3D1 (one pump) after an additional 30000 <i>s</i> of simulation time	93
6.33	Fuel temperature evolution in the six core channels during the extended simulation A3B1C3D1 (one pump)	94
7.1	Schematic of the enlarged fuel rod diameter due to candling of melt	96
7.2	Comparison of simulation A3B3C1D4 with 10 % higher BLOCKAGE values on the left and simulation A3B3C1D4N with 10 % lower BLOCKAGE values on the right five minutes into the reflooding (upper row) and at the end of the simulation (lower row)	97
7.3	Comparison of the hydrogen production during the three simulations investigated in the BLOCKAGE study	98
7.4	Comparison of the oxidation heat produced during the three simulations investigated in the BLOCKAGE study	98

7.5	Porosity evolution in Rod 3 during the simulation with decreased BLOCKAGE values	99
7.6	Comparison of the reflooding evolution during the three simulations investigated in the BLOCKAGE study with decreasing BLOCKAGE values from top to bottom (default values in the middle)	100
7.7	Comparison of simulation A5B3C1D4 using the AIDA module on the right and simulation A5B3C1D4N not using the AIDA module on the left at the moment of the first relocation of melt to the lower plenum (upper row) and after 10500 s simulation time (lower row)	102
A.1	Input for the AIDA module, part I	108
A.2	Input for the AIDA module, part II	109
A.3	Input for the GCSM control signals used by the AIDA module	110
A.4	Input for the ECORE module, part I	111
A.5	Input for the ECORE module, part II	112
A.6	Input for the ECORE module, part III	113
A.7	Input for the GCSM signals used for the simulation of the emergency cooling preparation signal	114
A.8	Input for the GCSM process signals used as observation values on which the reactor control system is based	115
A.9	Input for the GCSM signals used for the reflooding simulation, part I .	116
A.10	Input for the GCSM signals used for the reflooding simulation, part II .	117
A.11	Input for the GCSM signals used for the reflooding simulation, part III .	118
A.12	Input for the GCSM signals used for the reflooding simulation, part IV .	119
A.13	Input for the GCSM signals used for the reflooding simulation, part V .	120
A.14	Input for the GCSM signals used for the reflooding simulation, part VI .	121
A.15	Input for the GCSM signals used for the reflooding simulation, part VII .	122

Symbols and Abbreviations

α	Void fraction
D_h	Characteristic length
ϵ	Porosity
\vec{f}	Wall force
h	Enthalpy
i	Index used for interface
L	Index used for liquid
m	Index used for mean values
p	Pressure
Ψ	Source term for mass flux
\dot{q}	Heat flow
τ	Shear stress
V	Index used for void
\vec{w}	Velocity
AC	Alternating Current
AIDA	Analysis of the Interaction between Core Debris and the RPV during Severe Accidents
AMISUL	Parameter for the mass of molten core material in ATHLET-CD
ASTEC	Accident Source Term Evaluation Code
ATHLET-CD	Analysis of THERmalhydraulics of LEaks and Transients - Core Degradation
BDBA	Beyond Design Basis Accident
BWR	Boiling Water Reactor
CCO	Cross Connection Object
CESAM	Code for European Severe Accident Management (Project name)
CFD	Computational Fluid Dynamics
COCOSYS	Containment Code System
CRTA	Temperature of the absorber rod material
CRTC	Temperature of the absorber rod cladding
CV	Control Volume
DAtF	Deutsches Atomforum e.V. (German Atomic Forum)
DBA	Design Basis Accident
DC	Direct Current
EBS	Extra Borating System
ECCS	Emergency Core Cooling System
ECPS	Emergency Cooling Preparation Signal (Notkühlvorbereitungssignal)
ECORE	Name of the core degradation module in ATHLET-CD
FEBE	Forward-Euler Backward-Euler

FIPISO	ATHLET module for nuclide properties
FIPREM	ATHLET module for fission product and aerosol release
FUNGEN	Function generator in the GCSM module of ATHLET
GCSM	General Control Simulation Module
GRS	Gesellschaft für Anlagen- und Reaktorsicherheit gGmbH
HECU	ATHLET module for heat conduction and heat transfer
HCO	Heat Conduction Object
HPI	How Pressure Injection (System)
ICARE	Interprétation des Cœurs Accidentés pour les Réacteurs à Eau
IKE	Institut für Kernenergetik und Energiesysteme der Universität Stuttgart (Institute of Nuclear Technology and Energy Systems)
IRSN	Institut de radioprotection et de sûreté nucléaire (Institute for Radiological Protection and Nuclear Safety)
KSB AG	Klein, Schanzlin & Becker (German pump manufacturer)
LOCA	Loss Of Coolant Accident
LPB	Landeszentrale für politische Bildung (Centre for Political Education)
LPI	Low Pressure Injection (System)
LUHS	Loss of Ultimate Heat Sink
MBLOCA	Mid-sized Break Loss Of Coolant Accident
MELCOR	Methods for Estimation of Leaks and Consequences of Releases (Code name)
MEWA	Melt Water Interaction (Code name)
MPI	Middle Pressure Injection (System)
NPP	Nuclear Power Plant
OREST	ATHLET module for nuclide properties
PSL	Pressurizer Surge Line
PWR	Pressure Water Reactor
RCS	Reactor Coolant System
RPV	Reactor Pressure Vessel
RUB-LEE	Ruhr-Universität Bochum - Lehrstuhl für Energiesysteme und Energiewirtschaft (Chair of Energy Systems and Energy Economics)
SAMG	Severe Accident Mitigation Guideline
SBO	Station Black Out
SCRAM	Term for the emergency shut-down of a nuclear reactor (Safety Cut Rope Axe Man)
SOPHAEROS	ATHLET module for fission product and aerosol transport
SURGE	ATHLET variable, characterizing the water injection from the accumulators through the pressurizer surge line
TB	Temperature of the fuel
TC	Temperature of the cladding
TF	Temperature fluctuation
TFD	ATHLET module for thermo fluid dynamics
TL	Temperature of the water
TV	Temperature of the steam
VCS	Volume Control System
WASA-BOSS	Weiterentwicklung und Anwendung von Severe Accident Codes - Bewertung und Optimierung von Störfallmaßnahmen (Project name)
WWER	Water-Water Energy Reactor (Russian pressure tube reactor type)

1 Introduction

1.1 Motivation

Since the world's electricity demand is steadily increasing due to rising population and the high consumption of electricity by the lifestyle of foremost industrialized western nations, the need for clean and sustainable energy has never been more pressing than now. Nuclear technology has given the world the most efficient and clean energy source while at the same time being comparatively cheap and environmentally friendly. Most of the world's highly industrialized nations use nuclear power in combination with fossil energy sources like gas, oil and coal as well as renewable energy supplies like wind, water and sun, to reliably supply their industry and private households around the clock with affordable electricity.

In spring of 2011 the world witnessed one of the most devastating accidents in a nuclear facility in history, following the heaviest earthquake and highest Tsunami ever recorded in Japan [5]. The Tōhoku earthquake with its magnitude of $9.0/M_W$ or $8.4/M_{jma}$ occurred not far from the Sanriku coast of Japan, and only about 130 km from the metropolis of Sendai. It led to massive destruction of vast regions of the Miyagi prefecture and thousands of deaths, and was also the trigger of a massive Tsunami, which hit the coast only 50 minutes after the earthquake started [6].

Though not nearest to the epicenter, the power plants at the Fukushima Daiichi plant site had the most trouble in dealing with the earthquake and following Tsunami. The earthquake was of a very high magnitude, but did not damage the power plant too much, so the emergency reactor shutdown was initiated automatically. Due to the earthquake, all off-site power supply had been lost and the emergency diesel generators were started according to emergency protocol and supplied the safety systems and functions of all six plants. The flooding of the plant site by the Tsunami then had two major impacts on the nuclear reactors. First, the basements containing the diesel generators were flooded, and thus all but one generator (which supplied units 5 and 6 successfully) failed and emergency power supply was lost in units 1 to 4, leading to a station blackout (SBO) condition. Second, the ultimate heat sink (in this case the ocean) was lost when the sea water pumps were flooded, leading to a delayed shut-down of the existing passive core cooling functions. There were implied accident mitigation actions like water injection into the reactor through fire engines, but they were not successful and in the end reactors 1 to 3 experienced a nuclear core meltdown with hydrogen release to the containment, which led to hydrogen explosions in the reactor buildings [7].

The nuclear industry is expanding worldwide and many countries are currently not only planning and building new facilities but operating older fleets of nuclear power

1 Introduction

plants as well. The accident in Fukushima renewed the world's public awareness of nuclear hazards, and led to high safety requirements for new nuclear facilities as well as the so called „stress tests“ , which were performed for many existing nuclear power plants in order to assess their capability to deal with beyond design basis accidents. As a result, the authorities demand to make existing facilities safer by retrofitting new and mainly passive cooling systems into them. The existing GEN II reactors already include safety and emergency core cooling systems (ECCS) like the passive accumulators or active water injection systems. But many of these systems rely on AC or DC power supply in order to work properly, and Fukushima revealed that the risk of a total SBO in combination with a simultaneous loss of ultimate heat sink is quite real. Also it brought to mind that - since nuclear power plants are very safe in comparison to other industrial facilities - due to the complexity, there are still uncertainties in the modeling and simulation of reactor accidents with core melting.

Those so called beyond design basis accidents (BDBA) - even though they are very unlikely to ever happen - have the potential to completely destroy a nuclear facility and put the health of on-site personal and even civilians at risk, if no counter-measures are taken. This is why along with new generations of power plants, new and adapted safety systems and procedures have to be developed for existing reactor types, in order to keep nuclear power plants safe and technologically up to date.

In order to develop and assess accurate measures to counteract a potential core meltdown, we need to know as much details as possible about those beyond design basis conditions and what exactly the melting core looks like. Since experiments with nuclear fuel are complicated and dangerous, research in the BDBA area is forced to strongly use simulation tools like MELCOR (**M**ethods for **E**stimation of **L**eaks and **C**onsequences of **R**eleases) [8–10], ASTEC (**A**ccident **S**ource **T**erm **E**valuation **C**ode) [11] and ATHLET-CD (**A**nalysis of **T**hermalhydraulics of **L**eaks and **T**ransients - **C**ore **D**egradation). So in recent years, these tools were enabled to simulate core melting accidents and cover the whole sequence of an accident, from full-load operation over water loss and core melting, to hydrogen production and source term evaluation.

The main strategy to stop a core melting accident already in progress is to flood the reactor pressure vessel (RPV) with water as soon as possible, given that the RPV is still intact. As long as the core area is covered by water, the generated heat can be removed either by convective heat transfer or through evaporation. Also, the water filters the fission products and protects the surroundings from radiation.

On the other hand, the flooding of a melting core can lead to adverse effects like risk of explosion due to enhanced hydrogen production or embrittlement of the core material and the formation of debris. All those phenomena can have an effect on the evolution of the core melting accident, thus changing the chances of terminating the accident.

Even though Germany has decided its nuclear phase-out in the aftermath of Fukushima, there is still a lot of work left to do in the nuclear sector of the country. This does not only cover the years of operation left, but also decommissioning of the old nuclear facilities as well as waste treatment. Since Germany has many decades of experience with nuclear power plants, the country's experts will continue to contribute to the progress in nuclear technology by doing relevant research in different scientific topics.

In order to keep its expertise and competence, the government is funding research projects, in which a number of research institutes and universities come together to work on pressing safety matters in the field.

This thesis is embedded in the German joint research project WASA-BOSS (Weiterentwicklung und Anwendung von Severe Accident Codes - Bewertung und Optimierung von Störfallmaßnahmen), which started in 2013. Its goal is to simulate certain severe accidents in German pressurized water reactors (PWRs) and boiling water reactors (BWRs), and to develop and assess the influence of severe accident measures on the accident progression, in order to provide a basis for severe accident mitigation guidelines (SAMGs) for these power plants.

1.2 State of the art

1.2.1 The KONVOI type pressurized water reactor

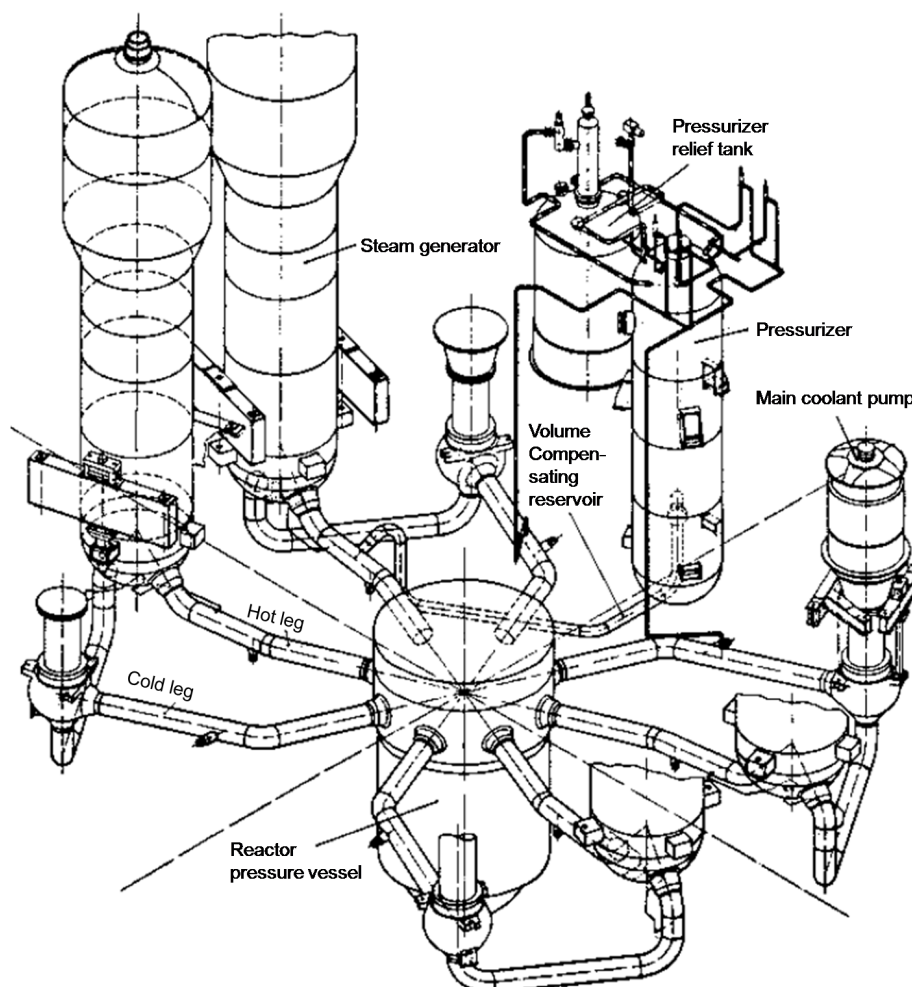


Figure 1.1: Schematic of a KONVOI type pressure water reactors primary system [1]

1 Introduction

The standard KONVOI type pressure water reactor consists of two separate water / steam cycles called the primary and secondary system. The primary system contains the reactor pressure vessel housing the reactor core and four water loops, each leading hot water from the core through the hot leg to a steam generator and through the main coolant pump in the cold leg back into the core. This configuration can be seen in figure 1.1, where the RPV is shown as well as the four identical loops. There is only one major difference between one of the loops and the other three, which is the connection of the pressurizer surge line to one of the cold legs. The surge line leads to the pressurizer, which regulates the pressure of the primary system and serves as compensation tank for small changes of the water inventory as well. The pressurizer is connected to a pressurizer relief tank, which serves as a collecting vessel, in which steam from the primary loop can be condensed in case of over-pressurization.

The steam generator serves as a heat exchanger between the primary and secondary circuit. The hot water coming from the core flows through more than 4,000 small U-tubes, giving off its heat through the metal walls to the water on the secondary side of the steam generator. Since the pressure in the secondary system is only around 7 MPa , the water on the secondary side will evaporate and the resulting steam is guided onto the turbine. From there, the steam is guided into condensers, and from there the water flows back into the steam generator secondary sides.

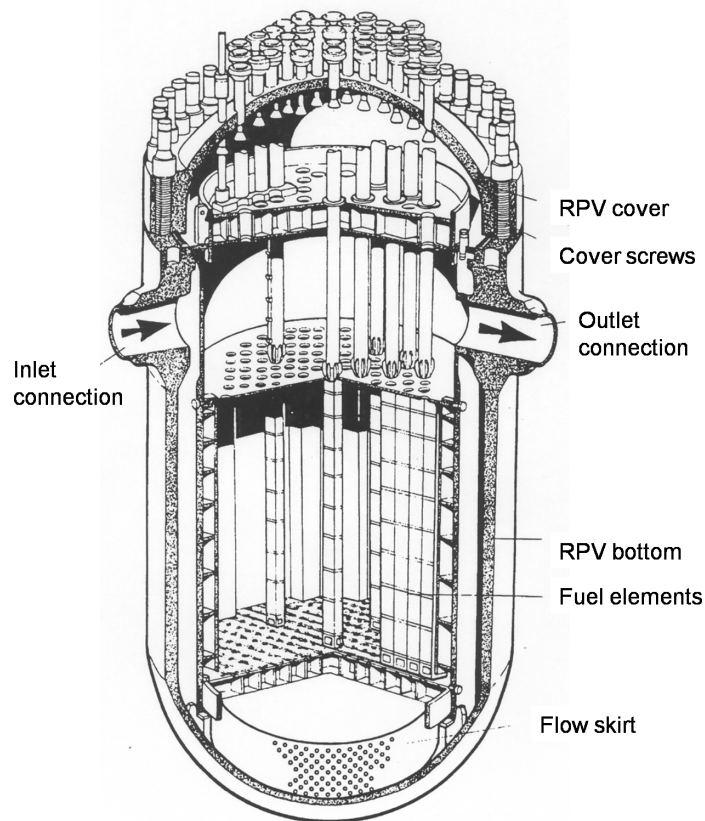


Figure 1.2: Schematic of a reactor pressure vessel of a KONVOI type pressure water reactor [1]

The reactor pressure vessel is the heart of every nuclear power plant. A typical construction is shown in figure 1.2, with one exemplary inlet and outlet connection not

showing the other six, which surround the RPV. Positioned in the lower half of the RPV is the fuel element rack holding nearly 200 fuel elements, while the upper space of the RPV is mainly used for the control rod structures. The area below the fuel element rack is called lower plenum, while the space above the control elements is called upper head.

1.2.2 Emergency core cooling systems in the design of a KONVOI type pressure water reactor

A typical KONVOI type PWR features four methods of injecting water into the primary system during a loss-of-coolant-accident (LOCA), which are part of the design basis (see fig. 1.3):

1. The high pressure injection system (HPI) shown in red,
2. the passive accumulator injection (ACCU) shown in orange,
3. the low pressure injection system (LPI) shown in green and
4. the sump circulation mode shown in blue.

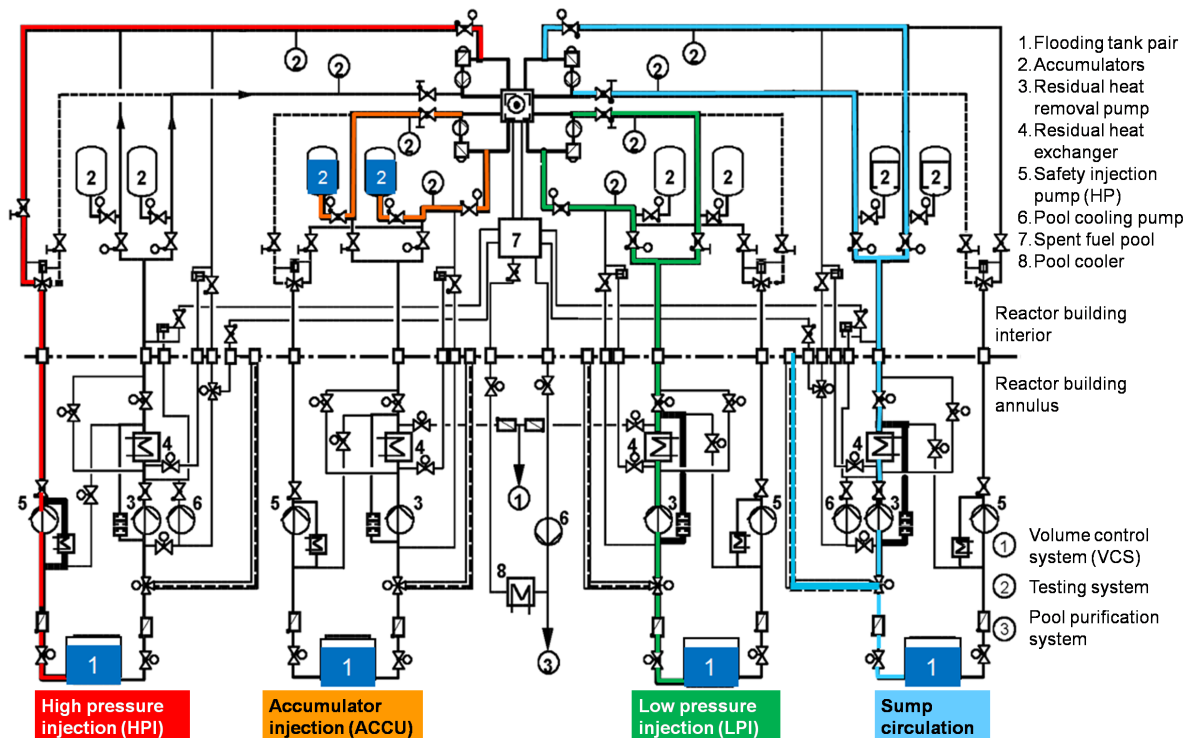


Figure 1.3: Schematic of the different emergency core cooling systems in a KONVOI type pressure water reactor [2]

The four pumps of the high pressure injection system (red) feed water from the flooding tanks into the four hot legs of the primary system with a maximum injection rate of 77 kg/s per pump and a pressure head of 11 MPa . It is possible for the operator to switch the injection location to the cold legs if necessary.

1 Introduction

There are eight passive accumulators (orange) present, one connected to each leg. Each accumulator contains 45 m^3 of water and is separated from the primary circuit by a check valve, which opens below a pressure of 2.6 MPa in the primary circuit. Usually, not the whole water inventory is emptied into the primary circuit, because nitrogen is used as a topper to keep the pressure inside the accumulators and the nitrogen is not supposed to reach the primary circuit. For this reason, there is an implemented „accumulator level low“ signal, stopping the injection before nitrogen can be injected into the primary circuit.

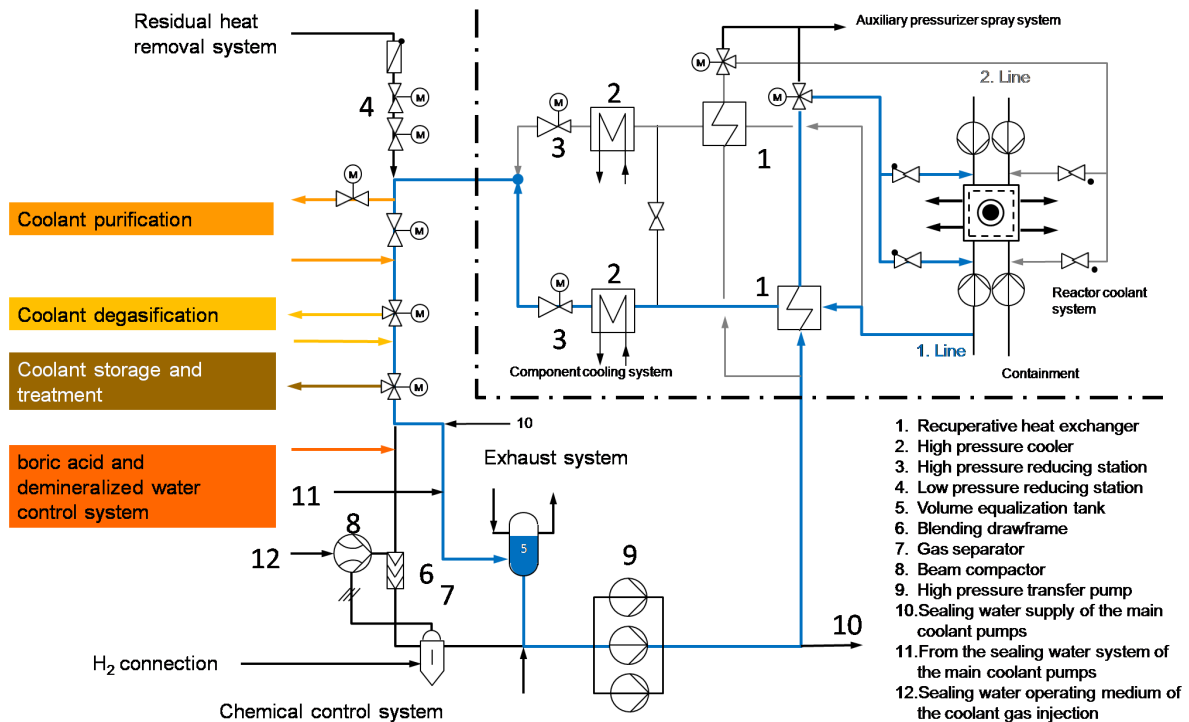


Figure 1.4: Schematic of the volume control system in a KONVOI type pressure water reactor [2]

The four pumps of the low pressure injection system (green) feed water from the flooding tanks into the eight legs of the primary system with a maximum injection rate of 325 kg/s per pump and a pressure head of 1.07 MPa . The system is designed to be switchable between pure hot or cold leg injection and a parallel injection into both legs with a 50 % flow rate per leg.

The sump circulation mode (blue) is designed for a continued core cooling operation after a loss-of-coolant accident. In case of a leak in the primary systems piping, a lot of water will leave the primary system, partially evaporate and condensate on the containment walls. In the end, the water will flow down into the reactor cavity called „sump“ and accumulate there. As soon as the fresh water supply from the flooding tanks is drained, the sump circulation mode is activated, sucking the water from the sump, cooling and cleaning it and feeding it back into the primary system through both the hot and the cold legs. Since the core is releasing heat continuously, the sump circulation will become ineffective over time, but it will create a grace period during which an external water supply can be established.

There is another systems directly connected to the primary system, which is usually not used in case of an accident: the volume control system (VCS). The volume control system regulates the water inventory of the primary system and hosts a lot of other systems, which preserve the water quality and purity, extract gases from the water, regulate the level of boric acid and more.

The schematic of the volume control system can be seen in figure 1.4. It takes water from the residual heat removal system, and feeds water directly into the four cold legs of the primary system. Each feed line contains a pump with a maximum injection rate of 35 kg/s . The maximum pressure head has to be at least 17 MPa , since the system working during the reactors operation when the primary pressure is 16.7 MPa .

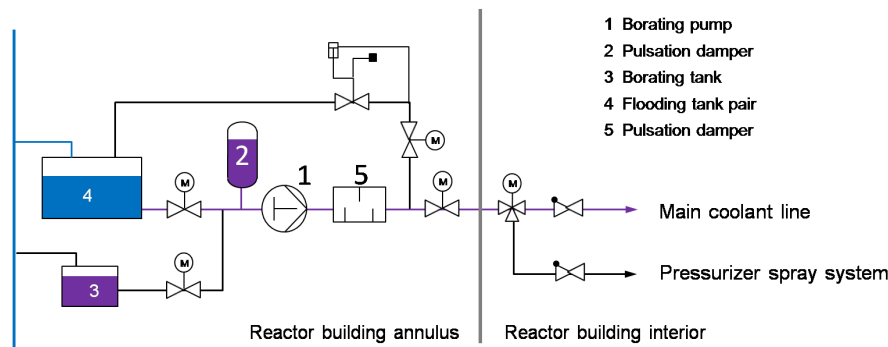


Figure 1.5: Schematic of the extra borating system in a KONVOI type pressure water reactor [2]

Another system connected to the primary system is the extra borating system (EBS). Its main purposes are the regulation of the content of boric acid in the primary system as well as the safe shut-down of the reactor in case the control rod system is not operation. The EBS can poison the reactor with boric acid, which will act as a neutron poison and stop the chain reaction. Its schematic is shown in figure 1.5.

1.2.3 The German Risk Study, Phase B

In the 1981, the German Risk Study, Phase B [12], was started in order to analyze and investigate accident sequences in German nuclear power plants (using Biblis B as a reference plant) and the resulting risks in a more detailed manner than during Phase A, the results of which had been published in 1979. With the German Risk Study, Phase A, an extensive risk analysis had been performed for the first time in the Federal Republic of Germany, using mainly the assumptions and methods of the WASH-1400 [13] study.

The Phase A study focused on the potential risk of a nuclear power plant on the public health, and the comparison of this risk to other civil or natural risks. The results of Phase A led to a variety of safety enhancements in the German nuclear power plants and showed to potential of risk studies in general. Phase B then focused on the subject of accident behavior, analyzing the development of accident sequences, the resulting loads on the power plant and the performance of the ECCS.

1 Introduction

The results of Phase B show the importance of accident management measures, because it revealed additional safety provisions, even when the implemented safety systems do not intervene as planned and the design basis is exceeded. Those safety provisions can be used for plant internal emergency measures in order to reduce the risk resulting from the accident. This might be the mastery of the accident or - if this is not possible - at least the reduction of the damage inflicted by the accident. It was shown in Phase B that an additional safety level can be created beyond the existing design basis levels.

The analysis of possible damage inflicted by the accident revealed great uncertainties, especially in the area of extreme accident events, which might be highly improbable but would also cause an enormous release of radioactivity to the environment. The results of Phase B were used to reconsider existing safety assessments and to refine the safety concept of the German nuclear power plants. [12, 14]

1.2.4 Phenomenology of a core melt-down

During a loss-of-coolant accident (LOCA) in an NPP, the fuel rods will heat up and degrade if not water can be supplied to the primary system. The water loss through the leak sooner or later leads to an uncovering of the core starting from the top. Due to the decay heat, the core materials will heat up, which at first will increase the gas pressure inside the fuel rods, leading to a ballooning effect. The core melt-down phenomenology can be seen in figure 1.6, starting from the left.

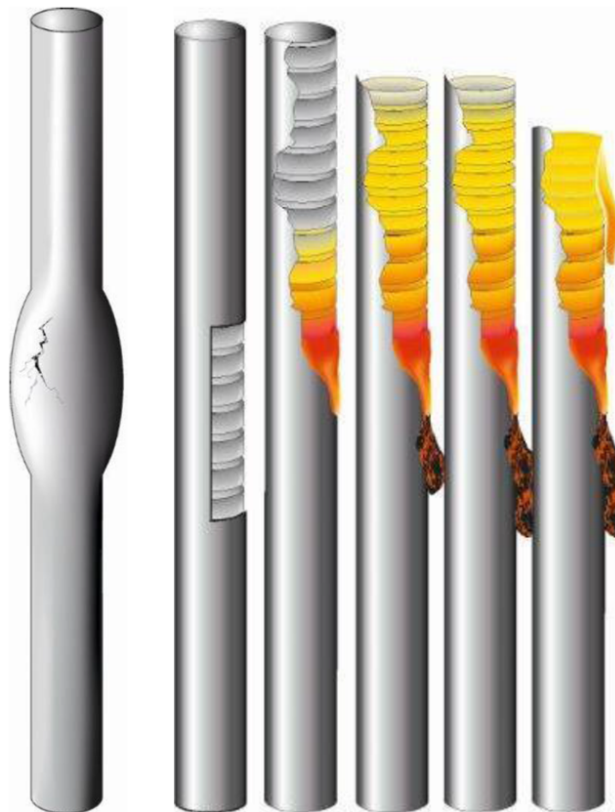


Figure 1.6: Phenomenology of the fuel rod degradation process [3]

At some point the fuel rod cladding will burst and melt, leaving the fuel pellets exposed. The melting cladding material will candle down to lower and colder parts of the core, where it freezes and forms blockades between the still intact fuel rods. The fuel pellets start melting later, when the temperature reaches the melting point of the uranium oxide.

Figure 1.7 shows the core degradation process as modeled in ATHLET-CD. Note that ATHLET-CD only simulates half of each rod and mirrors the results. In the initial state the fuel rod consists of the fuel pellets (solid UO_2 , shown in yellow) and the cladding material (zirconium, shown in black). With rising temperatures, a layer of zirconium oxide (light grey) forms on the outer surface of the cladding. This process takes place during operation and is not specific to an accident sequence.

The ballooning of the cladding leads to a failure of the cladding, releasing eutectic (ocher) and metallic (orange) melt, which starts to candle down the fuel rods outer surface. When the melt reaches lower and thus colder core regions, possibly even hitting water, metallic crusts (brown) are formed between the rods, which will eventually block the path for water and steam. Rising temperatures eventually lead to the melting of the fuel pellets, releasing ceramic melt (red), which can form ceramic crusts (dark red) in lower core regions as well.

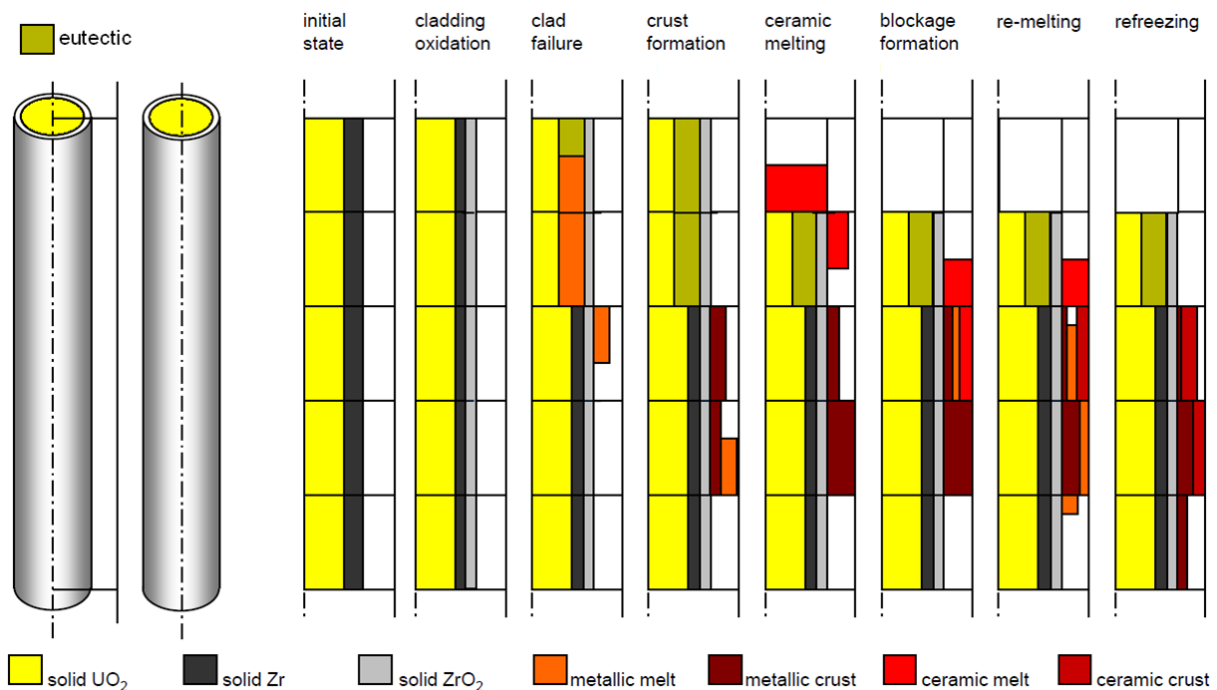


Figure 1.7: Schematic representation of the fuel rod degradation process as simulated by ATHLET-CD [3]

The time scale for a core melt-down is subject to uncertainties, especially depending on the size of the leak and the amount of water injected into the primary system e.g. by passive accumulators or other ECCS. Exemplarily, the accident in TMI-2 in 1979 can be used as a reference. This accident is commonly divided into seven phases [15–17]:

Phase 1: LOCA (duration ca. 100 *min*)

Phase 2: Core heating without available RCS or ECCS (duration ca. 74 *min*)

1 Introduction

Phase 3: Partial core reflooding and formation of a debris bed (duration ca. 6 min)

Phase 4: Formation of a molten pool inside the debris bed (duration ca. 20 min)

Phase 5: Total core reflooding (duration ca. 24 min)

Phase 6: Relocation of core material to the lower plenum (duration ca. 2 min)

Phase 7: Establishment of steady cooling conditions

The accident serves as the only core meltdown of reactor scale, because all experiments performed since had smaller geometries. This is the reason, why all severe accident codes have to be tested in the simulation of the TMI-2 accident, in order to assess effects caused by the 3D geometry of the reactor and scale effects that might not appear in smaller experiments [16, 17]. The TMI-2 accident is of great value to this work, because the reactor not only went through the full core degradation process, but also experienced a reflooding during the degradation, which in this case led to a coolable condition inside the RPV, even though not all the fuel could be retained in the core area. The incident proved that a core meltdown can be stopped under specific conditions and serves as a basis for all the reflooding variations discussed in this work. Nevertheless it cannot be compared directly, because the core degradation took place under high pressure conditions because of the small leak size, while the pressure in case of an MBLOCA decreases rapidly to a level below 1 MPa.

1.2.5 The Severe Accident Mitigation Guidelines (SAMGs)

All the emergency operating procedures (EOPs) implemented in nuclear power plants have the goal to keep the core integrity and supply a heat sink for the decay heat in order to prevent radioactive releases from the power plant to the environment. However, due to unforeseen events, operator errors or a combination of events, severe accidents with damage to the core are possible.

For this reason, severe accident mitigation guidelines have been developed. They no longer have the goal to keep the core intact, but assume that core integrity has been lost already. Thus they focus on preventing / minimizing the radioactive releases to the environment and the supply of a heat sink in order to cool the degrading core as fast and reliable as possible.

There are different techniques applied in Severe Accident Management Guidelines, which can be categorized into three categories: [18, 19]

Measures applied to keep the integrity of the barriers „Reactor Pressure Vessel“ and „Reactor Cooling System“

In order to keep the integrity of the RPV and / or RCS, it is of highest importance to cool the degrading core while keeping the pressure low enough so the RPV and RCS do not fail due to overpressure. Mitigation strategies can include the injection of water into the RPV and RCS, for example using the ECCS or systems like the VCS and EBS, or a spray system, which is implemented into the RCS of boiling water reactors. In case of a PWR, the restart of one or more reactor coolant pumps (RCPs) can enhance the

water flow into the RPV by establishing a forced water convection cycle. The supply of water to the core reduces the heat inventory and thus the systems pressure. Another strategy to reduce the pressure can be the opening of safety valves, which would lead to a controlled release into the pressure relief tank (PWR) or condensation pool (BWR).

To remove the heat from the core, it is important to keep the steam generators working, which is why water has to be supplied to the steam generators in parallel, too. A depressurization of the steam generators can be necessary as well, especially when the pressure of the primary system is reduced.

Another mitigation measure - depending on the reactor configuration - can be the external cooling of the RPV. This would remove heat through the RPV wall and could possibly prevent a creep failure of the RPV.

Measures applied to keep the containment integrity

In order to keep the integrity of the containment barrier, measures might have to be taken, which deal with the dangers induced by hydrogen deflagration or detonation. These measures include the operation of hydrogen recombiners or igniters, which shall lead to a controlled burning of the hydrogen inside the containment before the risk of a hydrogen detonation can arise. Since not only hydrogen but also oxygen is necessary to be present for a deflagration or detonation reaction, the inerting of the containment atmosphere using non-condensable gases or possibly steam is an option as well.

Venting of the containment by using the filtered venting system might have to be done in order to reduce the risk of a catastrophic containment failure due to overpressure. This would lead to a source term to the environment, but it would be a rather small one and could be released in a controlled manner over a certain time, thus preventing higher contamination. Also, the filtered venting system would reduce the amount of radioactivity released, as long as the system's maximum capacity is not exceeded. A filtered venting system is installed in all German nuclear power plants.

New built nuclear power plants also include passive containment cooling systems, releasing huge amounts of water to the outside of the steel liner in order to both dissipate the heat from the containment and reduce the pressure. Another passive containment cooling concept is the operation of building condensers, which would replace the steam generators as the primary heat sink under severe accident conditions.

Measures to minimize the radioactive releases

If radioactive releases have taken place into the reactor building or even into the surrounding buildings, measures have to be taken to minimize the release to the environment. These measures can include the spraying or even flooding of the reactor building or the spent fuel pool, depending strongly on the availability of appropriate systems and water. A venting of the affected buildings might be inevitable if the pressure rises and a failure due to overpressure cannot be ruled out. Another measure

1 Introduction

might be the spraying of the containment in order to wash out released fission products and thus reduce the radioactive releases through the containment building or auxiliary buildings.

In-vessel and ex-vessel corium melt retention concepts

In reactors of newer generations, in-vessel and ex-vessel melt retention strategies have been implemented in order to retain the core melt inside the containment building in case of a severe accident with core melting. The in-vessel melt retention mainly focuses on cooling the melt and RPV while the melt is still inside it, thus preventing the RPV failure and melt release to the containment. The ex-vessel melt retention strategies all come down to some kind of core catcher, which is located below the RPV and shall spread the corium over a certain area in order to enlarge its surface. The corium is then cooled by water, sometimes from the top, sometimes from nozzles in the core catcher below. In most concepts, sacrificial concrete is provided and shall condition the corium melt to become less viscous and reduce the temperature of the mixture as well.

1.3 Objective of this work

The severe accident mitigation is one of the major research fields in the community of nuclear energy, and has even gained attention and funding since the accident in Fukushima in 2011. SAMGs have been implemented in many countries of the world, but there remain large uncertainties concerning core degradation sequences. This is mainly due to the fact that there have not been many reactor accidents with core-meltdown, luckily. Experiments with nuclear fuel are expensive and potentially dangerous and can never be at reactor scale, making interpolation processes rather uncertain. This is why the simulation of severe accidents has gained increasing importance for the provision of knowledge on core degradation sequences, which in turn is essential for the development of SAMGs and other systems to create safer power plants for the future.

Against this background, the German Federal Ministry of Education and Research has funded the WASA-BOSS project, which brought together the top German nuclear research facilities in order to exchange and extend the knowledge on severe accidents and to assess the implemented SAMGs in Germany.

As part of the project, the IKE investigated a core degradation scenario using the German severe accident code system ATHLET-CD. The goal of this work was to simulate reflooding of the degrading core in order to assess the effectiveness of the reflooding using the ECCS and to propose potential optimizations to the SAMGs.

The first part of this work deals with the question, where the coolability limits are and up to which amount of molten core material a stable and coolable condition can be reached by reflooding the RPV. In this context, the way to judge coolability is assessed as well, because different criteria are possible. The question whether a middle pressure

1.3 Objective of this work

injection system might be more effective than the standard high and low pressure injection systems will be investigated, as well as a variety of system configuration, which differ in the injection location and the number of available pumps.

The results are supposed to be used for the optimization of the current state of SAMGs as well as for the design of new generations of nuclear power plants, in order to create more effective safety measures. A critical assessment of the results will contribute to the current state of modeling severe accidents with the system code ATHLET-CD and highlight improvement possibilities.

This means specifically that an assessment of the chances to successfully cool a degrading PWR core is performed, and an extensive parametric study shall enable a comparison of the different reflooding approaches. According to Hering et al. [20], reflooding performed in experiments or simulated, has mainly been performed with water mass injection rates $> 1 \frac{g}{s \cdot rod}$ (57.9 kg/s , assuming 57,900 fuel rods for a full sized PWR core), which is why simulations with lower injection rates have been performed for this work as well.

From the simulations performed for this work, a recommendation is derived as to which strategy might be preferable in the course of a severe accident similar to the one simulated here. Another point of interest is the evaluation of possible risks arising due to the water injection into the degrading reactor core, such as hydrogen production, which is part of the discussion.

2 The code system ATHLET-CD

For the simulations presented in this thesis, the German Severe Accident Code ATHLET-CD was used. This code system is developed by GRS. The Institute of Nuclear Technology and Energy Systems (IKE) at the University of Stuttgart contributes to the development of ATHLET-CD especially through models for the late phase of core degradation.

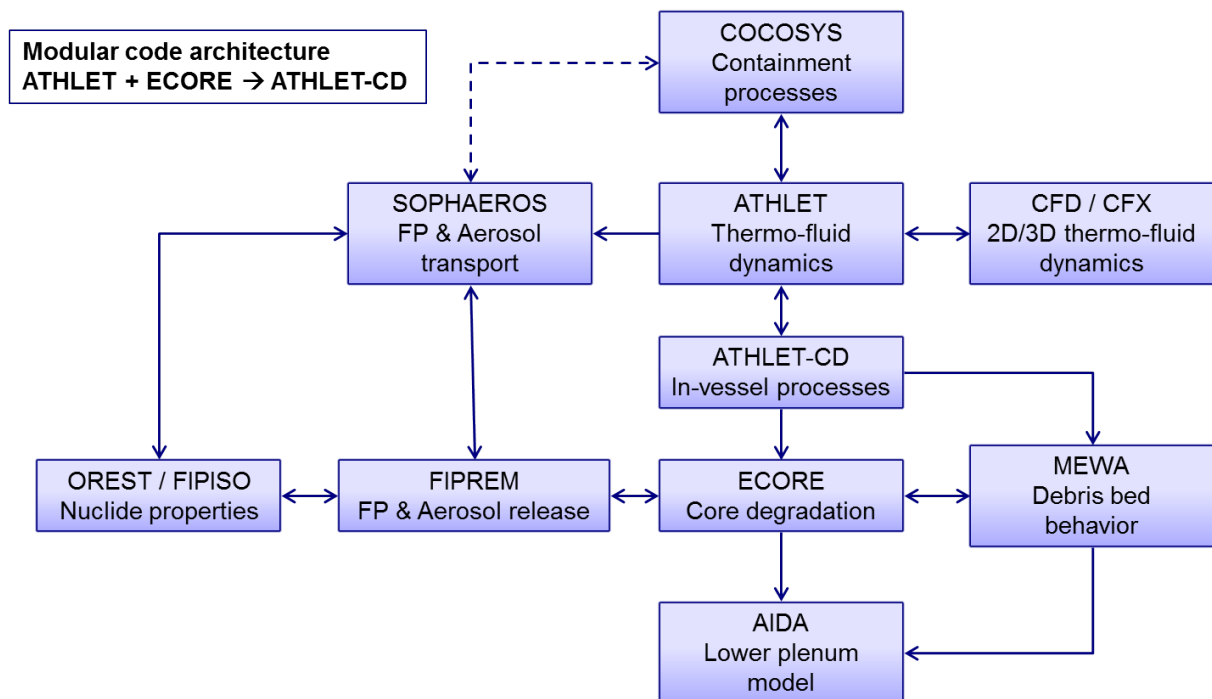


Figure 2.1: Overview of the modular code architecture of the ATHLET code system [3]

The thermal-hydraulic system code ATHLET-CD is designed to simulate the thermal-hydraulics of light water reactors, including DBAs and BDBAs. The highly modular code contains different optional and non-optional modules, so that the user can optimize the simulation tool for its particular purpose. Figure 2.1 shows a schematic of the ATHLET code system's architecture. The basic module of the code system is called ATHLET as well and contains the simulation models for thermo fluid dynamics, heat conduction and transfer, neutronics and reactor controls. The module ECORE is responsible for the simulation of the behavior of core materials. The common combination of the modules ATHLET and ECORE is called ATHLET-CD and was used for the purpose of this work, namely version 3.0A.

For the simulation of core melting accidents, the module AIDA plays an important role, since it simulates the transfer of molten corium to the lower plenum of the RPV, as well as the heat transfer to the vessel wall. The MEWA module for debris bed behavior is currently being extended at the IKE to simulate three dimensional beds, and shall be able to couple to the ATHLET code system soon.

In addition, there are modules available for the release and transport of fission products and aerosols (FIPREM and SOPHAEROS), as well as nuclide properties (OREST and FIPISO). It is possible, to couple the ATHLET code system to the containment code COCOSYS in order to simulate a severe accident with release to the containment until containment failure occurs. For the simulation of 2D- or 3D-thermo fluid dynamics, several common CFD / CFD codes can be used. For the simulation conducted in this work, only ATHLET, Ecore and AIDA were used.

2.1 Thermo fluid dynamics (TFD)

To simulate the thermo-fluid-dynamic behavior of the coolant, the user has to specify the whole piping system with all its geometrical and fluid dynamic properties. Therefore different kinds of objects are available, basically pipes and branches, but special objects like a steam water separator as well. Each object can be subdivided into numerous cells, the so-called control volumes (CVs), in order to refine the simulation's resolution. All objects have to be coupled via junctions, in order to provide valid flow paths (see fig. 2.2).

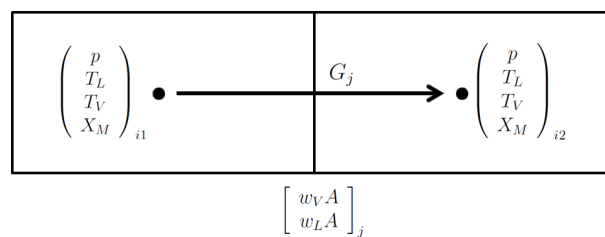


Figure 2.2: Schematic representation of two thermo fluid dynamic control volumes, connected by a junction

In principle, mass and energy conservation is based on the CVs, while the momentum balance is based on the junctions. The user can chose between the classic 5-equation model and a two-fluid model with separate momentum balance equations for liquid and vapor. The two-fluid model (or six equation model) treats the liquid and vapor phases of the coolant independently, so that for both phases the equations for mass, energy and momentum have to be solved:

Liquid mass:

$$\frac{\partial ((1 - \alpha) \rho_L)}{\partial t} + \nabla \cdot ((1 - \alpha) \rho_L \vec{w}_L) = -\Psi \quad (2.1)$$

Vapor mass:

$$\frac{\partial (\alpha \rho_V)}{\partial t} + \nabla \cdot (\alpha \rho_V \vec{w}_V) = \Psi \quad (2.2)$$

Liquid energy:

$$\begin{aligned} & \frac{\partial \left[(1 - \alpha) \rho_L \left(h_L + \frac{1}{2} \vec{w}_L \vec{w}_L - \frac{p}{\rho_L} \right) \right]}{\partial t} + \nabla \cdot \left[(1 - \alpha) \rho_L \vec{w}_L \left(h_L + \frac{1}{2} \vec{w}_L \vec{w}_L \right) \right] \\ & = -p \frac{\partial (1 - \alpha)}{\partial t} \end{aligned} \quad (2.3)$$

$+ \vec{\tau}_i \vec{w}_L$	shear work at the phase interface
$+ (1 - \alpha) \vec{\tau}_i (\vec{w}_V - \vec{w}_L)$	dissipation due to interfacial shear
$+ (1 - \alpha) \rho_L \vec{g} \vec{w}_L$	gravitational work
$+ \dot{q}_{WL}$	heat flow through structures
$+ \dot{q}_i$	heat flow at the phase interface
$+ \Psi (h_{\Psi,L} + \frac{1}{2} \vec{w}_\Psi \vec{w}_\Psi)$	energy flow due to phase change
$+ S_{E,L}$	external source terms

with

$\vec{w}_\Psi = \vec{w}_L$	for evaporation
$\vec{w}_\Psi = \vec{w}_V$	for condensation

Vapor energy:

$$\begin{aligned} & \frac{\partial \left[\alpha \rho_V \left(h_V + \frac{1}{2} \vec{w}_V \vec{w}_V - \frac{p}{\rho_V} \right) \right]}{\partial t} + \nabla \cdot \left[\alpha \rho_V \vec{w}_V \left(h_V + \frac{1}{2} \vec{w}_V \vec{w}_V \right) \right] \\ & = -p \frac{\partial \alpha}{\partial t} \end{aligned} \quad (2.4)$$

$- \vec{\tau}_i \vec{w}_V$	shear work at the phase interface
$+ \alpha \vec{\tau}_i (\vec{w}_V - \vec{w}_L)$	dissipation due to interfacial shear
$+ \alpha \rho_V \vec{g} \vec{w}_V$	gravitational work
$+ \dot{q}_{WV}$	heat flow through structures
$+ \dot{q}_i$	heat flow at the phase interface
$+ \Psi (h_{\Psi,V} + \frac{1}{2} \vec{w}_\Psi \vec{w}_\Psi)$	energy flow due to phase change
$+ S_{E,V}$	external source terms

with

$\vec{w}_\Psi = \vec{w}_L$	for evaporation
$\vec{w}_\Psi = \vec{w}_V$	for condensation

Liquid momentum:

$$\frac{\partial ((1 - \alpha) \rho_L \vec{w}_L)}{\partial t} + \nabla ((1 - \alpha) \rho_L \vec{w}_L \vec{w}_L) + \nabla ((1 - \alpha) p) = \quad (2.5)$$

$+\vec{\tau}_i$	interfacial friction
$-(1 - \alpha) \vec{f}_W$	wall friction
$-\Psi \vec{w}_\Gamma$	momentum flux due to phase change
$-(1 - \alpha) \rho_L \vec{g}$	gravitation
$+\alpha (1 - \alpha) (\rho_L - \rho_V) \vec{g} D_h \nabla \alpha$	water level force
$+\alpha (1 - \alpha) \rho_m \left(\frac{\delta \vec{w}_R}{\delta t} + \nabla \vec{w}_R \right)$	virtual mass
$+S_{I,L}$	external momentum source terms (e. g. pumps)

Vapor momentum:

$$\frac{\partial (\alpha \rho_V \vec{w}_V)}{\partial t} + \nabla (\alpha \rho_V \vec{w}_V \vec{w}_V) + \nabla (\alpha p) = \quad (2.6)$$

$-\vec{\tau}_i$	interfacial friction
$-\alpha \vec{f}_W$	wall friction
$+\Psi \vec{w}_\Gamma$	momentum flux due to phase change
$-\alpha \rho_V \vec{g}$	gravitation
$-\alpha (1 - \alpha) (\rho_L - \rho_V) \vec{g} D_h \nabla \alpha$	water level force
$-\alpha (1 - \alpha) \rho_m \left(\frac{\delta \vec{w}_R}{\delta t} + \nabla \vec{w}_R \right)$	virtual mass
$+S_{I,V}$	external momentum source terms (e. g. pumps)

with

$$\rho_m = \alpha \rho_V + (1 - \alpha) \rho_L$$

$$\vec{w}_R = \vec{w}_V - \vec{w}_L$$

The ATHLET-CD code system performs spatial integrations on the basis of a finite-volume approach, which leads to a set of first order differential equations, also called the 2M model: two equations per CV stemming from mass conservation, two from energy conservation and two equations per junction for momentum conservation. For the integration, a change in the geometry of flow channels and structures is neglected, as well as the dissipation energy and potential energy distribution to the energy balance equations [21].

If alternatively the five equation model (or 1M model) is applied, the momentum equations of liquid and vapor are combined to a momentum equation for a two-phase mixture:

$$\frac{\partial (\rho_m \vec{w}_m)}{\partial t} - \vec{w}_m \frac{\partial \rho_m}{\partial t} + \rho_m \vec{w}_m \nabla \vec{w}_m + \nabla \left(\alpha (1 - \alpha) \frac{\rho_V \rho_L}{\rho_m} \vec{w}_R \vec{w}_R \right) + \nabla p = \quad (2.7)$$

$$\begin{aligned}
 +\vec{f}_W & \quad \text{wall friction} \\
 +\rho_m \vec{g} & \quad \text{gravitation} \\
 +S_{I,m} & \quad \text{external momentum source terms}
 \end{aligned}$$

where

$$\vec{w}_m = \frac{1}{\rho_m} (\alpha \rho_V \vec{w}_V + (1 - \alpha) \rho_L \vec{w}_L)$$

In case of the five equation model, the momentum conservation equation for the mixture is complemented by a set of empirical algebraic laws describing the slip between the phases as a function of the void fraction and mixture velocity. This model is called the drift-flux model and it allows for the explicit calculation of the liquid and gas velocities [21].

There are two different kinds of CVs available in the ATHLET-CD code: the homogeneous CV, and one with a mixture level inside. In the homogeneous CV, liquid and vapor, as well as non-condensable gases are evenly distributed, while the CV with mixture level is automatically divided in two sub-CVs. The upper sub-CV contains vapor with droplets as necessary, while the lower sub-CV contains water with bubbles as necessary. If the mixture level approach is applied, the five equation model has to be used for the corresponding CVs.

Independent of the chosen CV type and balance equation model, a number of important non-condensable gases can be simulated, which are hydrogen, nitrogen, oxygen, air, helium and one user defined gas. They are basically treated as ideal gases and are simulated to have the same temperature and velocity as the vapor.

In addition, the boron tracking model can be used to simulate the transport of boric acid, which is dissolved in the liquid phase of the coolant only, through the system.

For the coolant not only light water is available, but also heavy water, helium and some liquid metals. For the simulation of leakages, specific models for critical flow and critical discharge have to be applied. For more information on the thermo fluid dynamic properties of the ATHLET-CD simulation tool, see Austregesilo et al. [21].

2.2 Heat conduction and heat transfer (HECU)

The HECU module simulates one-dimensional heat conduction in solid materials with up to three material zones separated by a gap. A HECU object can be coupled to a thermo fluid dynamic CV on one or both sides, in order to allow heat transfer between two CVs or between a CV and the environment.

$$\underbrace{\int_V W \cdot dV}_{\text{rate of heat generation}} = \underbrace{c_P \cdot \rho \cdot \int_V \frac{\delta T}{\delta t} \cdot dV}_{\text{rate of change of internal energy}} + \underbrace{\int_S \vec{q} \cdot d\vec{A}}_{\text{heat flow crossing the boundary}} \quad (2.8)$$

2 The code system ATHLET-CD

The basic assumptions made for the heat conduction theory are that the solid material is homogeneous and isotropic and has no dependencies on pressure. Phase changes of the material are neglected as well. The basic equation to be solved by the HECU module is the conservation of energy inside of the heat conduction objects (HCOs) 2.8.

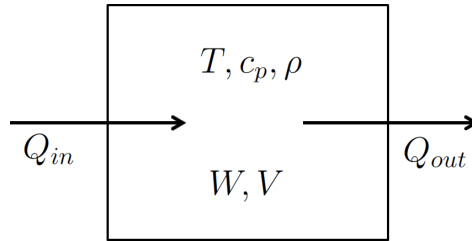


Figure 2.3: Schematic representation of the energy balance in an exemplified heat conduction layer

Figure 2.3 shows an exemplified heat conduction layer. The application of equation (2.8) to this layer under the assumption of uniform heat generation distribution, temperature and material properties leads to the following equation:

$$\underbrace{Q_{in}}_{\text{rate of heat flow into layer}} + \underbrace{W \cdot V}_{\text{rate of heat generation in the layer}} = \underbrace{Q_{out}}_{\text{rate of heat flow out of the layer}} + \underbrace{\rho \cdot c_P \cdot V \cdot \frac{dT}{dt}}_{\text{rate of change of internal energy in the layer}} \quad (2.9)$$

The specific equations for the heat flow into and out of the layer depend on the geometry of the layer, which can be cylindrical, flat or spherical. HECU also handles the heat transfer between the fluid and the solid structures.

In principle, the ATHLET-CD simulation tool divides the heat transfer into four main regimes, which are:

- Level I: Heat flow from fluid to wall
- Level II: Heat flow from wall to fluid
- Level III: Transition boiling
- Level IV: Stable film boiling

For every regime, and several sub-regimes, different correlations for the calculation of heat transfer coefficients are applied, while the user has a variety of options to control the transition between nucleate boiling and film boiling. Details can be found in the ATHLET Input Data Description [22].

Also, the HECU module separately accounts for condensation and evaporation directly on heating or cooling surfaces and offers the option for a quench front model for both top and bottom flooding conditions.

2.3 Time advancement procedure (FEBE)

Through the spatial integration of the conservation equations over control volumes and junctions, the system of spatial differential equations is transformed into a system of coupled differential equations (see section 2.1). To determine a numerical solution for an initial value problem of this large system of ordinary differential equations, the ATHLET-CD code uses the FEBE-method (**F**orward-**E**uler - **B**ackward-**E**uler) [21].

$$\frac{dy}{dt} = f(y, t), \quad \text{with initial values} \quad y(t_0) = y_0 \quad (2.10)$$

The solution variables y_i depend only on time, and describe the temporal evolution of the thermo-fluid-dynamic state of the system. The number of variables y_i , and thus differential equations, depends on the number of CVs and their junctions, and on the number of solution variables in every basic element.

The ATHLET-CD code approximates the time derivatives \dot{y}_i to be only dependent on the solutions variables of a few adjacent elements, using spatial approximation algorithms:

$$\frac{dy_i}{dt} = f_i(y_{i-i_L}, \dots, y_{i-1}, y_i, y_{i+1}, \dots, y_{i+i_R}, t) \quad (2.11)$$

By applying this method in the ATHLET-CD simulations, three types of methodical errors occur:

1. Errors in the physical models. These errors have to be minimized by comparing simulation results with experiments and by improving the models, if necessary.
2. Errors due to spatial discretisation. To minimize these errors, the discretisation has to be refined until the differences between the results have diminished to an acceptable level. It has to be noted that in practice this refinement is only possible up to a limited amount of control volumes, because the finer the discretisation becomes, the higher will be the simulation time.
3. Errors caused by the time discretisation. This kind of error is limited by the applied time advancement procedure in the integration of the differential equation system.

The time advancement procedure in the ATHLET-CD simulations consists of two steps [23]. In the first step the system of differential equations is solved with the linear implicit Euler method, using a time step considerably bigger than the one supposed to get accurate solutions. In order to control the local discretisation error produced by this method, a second stage is applied in which another solution is calculated taking two steps with half the time step size. From those two solutions an extrapolation of the solution value for a time step size $\Delta t \rightarrow 0$ is performed, and the difference between the actual and extrapolated value is compared against the given error bound. If the

difference is of an acceptable value, the extrapolated value is taken as the solution, and the simulation moves on to the next time step. If not, another solution is calculated at one third of the time step. Then the extrapolation is done again with the three available solutions, and again the result is compared against the error bound. The FEBE method could continue this to higher orders (4^{th} , 5^{th} , etc.), but it stops at 3^{rd} order by default. If the estimated error does not satisfy the accuracy criterion by then, the whole step is restarted, with a new basic time step reduced by at least a factor of two. This is repeated until the time step size has become so small that it is below the lower limitation given by the user as input value. In this case the code stops with an error status.

2.4 General simulation control (GCSM)

To simulate the balance-of-plant systems, the general control simulation module (GCSM) is used. It is a block-oriented language, which describes the control and protection systems of the simulated nuclear power plant. [24] Every GCSM control element is restricted to a maximum of four input values, and gives only one output value.

The GCSM provides interface data to the simulation of the thermal dynamic plant behavior by means of process signals like temperature and pressure values and control signals or hardware actions such as valve positions. There is a total of 41 process signals and 26 different hardware actions available, which are described in detail in Austregesilo et al. [21].

In GCSM, a set of interconnected signals is used to simulate the whole control system of the power plant. There are 25 basic control elements (e.g. SWITCH, ADDER, ...) and three special control elements available, which can be coupled by the user input for the simulation of complex systems.

2.5 Core degradation (ECORE)

ATHLET can be used together with the module HECU (see Section 2.2) to simulate the thermal behavior of fuel and control rods adequately as long as the initial geometry remains intact. However, when insufficient cooling leads to a heat-up of the core beyond approximately $1100K$, core degradation sets in and leads to the chemical and melting phenomena listed in Table 2.1. In order to be able to simulate these processes as well, ATHLET is coupled with the module Ecore. This version, which can also be used to simulate severe accidents with core melting, is called ATHLET-CD. The module Ecore aims at modeling of the most relevant processes in the reactor core, up to complete failure of the core. Quite detailed models are available for the early phase of core degradation, which is characterized by the still mostly intact rod bundle geometry.

Table 2.1: Phenomena important for the degradation process and their occurrence temperatures

Temperatures	Phenomenon
1100 K	Melting of absorber material (AIC), thus failure of the control rods
1220 K	Eutectic interaction of both Fe and Ni with Zr and thus interaction of the fuel rod cladding with the spacers and possible penetration of the cladding
1400 K	Formation of liquid U due to UO_2/Zr interaction (insignificant)
1500 K	Liquefaction of inconel/Zr and thus start of rapid Zr oxidation and cladding embrittlement
1650 K	Melting of inconel
1720 K	Melting of stainless steel
2030 K	Melting of zircaloy-4
2170 K	Formation of $\alpha Zr(O)/UO_2$ eutectics
2245 K	Melting of $\alpha Zr(O)$
2670 K	Formation of $\alpha Zr(O)/UO_2$ and U/UO_2 monotectics
2750 K	Melting of UO_{2-x}
2810 K	Formation of liquid phase of oxidic $UO_2 - ZrO_2$ -eutectics
2900 K	Melting of UO_{2+x}
2960 K	Melting of ZrO_2
3120 K	Melting of UO_2

The model approach followed in Ecore is one of representative rods, which can be either fuel or control rods. Representative fuel rods consist of fuel pellets separated from the cladding by a gas filled gap, while the control rods are composed of absorber pellets enclosed in the cladding of the guide tube. The representative rods are axially meshed in order to describe axial profiles of temperature, layer thickness, etc. Usually, the core will be divided into several concentric rings, with one representative fuel and one representative control rod, simulating the N_{fuel} and $N_{control}$ rods in this ring. Then, each ring is typically associated to a separate thermal-hydraulic channel.

The idea of the representative rod concept is that within certain parts of the core many rods have the same fission (or decay) power and are subject to approximately the same thermal-hydraulic boundary conditions. Thus, it is sufficient to model the behavior of very few rods to describe the behavior of a whole core. A further advantage of the concept of representative rods is that the modeling can take into account effects that occur at the rod level in a very detailed manner, like the formation of melt and its relocation along the rod in streaks. This strength however becomes a weakness when interactions between several rods become important, like when the melt produced along several rods starts to merge and forms blockages or possibly a molten pool in a later stage.

The processes modeled by the Ecore module include:

- The thermal behavior of the rods:
 - radial heat conduction inside the fuel, heat transfer through the gap and conduction through the cladding,

2 The code system ATHLET-CD

- axial heat conduction in the rod,
 - convective heat transfer with the surrounding fluid in single- and two-phase regimes and
 - radiative heat transfer between neighboring rods and to surrounding structures at the top, bottom and radial core boundaries.
- The cladding's mechanical behavior: deformation and creep of the cladding (ballooning) due to the difference between the rod's internal pressure and the system pressure up to possible mechanical failure (clad burst).
 - Exothermic reactions between cladding and steam (cladding oxidation), leading to formation of a ZrO_2 protective layer and hydrogen.
 - The formation and relocation of melt (absorber, metallic and oxidic).

Further models and modules in ATHLET-CD deal with fission product release and transport in the primary system (modules FIPREM and SOPHAEROS) as well as with the formation and behavior of debris beds during the late phase of core degradation (module MEWA). Since these have not been used in the present work, they are not discussed further here.

2.5.1 Cladding oxidation

At temperatures above ca. $900^\circ C$ the chemical reaction between the cladding material and steam becomes significant. The oxidation of Zr by steam is described by the formula:



This reaction is strongly exothermic and contributes significantly to the core heat-up. Various experiments have shown that the oxidation phenomenon is essentially non stationary and controlled by oxygen diffusion, which leads to growth of a protective layer (ZrO_2), consuming the initial cladding material during the process. The chemical reaction kinetics can be approximated by rate laws of the form:

$$\frac{dX^2}{dt} = K \quad (2.13)$$

where X is the layer thickness of the ZrO_2 layer. From the growth rate of the ZrO_2 layer, the amount of hydrogen as well as the reaction heat can be calculated, taking into account the reaction equation 2.12. The temperature dependent kinetic oxidation constant K is determined from experiments and usually given as an Arrhenius formulation of the form:

$$K = A \cdot \exp\left(-\frac{\Delta E}{RT}\right), \quad (2.14)$$

where T is the temperature in Kelvin, R the perfect gas constant in $J/(molK)$, A the rate factor and ΔE the activation energy.

The values of A and ΔE come from experimental correlations, for which ATHLET-CD leaves the user to choose between two correlations for the low temperature range:

- The Cathcart model with a temperature range of 1273 K to 1800 K and
- the Leistikow model with a temperature range of 1173 K to 1800 K ,

and two for the high temperature range:

- the Urbanic/Heidrick model with a temperature range of 1900 K to 2100 K and
- the Prater/Courtright model with a temperature range of 2600 K to 2673 K .

The Urbanic/Heidrick model can only be combined with the Cathcart model. Between the low and high temperature range, a so-called transition range is modeled by ATHLET-CD, where the values for the low and high temperature regimes are linked by interpolation. It should be noted that the ranges of validity given in the literature for the above correlations cover a larger range. Furthermore, ATHLET-CD extrapolates the correlations beyond the validity ranges given above.

From equation 2.13 and 2.14 it can be deduced that the reaction rate increases with temperature and decreases with oxide layer thickness (i.e. with duration of the oxidation process). The oxidation rate calculated by equation 2.13 can only be reached if sufficient steam is available. However, as steam is consumed and hydrogen is produced in the reaction, the so-called „steam starvation“ condition causes the oxidation reaction to cease. In ATHLET-CD, the reaction rate is progressively driven to zero below a limiting steam concentration (default value of 10 %).

2.5.2 Melting and melt relocation

The modeling in ATHLET-CD distinguishes between melting processes taking place at different temperature levels:

- Melting of absorber material, starting at 1073 K (default value for the AgInCd absorber material).
- Formation of metallic, Zr-rich melt due to melting of cladding material and partial dissolution of fuel (UO_2) by diffusive and convective processes, see Hofmann et al. [25] and Kim et al. [26]. The default value for the starting temperature of this process (parameter TAM) is 2250 K for Alpha-Zr (pre-oxidized cladding). In case of Beta-Zr (non-oxidized cladding), a value of 2033 K is recommended.

- Formation of oxidic melt composed of UO_2 and ZrO_2 . The default value for the starting temperature of this process (parameter TCOMPL) is 2600 K (recommended for ceramic mixtures with metallic inclusions). This recommendation results from Phébus experiments, where massive relocation of oxidic material has been observed well below the melting temperature of the UO_2 / ZrO_2 eutectic.

In ATHLET-CD it is assumed that melt is generated in-situ, kept in place by an outer oxide shell with higher melting temperature. Melt relocation is assumed to start when this shell fails. The failure criteria combine oxide layer thickness and temperature, i.e. failure is assumed when a certain threshold temperature is exceeded, whereby the threshold temperature is lower for smaller layer thicknesses [27].

Melt relocation is modeled as a candling process, assuming that melt flows downwards as rivulets along the outside of the cladding. The velocity of the melt is calculated from a simplified momentum balance for film flow. The melt exchanges heat with the cladding during the relocation to lower, colder locations. Re-freezing (crust formation) occurs when the melt temperature falls below the solidification temperature, which is by default 50 K lower than the melting temperatures TAM and TCOMPL. Crust may re-melt later, when the temperature exceeds the melting temperature, restarting the candling process. Details on the modeling of the candling process are given by Kronenberg [28].

2.5.3 Effect of blockages on thermal hydraulics and melt relocation

The geometrical changes induced by the core degradation processes influence the thermal-hydraulics as well as the interaction between rods. This includes effects like

- (partial) blocking of flow paths perpendicular and parallel to the rods due to ballooning or crust formation, which causes reduced cooling by the fluid (especially during reflooding) as well as reduced availability of steam for oxidation,
- opening of preferential flow paths through voided regions created by the failure of rods and
- melt accumulation on top of blockages (crusts), leading to sideways spreading and finally to molten pool formation.

Such effects caused by the geometrical changes are taken into account within ATHLET-CD only in a simplified, parametric manner. The porosity ϵ , i.e. the fraction of open flow area to total area, is taken as an indicator variable. For intact rod geometry and typical values of rod diameter and pitch, the porosity ϵ is about 56 %. In the ATHLET-CD input, several threshold values for the porosity are defined according to Table 2.2, which also shows the recommended values.

- For $\epsilon \geq POPEN$, no difference to the intact geometry is taken into account. This means that voided regions ($\epsilon \rightarrow 1$) are also treated like intact geometry.
- For $POPEN > \epsilon \geq PCLSR$ the flow perpendicular to the rods is successively reduced to zero by increasing the drag loss coefficient for radial flow.

- For $PCLSR > \epsilon \geq PCLSX$ the flow parallel to the rods is successively reduced to zero by increasing the drag loss coefficient for axial flow. Simultaneously, the heat transfer between rods and fluids is also driven to zero.
- For $PCLSX > \epsilon \geq PCONV$ the radiative heat transfer between rods is artificially increased. It is assumed that melt rivulets coalesce and start to form a molten pool. The increase of radiative heat exchange shall mimic the heat transport by convection, which leads to a temperature equilibrium between neighboring rods.
- For $PCONV > \epsilon \geq BLOCKG$ the relocation velocity for melt flowing into a mesh is successively reduced to zero. Then, the porosity cannot become smaller than BLOCKG. This prevents „overfilling“ of a mesh with melt and melt can dam up above a blockage. However, according to the model in Ecore, melt can only flow parallel to rods, so melt columns of different height in neighboring rods do not lead to transverse flow, as it should be expected.

Table 2.2: Porosity boundaries used in the blockage module

Porosity	Description
30 %	Lower limit for open porosity (POPEN)
27 %	Lower limit of porosity to limit radial flow (PCLSR)
25 %	Lower limit of porosity to limit axial flow and convective heat transfer to fluid (PCLSX)
20 %	Lower limit of porosity to increase radiative heat transfer (PCONV)
10 %	Lower limit of porosity to limit candling of melt (BLOCKG)

2.6 Behavior of melt in the lower plenum (AIDA)

ATHLET-CD does currently not contain models that predict the relocation of melt (timing and path) from the core region to the lower plenum. It is up to the code user to define a signal that initiates the transfer of melt to the lower plenum and initiates the AIDA module. The processes occurring during melt relocation to the lower plenum are not modeled either. The user therefore has to specify the expected configuration of corium in the lower plenum in the input. According to the ATHLET-CD description [27], three potential configurations are available:

1. homogeneous (oxidic) melt pool,
2. debris bed (oxidic melt pool with overlying particles) and
3. stratified melt pool (metallic melt layer on top of oxidic pool).

Option 1. is recommended and was actually the only option that worked without numerical problems in the simulations performed in the frame of the presented work.

2 The code system ATHLET-CD

The AIDA module describes the thermal behavior of melt in the lower plenum as well as the structural response of the vessel wall. The molten pool is described using a point model, assuming a homogeneous temperature inside the pool. Heat transfer from the molten pool to the surrounding crust is calculated based on correlations for turbulent natural convective heat transfer derived from experiments. These correlations give the average Nusselt number as a function of the Rayleigh number. In the presented work, the correlation of Mayinger et al. [29] has been applied for the heat transfer from the melt to the upper crust and the correlation of mini-ACOPO for the heat transfer from the melt to the lower crust in contact with the vessel.

For the heat transfer to the lower crust, the average heat flux is superposed with a shape function depending on the polar angle, which is adapted to experimental measurements. This yields a heat flux distribution, which is peaked at the upper edge of the pool.

The crust thickness is calculated from a quasi-steady heat balance, taking into account heat conduction through the crust and, optionally, heat transfer through a gap between crust and vessel wall, which is calculated as a combination of the heat conduction of superheated steam and thermal radiation.

For the heat transfer from the upper crust to an overlying water pool, three regimes are distinguished: film boiling, nucleate boiling and sub-cooled boiling. For the calculation of the temperature distribution inside the vessel wall, the transient heat conduction equation is solved by means of a linear finite difference method in 1D or 2D. The calculated temperature development in the vessel wall is used to estimate the creep damage and potential failure of the wall. Three different models are available in ATHLET-CD for this. In the present work the correlation, which approximates results from the detailed ASTOR code has been applied. Further details on the AIDA module can be found in the GRS technical report GRS-A-2933 [30]. The input data for AIDA used in the simulations presented in this work as well as the GCSM signals used by the AIDA module are displayed in appendices A1 and A2.

2.7 State of the code validation

The ATHLET-CD code system is developed by GRS for many decades now, and has constantly been improved and validated with new and extended models, developed on the basis of advanced experiments. It is beyond the scope of this work to give a full overview of the validation state of the ATHLET-CD code, but it shall be made clear that especially the core degradation module ECORE has been extensively validated in the past 20 years.

The Input Data Description for the ATHLET-CD code system [27] gives only rudimentary information on the validation state of the ECORE module, but there has been validation from GRS as well as other institutions, such as RUB-LEE and KIT. There are papers and reports available, describing the validation of the ATHLET-CD code system by means of the following experiments, descriptions based on Jacquemain et al. [15] and Buck [31].

CORA and QUENCH

Between 1987 and 1993 the CORA facility at KIT was the scene of 19 out-of-pile experiments investigating the early core degradation phase. Fuel bundles representing a PWR, BWR or WWER design were tested, using electrically heated fuel rods to simulate the decay heat. The bundles also contained non-heated fuel rods and control rods in case of the PWR design, while for the BWR design absorber blades and fuel channels were included. Among other goals, the tests at the CORA facility aimed at the investigation of the oxidation behavior of the materials in order to better assess the resulting hydrogen generation. Another point of interest was the formation of liquid phases not due to regular melting, but due to material interaction (eutectic melting) or chemical interactions. This included an assessment of the dissolving of uranium and zirconium oxides by liquid zircalloy as well as relocation of molten material and its freezing, which lead to the formation of blockages in the test bundle.

Reflooding of the degrading test bundle was performed as well, in order to observe the fragmentation of embrittled fuel rods and the resulting formation of a debris bed. This part is of special interest for the present work, because during the reflooding some tests showed a massive production of hydrogen. Since the temperatures reached in the CORA facility did not exceed $2273K$, mainly the early phase of core melting was observed with some interesting results.

It was observed for example that the zircalloy oxidation starts at a temperature of $1373K$ in the upper part of the bundle, thus accelerating the core heat-up, spreading from there to upper and lower core regions successively. A number of influence factors for the oxidation propagation have been identified, such as the availability of zircalloy surfaces and steam, as well as the temperature evolution and cooling conditions (e.g. reflooding conditions). Another result of the CORA tests was that the liquefaction of the present materials often starts at temperatures lower than their individual melting temperature, which is a phenomenon mainly due to eutectic interactions and dissolving processes. For further information, see Hoffmann et al. [32].

The QUENCH program is a direct successor of the CORA program and resembles it in many aspects. A key difference is that legal requirements prohibited the further use of uranium fuel pellets, thus forcing the scientists at KIT to use fuel rod simulators made from zirconium oxide. As in the CORA facility, the fuel simulator rods had not been irradiated previously and were subject to in-pile heating, creating temperatures of up to $2000 K$ in order to survey the cladding behavior up to its failure and degradation behavior of the fuel rod assembly. For further information, see Sepold et al. [33].

Validation of ATHLET-CD has been performed on the tests CORA-13 [34–37], CORA-17 [38], CORA-28 [39, 40] and CORA-33 [41], as well as CORA-W1 [42] and CORA-W2 [43–46]. QUENCH01 [47], QUENCH06 [48, 49], QUENCH-10 [50] and QUENCH-11 [51, 52] have been part of the ATHLET-CD validation as well.

LOFT-FP

The LOFT-FP test assembly consisted of 121 UO_2 fuel rods with nuclear heating creating temperatures of up to $2400 K$. Different test were conducted in order to record

fuel degradation up to the release of fission products. At the end of the tests, the test section was flooded with water. Opposing all other experimental facilities, the LOFT-FP facility included a model of the primary circuit, thus creating more realistic reflooding scenarios. For further information, see Jensen et al. [53] and Nalezny [54], for the ATHLET-CD validation see Bestele [55].

Phebus FP

The Phebus FP test assembly consisted of 21 pre-irradiated fuel rods that were subject to in-pile nuclear heating, creating temperatures of up to 3100 K. As in the LOFT-FP tests, the experimental goal was to record fuel degradation up to the release of fission products. One of the key differences to the LOFT experiments was the pre-irradiation of the fuel rods in order to generate a realistic distribution of fission products in the fuel rods. Three tests have been performed in a bundle configuration, and the tests were terminated later in the core degradation process, thus generating a lot of interesting data for the late phase of core degradation, while most of the other experiments were terminated after or during the early phase of core degradation. For further information, see Clément et al. [56] and Schwarz et al. [57].

Validation of ATHLET-CD has been performed on the tests Phebus FPT-0 [58–60], FPT-1 [61–63] and FPT-4 [64], as well as Phebus SFD B9+ [65, 66], SFD 1-1 [67, 68] and SFD 1-4 [69]. The Phebus SFD AIC Test [70] was part of the validation, too.

There have been other experiments for the validation of ATHLET-CD, such as CODEX AIT-1 [71], the Halden Experiments IFA650.2 [72] and IFA650.3 [72, 73], NRU-FLHT-2 [74] and TMI-2 [75].

The validation simulations focused on different aspects of the experiments, and included the core melt-down behavior, the general thermal behavior of the fuel rod bundles and the oxidation reaction of the zirconium, as well as fission product release and transport. Most results were promising and ATHLET-CD was judged as adequate in the simulation of severe accident phenomena. In an OECD benchmark exercise, different code systems were tested on the simulation of the TMI-2 accident scenario, including ATHLET-CD simulations performed by GRS, IKE and RUB-LEE. The results confirm the validity of the simulation tools, and especially thermo fluid dynamic properties like the break mass flow rate and primary water mass showed a high degree of synchronization.

During the progression of the accident, the diversity of the results increased, because in the late phase modeling the user influence increases due to more uncertainties in the models. The deviations started to become distinct with the beginning of melt relocation in the core, and increased throughout the following degradation phases. As far as the relocation to and behavior in the lower plenum is concerned, the results of the benchmark differed quite a lot.

The benchmark results show that the validation state of the ATHLET-CD simulation code is quite adequate concerning the early accident sequence, up to and including core heat-up. During the core melting phase, the codes start to diverge and the late

in-vessel phase dealing mostly with behavior in the lower plenum reveals that the models used need improving, especially where the dependency on the user input is concerned. For the conducted simulations the most recent and thus highly validated version of ATHLET-CD has been used, which is why there has not been any further validation conducted in this work.

3 About the nuclear power plant

3.1 ATHLET-CD model of the reactors thermo fluid dynamic systems

The simulated reactor is a generic German PWR (KONVOI type), which has four loops and produces 1300 MW_{el} of power. Its nodalisation scheme is shown in figure 3.1. Of the four loops, the ATHLET-CD code simulates only two, thus assuming that the three intact loops behave identical. Loop A (on the left) represents the three intact loops and has all its quantities simply multiplied by three, while loop B (on the right) represents the loop with the leak next to the PSL indicated by the X. For the purpose of the present investigations, i.e. the simulation of a severe accident with loss of the primary heat sink, it is sufficient to replace the simulation of further components of the secondary system by boundary conditions.

3.1.1 The primary system

The primary system is simulated in two separate loops, each of them consisting of the steam generator U-tubes, connected to the hot and cold legs by the steam generator inlet and outlet. The cold legs host the main coolant pumps, and the hot leg in the broken loop contains the leakage and the PSL to the pressurizer. Because the accident scenario simulated in this work involves a leak with rapid depressurization, it was not necessary to simulate the relief valve and relief tank, nor is the spray line at the top of the pressurizer simulated.

The cold legs are connected to the downcomer of the RPV, which lies parallel to the core channels and the reflector, all connected at the bottom by the volume of the lower plenum. On top of the core channels, the upper plenum is simulated, as well as the connection to the hot legs.

As shown in figure 3.2, the thermodynamic part of the core area is simulated as six concentric core rings, each represented as an identical pipe object with a different multiplication factor < 1 to account for the area fraction of the core each channel represents. The included table shows the distribution of the core area to the six core channels.

To allow horizontal flow in the core, the core channels are connected by so-called cross-connection objects (CCOs). They generate junctions between all the control volumes of the two parallel pipes, which must be identical in length, elevation and nodalisation to allow the use of a CCO.

3 About the nuclear power plant

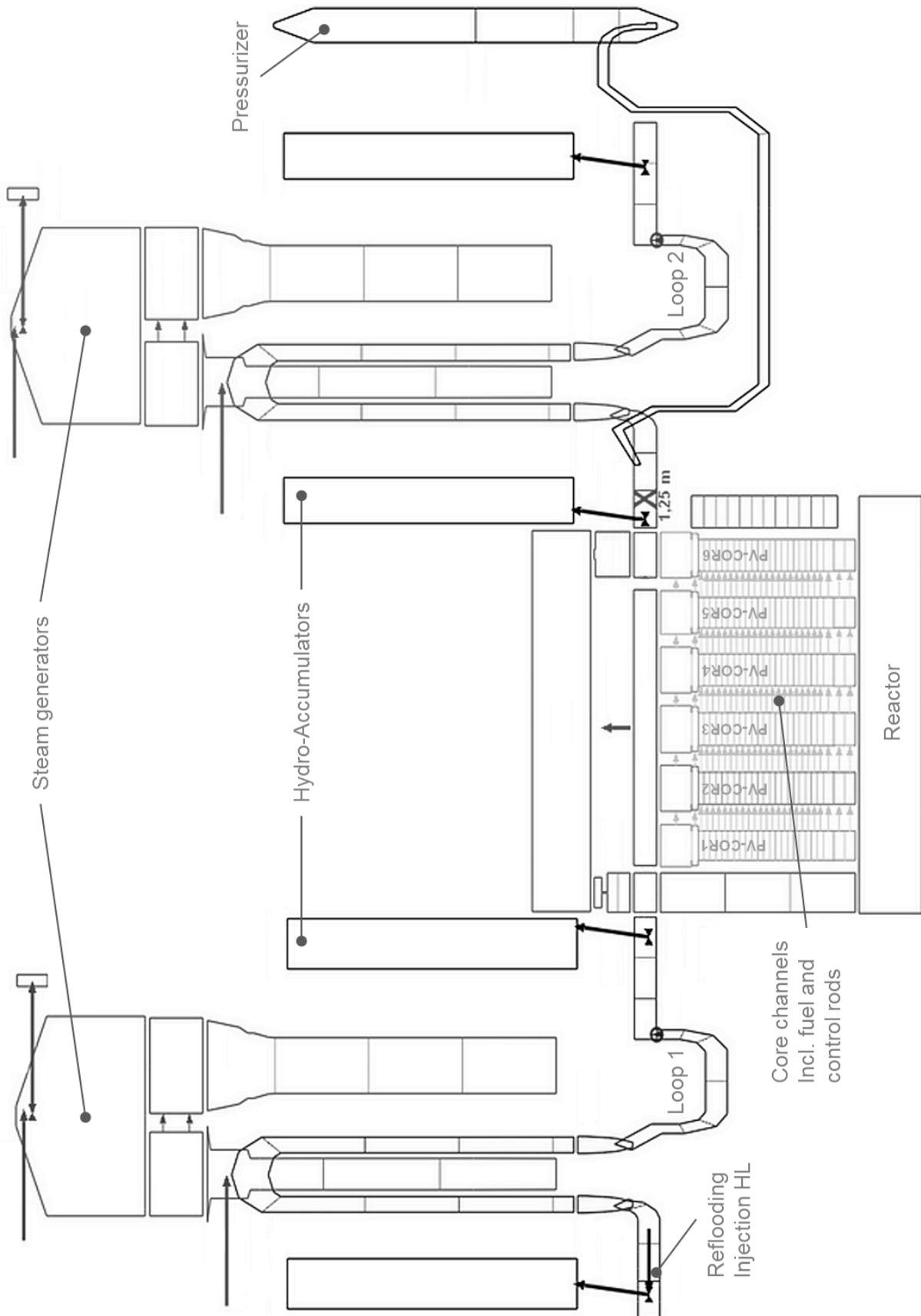


Figure 3.1: Graphical representation of the simulated reactor structure with an X indicating the location of the leak

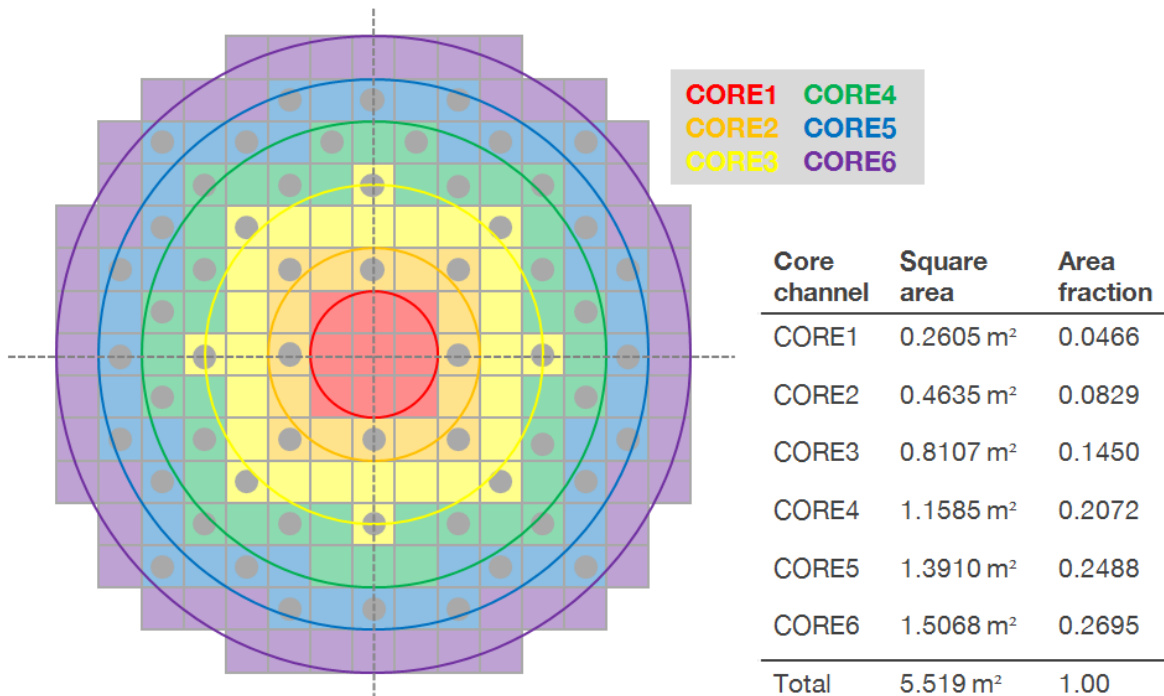


Figure 3.2: Graphical representation of the simulated core structure as six concentric core rings

3.1.2 Secondary systems

The secondary system contains only a representation of the steam generator secondary side, with a distinct representation of the riser and downcomer, containing a special water-steam-separator-object topped by the steam dome. A positive fill to the downcomer represents the feedwater injection and a negative fill in the steam dome represents the main steam line to the turbine. The steam dome also hosts a special object to account for the presence of a pressure relief valve. The turbine and the condensers are not simulated explicitly.

3.2 Emergency core cooling systems (ECCS)

The KONVOI-class PWRs have one passive and two active ECCSs in the primary loops. For every leg, there is a passive hydro-accumulator with a water volume of 45 m^3 , connected to the primary system by a check valve, opening below 2.6 MPa . The High and Low Pressure Injection (HPI / LPI) Pumps have to be supplied with electricity either via AC power or the emergency diesel generators. In the simulation, all (active and passive) injection systems are represented as fills, which are time-dependent boundary conditions specifying mass and enthalpy flow rates. They are connected to the primary loops by single junction pipes, in which the momentum balance is not calculated („massless pipe“). This way, the systems do not have to be modeled, and only their characteristics are fed into the simulation. For the high and low pressure injection pumps, their pump characteristics (see fig. 3.3) are given in tabular form.

3 About the nuclear power plant

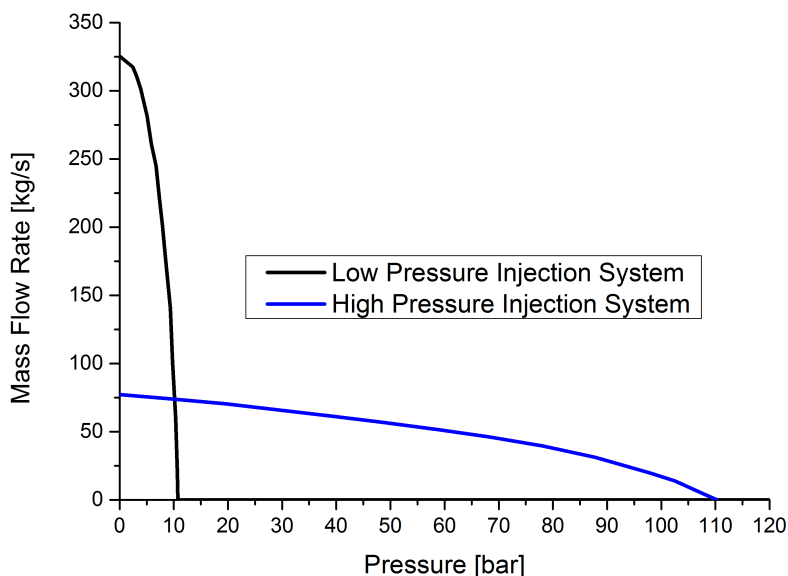


Figure 3.3: Pump characteristics of the low and high pressure injection pumps (HPI and LPI)

There is a pump dedicated to both HPI and LPI for each loop. Below 11 MPa, the HPI pumps can feed water either into the hot or cold legs of the loops with a maximum flow rate of 77 kg/s per pump. The LPI is connected to both hot and cold legs of each loop, and usually feeds 50%/50% into both legs simultaneously. It is possible, to close either of the connections to the hot or the cold legs, leading to an injection of 100% into the other legs. The LPI starts its injection below 1.1 MPa with a maximum flow rate of 325.4 kg/s per pump. Connected to the cold legs, the Extra Borating System (EBS) is modeled with a constant non-pressure dependent injection mass flow rate of 2 kg/s per pump. Since there is no specific information available on the Volume Control System (VCS), it was assumed to have a constant injection mass flow rate of 35 kg/s per pump.

3.2.1 Model parameters

All simulations presented in this work used the 5-equation model for the simulation of all the thermo fluid dynamic parts of the reactor core. Most of the simulated parts were treated as homogeneous, but in a few special objects a mixture level tracking was implemented, namely in the steam generators and core channels. The reason for this is that the position of the mixture level is crucial information within this area, whereas it is not so important in others e.g. in the piping system.

The only simulated non-condensable gas was hydrogen, because nitrogen and other gases were not judged as crucial for this kind of accident sequence. Nitrogen was only applied in the accumulators, which are topped by a nitrogen cushion, but the reactor protection system was assumed to close the accumulator check valves before any nitrogen could enter the primary system.

3.3 Properties of the reactor core

Since only the thermodynamic properties of the core are simulated by the ATHLET module itself, it is necessary to use the module Ecore for the simulation of all the properties of the fuel and absorber rods in the core, as well as their behavior during the accident. So for every core channel (CORE1 to CORE6), there is a corresponding radial core section (ROD1 to ROD6) defined in the input for the Ecore module, which specifies the number of fuel and control rods present. Table 3.1 shows the specifications used in the simulations. 57,900 fuel rods are simulated in total, as well as 2328 absorber rods. Assuming the standard 18x18 geometry for fuel elements in KONVOI type PWRs, this makes 324 rods per fuel elements (see right side of fig. 3.4). Of these 324 rods, 24 are left empty to take in the absorber rods, leaving 300 for fuel. So in total, the simulated core consists of 193 fuel elements, and 97 absorber rod assemblies.

Table 3.1: Simulation properties of the radial core sections in the Ecore module

Core channel	Fuel rods / elements	Absorber rods / assemblies	Radial power factor
ROD1	2,700 / 9	96 / 4	1.044
ROD2	4,800 / 16	576 / 24	1.0542
ROD3	8,400 / 28	480 / 20	1.0535
ROD4	12,000 / 40	960 / 40	1.0792
ROD5	14,400 / 48	192 / 8	1.032
ROD6	15,600 / 52	24 / 1	0.8565
Total	57,900 / 193	2,328 / 97	

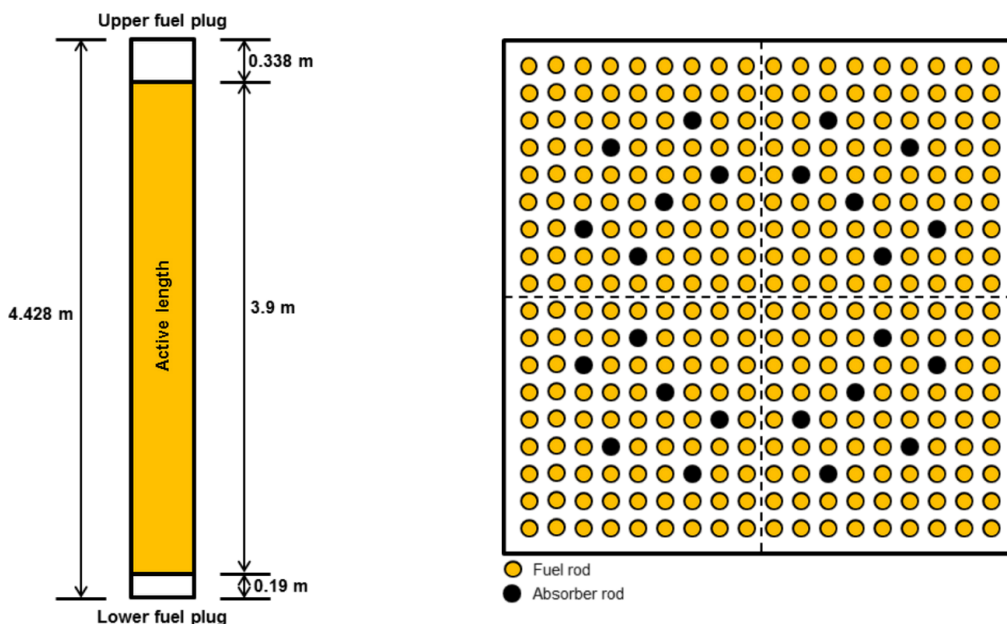


Figure 3.4: Structure of the simulated fuel rods (on the left) and schematic of the cross section of an 18x18-type fuel elements (on the right) [4]

3 About the nuclear power plant

The fuel rods are simulated as cylinders, consisting of UO_2 fuel pellets inside a Zircalloy cladding, which is modeled like α -Zr, and a small gap between pellets and cladding. Figure 3.4 shows the structure of a fuel rod on the left, which consists of an active fuel zone with a height of 3.9 m, which is edged by an upper and lower fuel plug of 0.338 m and 0.19 m height respectively.

The fuel rod is sub-divided into 22 nodes of which two represent the upper and lower fuel rod plugs. The 20 remaining nodes have the same height of 19.5 cm, as can be seen in figure 3.6. All the results and discussion in this work will refer to the nodes as described here. The elevation value refers to the lower boundary of the core area, meaning the position of the core support plate.

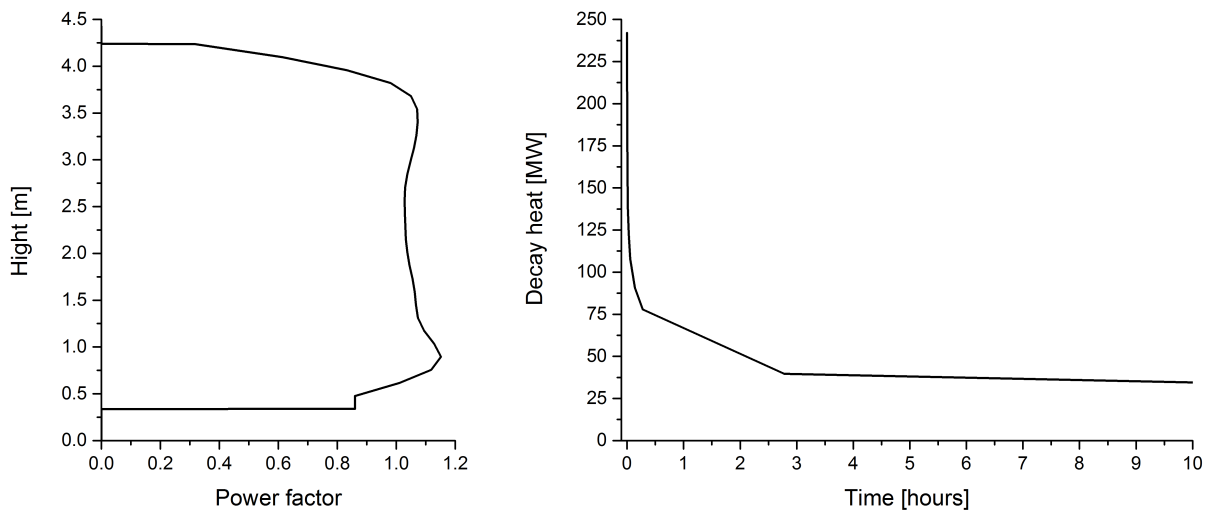


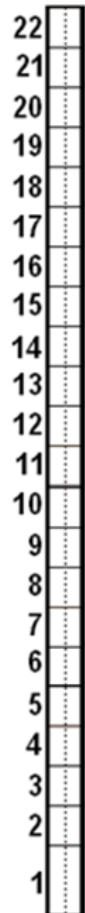
Figure 3.5: Axial power profile (on the left) and decay heat (on the right), both generated from the ATHLET-CD input tables with linear interpolation between the values

Figure 3.5 shows the axial power profile applied to the active zones of all the simulated rods uniformly, as well as the decay heat that is assumed to be produced by the reactor core after emergency shut-down. The decay heat is derived as percentage of the nominal (thermal) power of the core, which is 3.765 GW, and weighted with a radial power factor to account for a non-uniform radial power distribution caused by a low leakage core loading strategy (values given in tab. 3.1). This radial profile is also used in the steady state simulation of the reactor at nominal power.

3.3.1 Properties of the core materials

Figure 3.7 shows a cross section of a fuel rod, with the UO_2 pellet in orange, the Zircalloy cladding in grey and the gap in white. The center of a fuel rod represents one corner of the square fuel rod lattice, as can be seen on the right of figure 3.7.

The numbers 1 to 5 in figure 3.7 display the characteristic values of the fuel rod lattice, which are given in table 3.2. From these values, the gap width between fuel pellet and cladding can be derived to 0.085 mm, and the fluid cross section of one cell comes to 95.528 mm².



Node	Lower elevation	Height
22	4,95 m	0,19 m
21	4,755 m	0,195 m
20	4,56 m	0,195 m
19	4,365 m	0,195 m
18	4,17 m	0,195 m
17	3,975 m	0,195 m
16	3,78 m	0,195 m
15	3,585 m	0,195 m
14	3,39 m	0,195 m
13	3,195 m	0,195 m
12	3,00 m	0,195 m
11	2,805 m	0,195 m
10	2,61 m	0,195 m
9	2,415 m	0,195 m
8	2,22 m	0,195 m
7	2,025 m	0,195 m
6	1,83 m	0,195 m
5	1,635 m	0,195 m
4	1,44 m	0,195 m
3	1,245 m	0,195 m
2	1,05 m	0,195 m
1	0,712 m	0,338 m

Figure 3.6: Sub-division of the fuel rods (incl. upper and lower fuel rod plug) into 22 nodes

Table 3.2: Simulation properties of the fuel rod structure

Variable	Value
1 Radius of a fuel pellet	4.025 mm
2 Inner radius of cladding	4.11 mm
3 Fuel rod outer radius	4.75 mm
4 Minimum distance between fuel rods	3.4 mm
5 Distance between fuel rod centers	12.9 mm

3.3.2 Model parameters

An important part of a core melting accident is the oxidation of the zirconium present in the reactor core, because the chemical reaction produces hydrogen and is highly exothermic:



The oxidation model used for the cladding of the fuel rods and the absorber rods (Zircalloy, simulated like α -Zr) consists of four parts, depending of the temperature of the material as given in table 3.3.

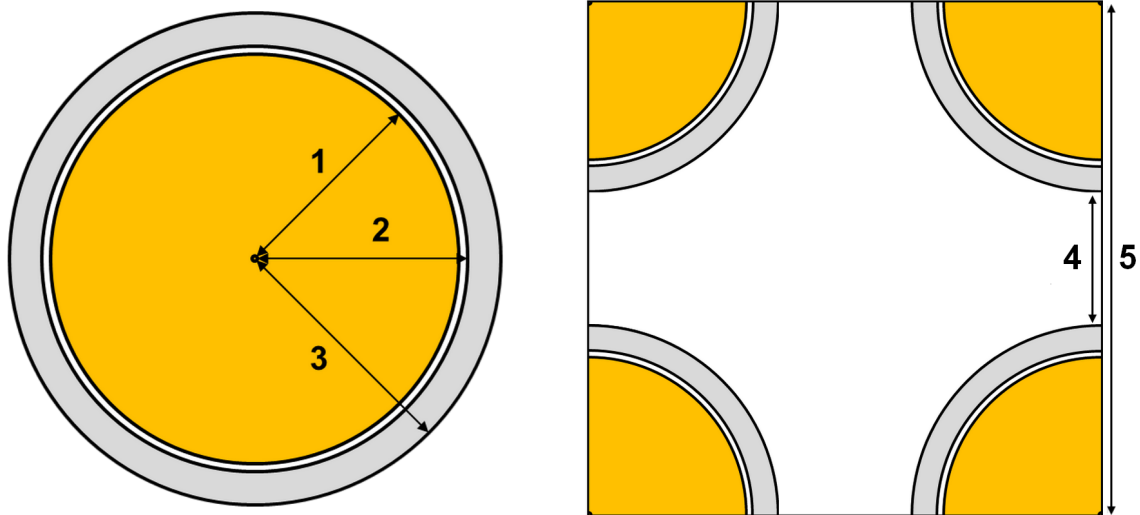


Figure 3.7: Cross section of a simulated fuel rod (on the left) and schematic of the smallest cell of the square fuel rod lattice (on the right)

Table 3.3: The four parts of the oxidation correlation

Part	Temperature range	Correlation
Part 1	1273 – 1800 K	Cathcart [76]
Part 2	1800 – 1900 K	Transition range
Part 3	1900 – 2100 K	Urbanic / Heidrick [77, 78] ¹
Part 4	2100 – 2700 K	Extrapolation range

Since the cladding is modeled like α -Zr, its melting temperature is set to 2250 K. The initial inner and outer cladding oxide layer thickness is assumed to be 6 μm .

For the simulation of the mechanical fuel rod behavior, an initial pressure of 3.2 MPa is set for the internal fuel rod pressure. The temperature of the fill gas is assumed to be 593 K at first, and the porosity of the UO_2 pellets is assumed to be 0.017. The fuel rods are simulated with a fuel rod plenum volume of $1 \cdot 10^{-5} \text{ m}^3$ each.

For the rod relocation model, table 3.4 gives an overview over the most important values assumed in the simulations.

For the absorber and control rods, table 3.5 shows the most important values given by the user via input. Since an encompassing description of the values for the ECORE module is beyond the scope of this chapter, the complete input used for the ECORE module can be found in appendix A3. The description of the parameters can be taken from the ATHLET-CD User's Manual [27].

¹against all evidence according to Schanz et al. [79]

Table 3.4: Overview of the most important values assumed in the simulation of rod relocation

Parameter	Value	Description
ILIQUI	1	Use of the Hofmann liquefaction model (KfK 4485, Jan. 1989)
IREMELT	1	Remelting of frozen material and blockage formation is simulated
DDTAL	$300 \cdot 10^{-6} \text{ m}$	Oxide layer thickness for the cladding failure criterion
TALLOW	$2.3 \cdot 10^3 \text{ K}$	Cladding failure temperature if oxide layer thickness is below DDTAL
DELTSL	50 K	Temperature difference for refreezing of the cladding material
IOXML	16	The crust oxidation correlation is the same as for the zirconium oxidation, see table 3.3
DHZRP	$22.5 \cdot 10^4 \text{ J/kg}$	Melt enthalpy of metallic Zr
ALAMSL	30 W/mK	Heat conductivity of the metallic crust
WSLMAX	0.06 m/s	Maximum candling velocity of the melt
DELSL	$1 \cdot 10^{-3} \text{ m}$	Film thickness of the metallic melt
TCOMPM	2600 K	Relocation or solidus temperature of UO_2
TCOMPL	2800 K	Pseudo temperature for UO_2 melting
DTSLUO	50 K	Temperature difference for refreezing of UO_2
DTACUO	30 K	Temperature difference for melt accumulation
DHZRO2	$2.25 \cdot 10^5 \text{ J/kg}$	Melt enthalpy of ZrO_2
DHUO	$1 \cdot 10^5 \text{ J/kg}$	Melt enthalpy of UO_2
ANYUO	$4 \cdot 10^{-3} \text{ m}^2/\text{s}$	Kinematic viscosity of the ceramic melt
ALAMUO	20 W/mK	Heat conductivity of the ceramic crust
WSLUO	0.03 m/s	Candling velocity of the UO_2 melt
DSLUIO	negative	The following equation is applied: $DSLUIO = \sqrt{\frac{3}{9.81} \cdot WSLUIO \cdot ANYUO}$

3.4 Use of the GCSM signals in the simulations

The CGSM part of the input deck used to conduct the presented simulation has a length of 1123 lines and consists of roughly 200 signals. It is understandably beyond the scope of this work, to describe all of them, or even show all the code.

But in order to explain how the signals have been interwoven in this input to generate a working reactor control system suitable to the investigated accident sequence, the emergency cooling preparation signal (ECPS) (in German „Notkühlvorbereitungssignal“ NKV) will be described. Appendix A4 shows the GCSM signals used for the implementation of the ECPS in the input.

The ECPS is labeled „CSIG09“ in the input, and has been given the signal type „OR“, in order to establish a logical OR link between the signals CSIG08, CSIG07 and CSIG06. The signals CSIG08, CSIG07 and CSIG06 represent a „two-out-of-three“ logic, where

3 About the nuclear power plant

Table 3.5: Overview of the most important values assumed in the simulation of absorber and control rod behavior

Parameter	Value	Description
NCRTOT	2328	Total number of control rods in the core
IWWER	0	Ag/In/Cd is used as control rod material
IWLCR	3	Radial and axial radiation is simulated as well as axial heat conduction
CRSTAB	$6.16 \cdot 10^{-3} m$	Outer radius of the control rod guide tube
CRHU	$5.55 \cdot 10^{-3} m$	Inner radius of the control rod guide tube
CRBA	$4.65 \cdot 10^{-3} m$	Outer radius of the control rod cladding
CRBIC	$4 \cdot 10^{-3} m$	Radius of the absorber material
CRHAC	$500 W/m^2 \cdot K$	Heat transfer coefficient between control rod and guide tube
CRTAM	$1073 K$	Melt temperature of the absorber material
ICROXM	16	The same oxidation correlation is used as for the zirconium oxidation, see table 3.3
CROXID	$6 \mu m$	Initial guide tube outer oxide layer thickness
CROXII	$6 \mu m$	Initial guide tube inner oxide layer thickness
CRTVER	$1523 K$	Failure temperature of the control rod and guide tube
CRDTSL	$50 K$	Temperature difference for relocation / refreezing
DHAIC	$9.56 \cdot 10^4 J/kg$	Melt enthalpy of absorber material
ALAMCR	$50 W/mK$	Heat conductivity of crust
CRWSL	$0.03 m/s$	Candling velocity of control rod melt
CRDELS	$1 \cdot 10^{-3} m$	Film thickness of the control rod melt

in each case two of the following signals lead to the activation of one of the aforementioned signals, resulting in the activation of the ECPS:

- CSIG08: CSIG02 AND CSIG03 (pressurizer level and containment pressure difference)
- CSIG07: CSIG01 AND CSIG03 (primary pressure and containment pressure difference)
- CSIG06: CSIG01 AND CSIG02 (primary pressure and pressurizer level)

with

- CSIG03: Pressure difference of the containment atmosphere to its nominal value is greater than $3 kPa$
- CSIG02: Pressurizer level below $2.28 m$
- CSIG01: Primary pressure below $11 MPa$

For the simulation of signal CSIG03 (containment pressure difference), the pressure control in the containment is turned on when the break in the hot leg occurs, using

3.4 Use of the GCSM signals in the simulations

signal NODELAY, which is then fed into the signal SPCONTAIN, which generates a function for the containment pressure, using values specified in table PCONTAIN.

For the simulation of CSIG02 (pressurizer level), the signal PSIG03 is compared to the given value of 2.28 m , while PSIG03 is the observation variable „water level in the pressurizer“.

CSIG01 works just like CSIG02, using the observation variable PSIG02 „pressure in the RPV upper plenum“, and comparing the variable to the given value of 11 MPa .

All the observation variables used in the simulations are shown in appendix A5. In ATHLET-CD they are called „process signals“, and simply measure the value of a certain variable called „VARTYPE“ at a certain location of the simulated reactor called „OBJECTNAME“.

4 The reference case

Since the primary research goal was to investigate the reflooding of a partially degraded PWR core, a scenario had to be chosen that would lead to a core meltdown, which could be achieved within reasonable simulation and computation times while covering all the relevant phenomena. In order to get a core meltdown, the water inventory has to be decimated, so it was obvious to choose a LOCA. The German risk study phase B [12] differentiates LOCAs into three categories, depending on the size of the leak:

- The large leak with a size from 500 cm^2 to the well-known double ended guillotine break (2F) with about $10,000 \text{ cm}^2$,
- the small leak with a size smaller than 25 cm^2 and
- the mid-sized leak in between.

The small sized leak does not give the reactor much trouble at first, because the water loss is slow and could easily be replaced without the core ever getting uncovered, even though the system would have to be vented regularly in order to dissipate the decay heat. If a total station blackout was assumed additionally, the core would eventually uncover and melt, but it would take a high amount of simulation time to get there, which was undesirable for performing several case studies. Also, researchers from HZDR (Helmholtz-Zentrum Dresden-Rossendorf) have already conducted simulations covering the SBLOCA scenario [80]. In case of a large break, the pressure in the primary system decreases rapidly below the response pressure of the LPI, which will fill the RPV before the core temperatures rise above $1000 \text{ }^\circ\text{C}$. Both the small and the large break scenarios were judged as controllable, quite contrary to the mid-sized leaks.

The trouble with mid-sized leaks is that the water loss is high enough to uncover the core, but the pressure decreases too slowly thus preventing an early start of the LPI. In the German risk study phase B [12] the leaks with sizes from 40 cm^2 to 380 cm^2 were judged as not controllable with the implemented measures of the core cooling systems and lead to a core melting accident. Thus, a mid-sized loss-of-coolant-accident (MBLOCA) was chosen as basic scenario.

4.1 The MBLOCA accident scenario

The initiating event is the opening of a medium sized leak of 200 cm^2 in the hot leg near the PSL. The location of the leak was chosen contrary to the German risk study

4 The reference case

phase B [12], because of two reasons: First, the inventory of the pressurizer can now be assumed to empty directly into the leak thus not contributing to the water inventory of the RPV during the accident. Second, the pressurizer is equipped with a spray line at its top that could be used to inject water into the primary system. With the chosen leak location, this possibility ceases to exist, accelerating the evolution of the core melting and leaving the operator with less reflooding options.

The accident evolution described in the following is summarized in table 4.1. Notice that the simulations include an initial calculation period at steady state conditions in order to have a well defined plant state at the time of the accident initiation at 1000 s, when the leak opens in the simulation.

The functionality of the high and low pressure emergency core cooling systems is assumed to be intact at first, as well as the injection of four out of eight hydro-accumulators. When the inventory of the flooding pool has been drained by the ECCS, a switch to sump circulation mode has to be performed in order to ensure a continuous core cooling. For the simulation, this switch is assumed to fail, causing the LPI to fail and leaving the reactor without further water injection into the primary system.

The failure of the LPI thus marks the switch from the design basis accident to a beyond design basis accident, because without continuous water supply, the core inventory will evaporate due to the decay heat, causing the core to dry out and melt. The underlying assumption here is that no other form of water injection can be established manually.

For the secondary side it is assumed that the turbine is isolated and that the secondary water injection into the steam generators fails as well, leaving the reactor without ultimate heat sink. These assumptions have been made, because they accelerate the core melting process resulting in shorter simulation times.

4.1.1 Thermal-hydraulic behavior during the accident evolution

The opening of the leak results in an immediate reactor shut-down, so that only the decay heat and the heat generated by chemical reactions have to be removed from the core. The leakage leads to a massive loss of coolant, which again causes a significant pressure drop in the primary system.

Figure 4.1 shows a graphical representation of four key values of the simulation in a standardized form, which will be used throughout this work. The ordinates on the left show the system pressure in dark green with a range from 0 to 17.5 MPa and the void fraction near the leak in light green with a range from 0.0 to 1.0. The ordinates on the right show the summarized injection mass flow rate in light blue with a range from 0 to 1400 kg/s and the leak mass flow rate in dark blue with the same range of values. The abscissa gives the simulation time in a certain interval, showing only the interesting parts of the simulation for the sake of clarity. This means that in the following only the early phase of the MBLOCA accident evolution will be discussed, which is the

Table 4.1: Important points of the MBLOCA accident progression

Event	Time
Break opening	1000 s
SCRAM	1006 s
HPI ON	1009 s
Start of accumulator injection	1598 s
LPI ON	1810 s
HPI OFF	1821 s
LPI failure	3852 s
Start of core uncovering	4157 s
Start of zirconium oxidation (AMIZO)	6410 s
Start of core melting (AMISUL)	6951 s
First sign of ballooning	7020 s
First occurrence of molten fuel (AMIUOL)	7436 s
First occurrence of metallic melt (AMIMRL)	7436 s
Start of candling	7526 s
Formation of a lower crust in the upper core region	7706 s
Failure of the crust	7928 s
First occurrence of ceramic melt (AMIKRL)	8201 s
First rod failure (ROD3)	8210 s
Start of melt relocation to lower plenum	8462 s
Complete core uncovering	9669 s
RPV failure in Node 12 (DAMAGE)	21740 s

same for all conducted simulations up to the point of reflooding. When the reflooding simulations are discussed in the following chapters, only the behavior after reflooding will be discussed, since the behavior before reflooding is the same as in the BaseCase simulation discussed here.

The early phase of the MBLOCA accident evolution with its characteristic points can be seen splendidly in figure 4.1. When the leak opens at 1000 *s*, the pressure drops significantly, and the leak and injection mass flow rates show high peaks. The peak in the injection rate is due to the emptying of the pressurizer inventory through the surge line (SURGE), while the HPI starts after 9 *s* and increases in injection rate because of the continuing pressure decrease. Nevertheless, the void fraction in the hot leg increases to about 90 % during HPI injection and starts to decrease just when four of the eight accumulators open at 1598 *s* and release their inventory of 180 *m*³ (4 x 45 *m*³) into the primary loops. At 1810 *s* the LPI is started, which leads to high peaks in the injection rate and to a correspondingly rising leak mass flow rate. The fluctuations stabilize at around 2500 *s*, and injection and leak mass flow rates remain the same level, until the flooding pool is empty because the switch to sump circulation failed at 3852 *s*, according to the assumption in the accident scenario. After the failure, the leak mass flow rate decreases as well, and the void rises subsequently until it reaches 100 % at around 5000 *s* and only steam leaves the system.

Figure 4.2 shows the injection mass flow rate broken down to the different injection systems. After the leak opening, first of all the pressurizer injects its inventory into the

4 The reference case

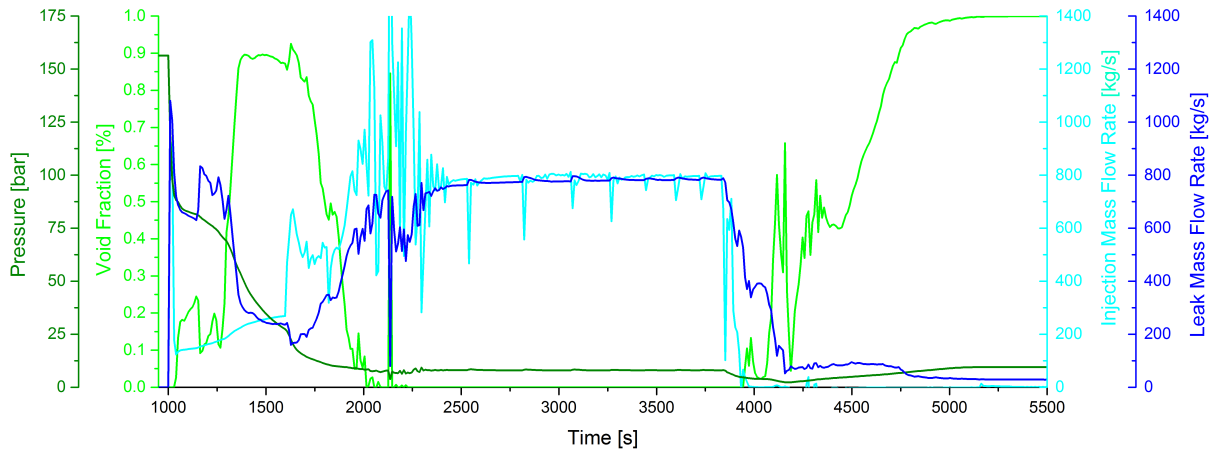


Figure 4.1: MBLOCA: Comparison of pressure and void fraction near the leak with the injection and leak mass flow rates during the early accident phase

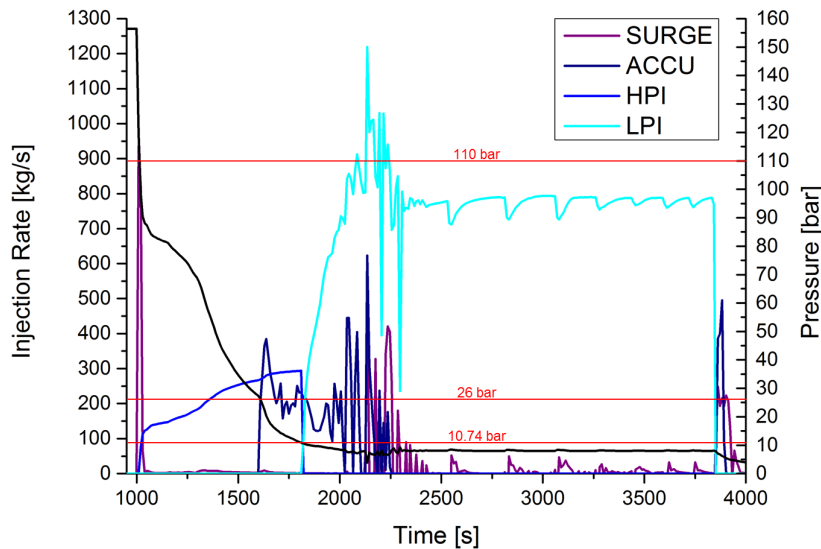


Figure 4.2: MBLOCA: System pressure and injection rates of the pressurizer, accumulators as well as high and low pressure injection systems. Legend: SURGE - Injection of the pressurizer, ACCU - Injection of the accumulators, HPI - Injection of the high pressure injection system, LPI - Injection of the low pressure injection system

primary system (SURGE). When the pressure drops below 11 MPa after 9 s , the HPI starts automatically and injects water into the three intact hot legs and the cold leg of the broken loop. The hydro-accumulator check valves open below a system pressure of 2.6 MPa , which is reached 598 s after the leak opening, because the injection rate of the HPI is not sufficient to overfeed the leakage. After 810 s and below 1.07 MPa , the LPI is started, which then cools the core by injecting water into both the hot and the cold legs. These three points in the accident sequence can be clearly identified in the evolution of the system pressure, as shown in figure 4.2. Through comparison to the water level evolution in the pressurizer, it can be determined that the LPI fills

the primary loops up to a height of about 2 m over hot leg level (3 m of water in the pressurizer).

Since a regularly working LPI would be sufficient to cool the reactor core constantly, it is assumed that the LPI fails as soon as the inventory of the flooding pool is drained (3852 s). At this time, a switch to sump circulation would be necessary, which is assumed to fail without an operator noticing. So from this time, there is no more water injection into the primary system.

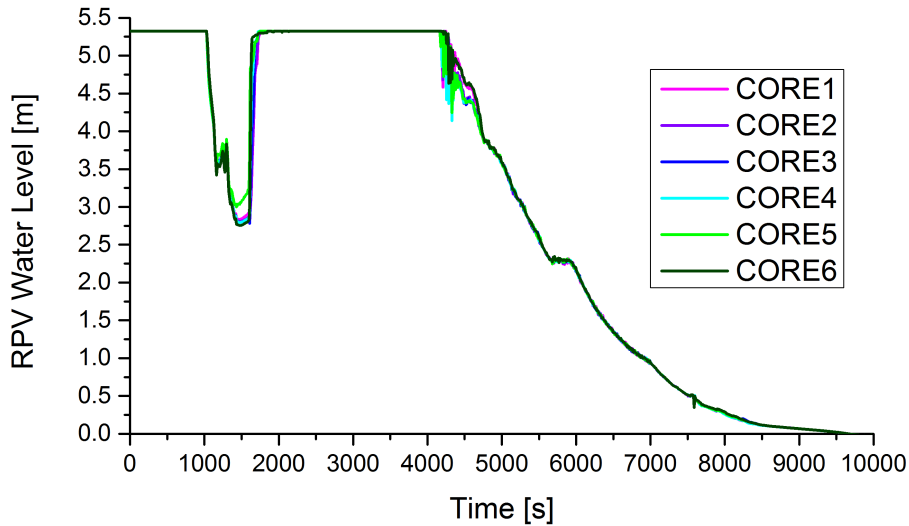


Figure 4.3: Water level evolution in the six core channels named CORE1 (innermost core channel) to CORE6 (outermost core channel)

The evolution of the collapsed water levels in the six concentric core rings can be seen in figure 4.3. The 0.0 m mark on the *RPV Water Level*-scale corresponds to the lower end of the active fuel rod zone. Around 1500 s the upper third of the active fuel rod zone is uncovered for a short time, before the LPI starts and fills the primary system way above core level. Since the LPI is assumed to fail at 3852 s , the water in the system evaporates successively and the final core uncovering begins at 4157 s . It has to be noted that figure 4.3 shows the collapsed water levels. Their height is evaluated by summarizing the water present in all nodes, and pretending that there are no boiling or other effects disturbing the surface of the water layer. In reality of course, there is no water surface since boiling and steam flow effects lead to a turbulent mixing.

4.1.2 Accident evolution in the core

From figure 4.4 can be seen that the core temperatures start rising at 6000 s and reach values of more than $2000\text{ }^{\circ}\text{C}$ roughly 20 min later. This is especially true for the temperatures of fuel (TB) and fuel rod cladding (TC), as well as for the vapor temperature (TV). The liquid temperature (TL) remains low, simply because there is no more water present in the core area at the time. The absorber rod temperature (CRTA) shows two distinct peaks due to material relocation from the node, before it rises to more than $2000\text{ }^{\circ}\text{C}$ as well, while the temperature of the absorber rod cladding (CRTC) follows the temperature of the fuel rod cladding (TC).

4 The reference case

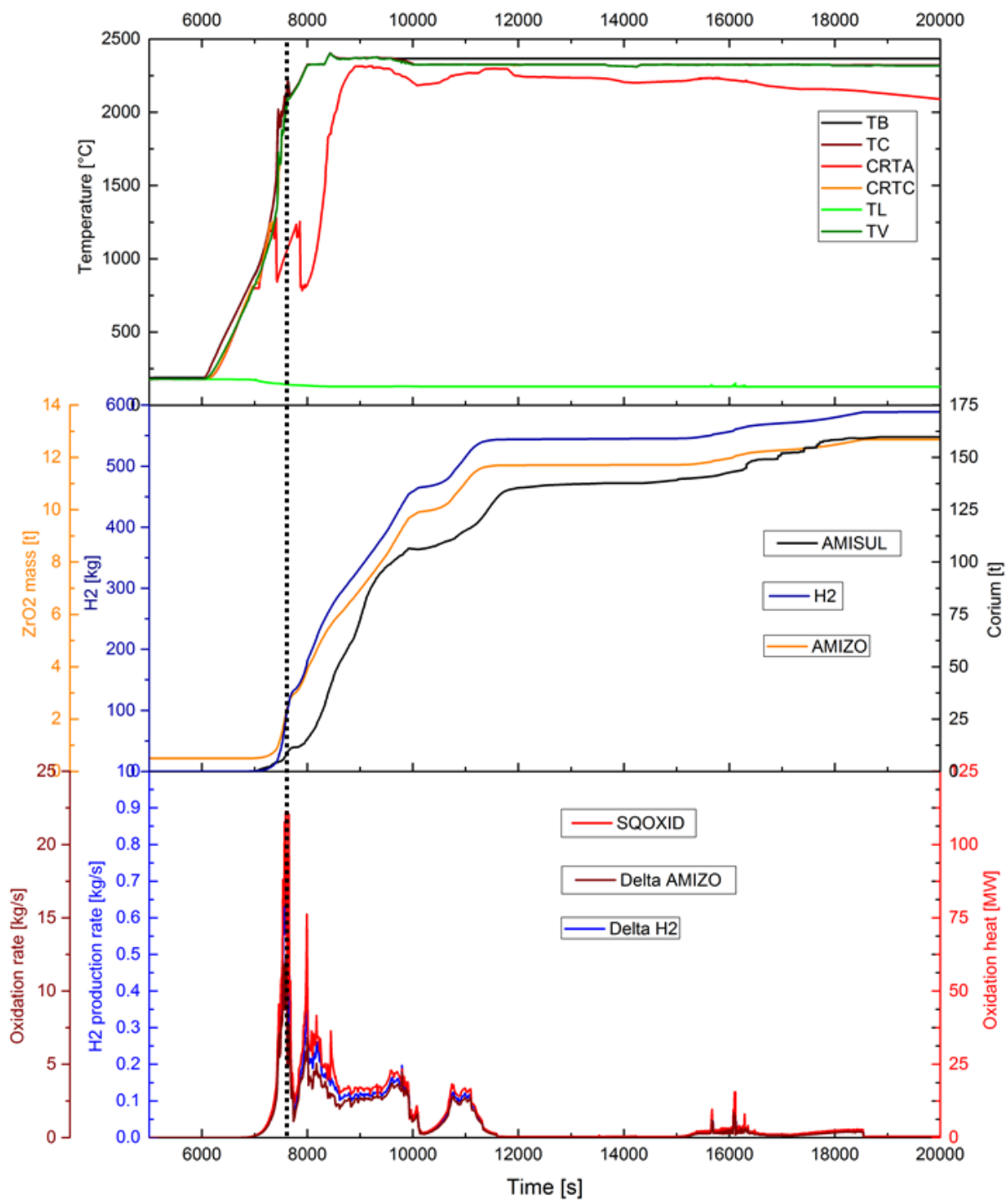


Figure 4.4: Top: Highest material temperatures in the core (TB - Fuel temperature, TC - Cladding temperature, CRTA - Temperature of the absorber rod material, CRTC - Temperature of the absorber rod cladding, TL - Liquid temperature, TV - Vapor temperature), middle: ZrO_2 mass (AMIZO), Hydrogen mass (H2) and mass of molten corium (AMISUL), bottom: Comparison of Zirconium oxidation rate (Delta AMIZO), hydrogen production rate (Delta H2) and the heat released by oxidation (SQOXID)

From 6410 s the amount of Zirconium oxide in the core starts to increase slowly, even though the cladding temperatures are still way below 1273 K. This might be due to the ATHLET-CD code extrapolating the Zirconium oxidation rate to temperatures below the Cathcart interval from table 3.3, but no corresponding information could be found in the manuals. From about 7200 s the amount of Zirconium oxide present in the core changes faster, reaching its peak oxidation rate of 12.5 kg/s at 7596 s. The oxidation rate drops to zero at 18550 s, when 40.05 % of the Zirconium have been oxidized. The zirconium oxidation results in a massive heat release with a peak value of more than 100 MW within 10 seconds, and the oxidation rate correlates with the hydrogen production curve and of course the heat release curve, which explains the observed temperature rise in the core. With the start of the zirconium oxidation the amount of zirconium oxide rises as well as the amount of molten core material, because the heat released by the oxidation is added to the decay and structural heat at that time.

Since the control rods consist of an alloy made from Indium, Cadmium and Silver, they show a low melting point of about 1073K, as given by the ATHLET-CD Users Manual [27]. Due to insufficient cooling, the temperature continues to rise, and reaches the melting temperature of the cladding (2030 K) at 7425 s in ROD1 Node 19. Only 20 s later the eutectic interaction between ZrO_2 and UO_2 leads to an early start of fuel melting.

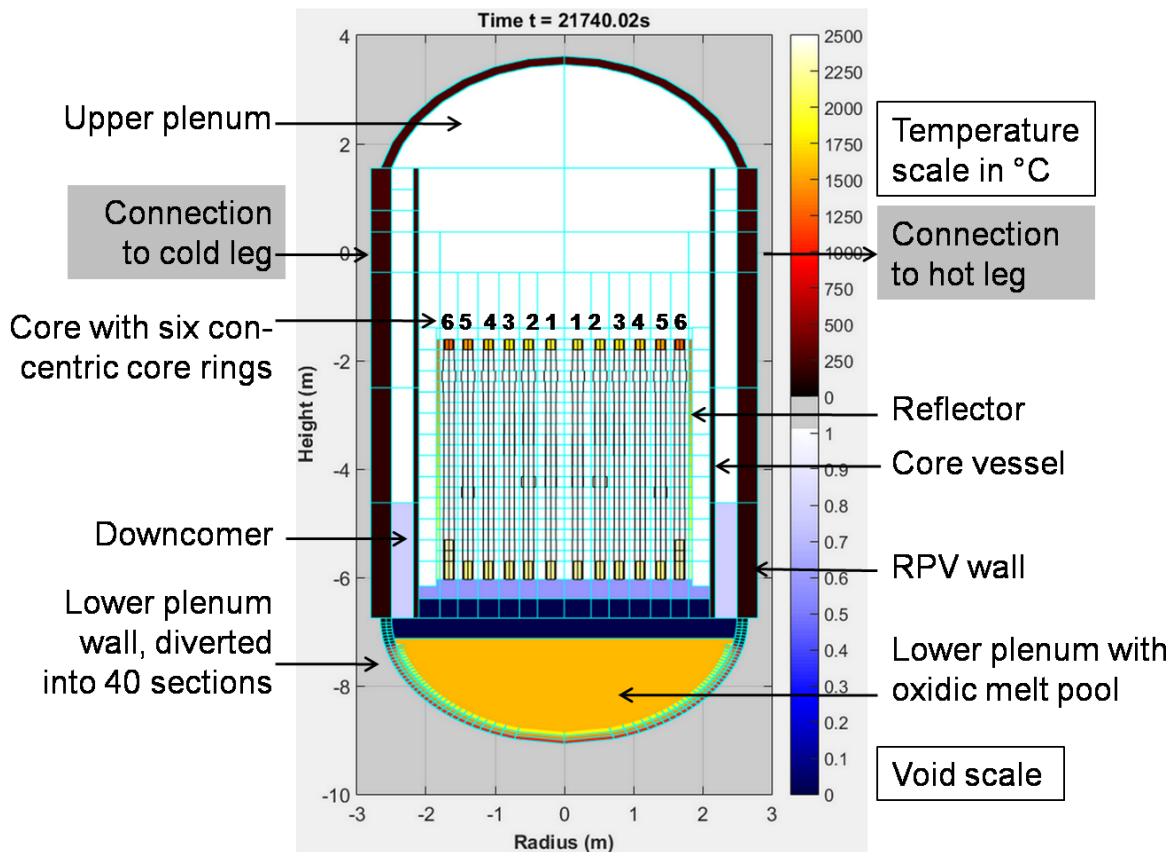


Figure 4.5: Core status when the RPV fails at 21740 s in Node 12

4.1.3 Accident evolution in the lower plenum

The ATHLET-CD code system has no model to predict when relocation of molten core material to the lower plenum starts. It is up to the user to provide adequate criteria. Here, it was decided that relocation by AIDA should be activated as soon as ceramic melt has been produced in the core area (ECORE). This is the case at 8462 s in the MBLOCA simulations and the lower plenum module AIDA is activated at that time. The activation of AIDA leads to an immediate relocation of 21.226 t of molten core materials from the core area (modeled by the Ecore module) to the lower plenum (modeled by the AIDA module). The ongoing core melting and the continuous relocation to the lower plenum lead in the end to a relocation of nearly the whole core inventory (about 156 t) to the lower plenum. Without mitigation measures the process of core melt-down takes about 5.7 hours from the opening of the leak, until at 21740 s the RPV failure is predicted according to the ASTOR failure criterion, which was chosen via input. Figure 4.5 displays the core status at the time AIDA predicts the RPV failure. Please note that ATHLET-CD simulates only half the of the RPV structures shown in figure 4.5, but it was decided to mirror the simulated half in order to generate a better picture of the RPV.

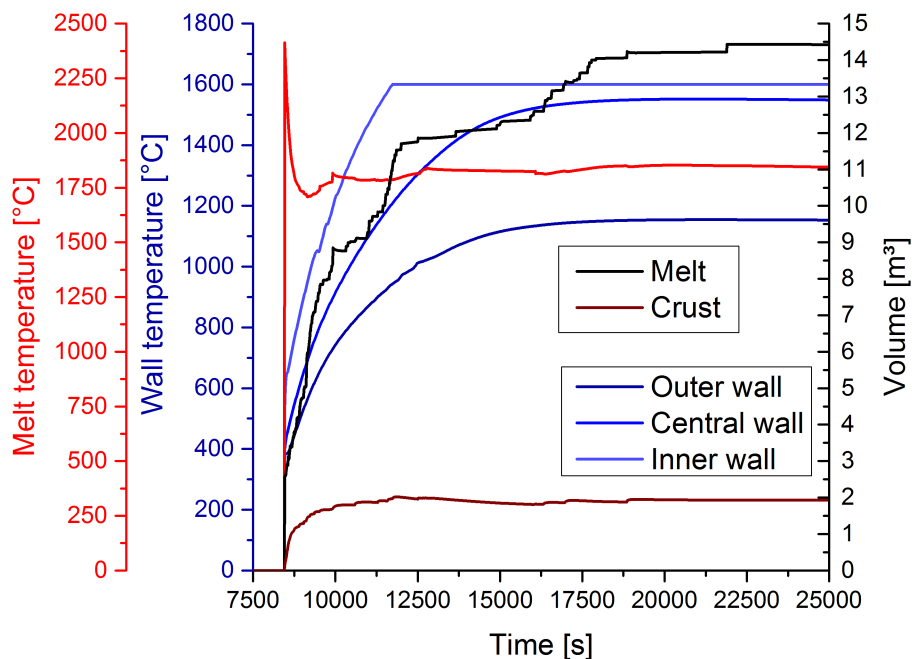


Figure 4.6: MBLOCA: Wall and melt temperatures in the lower plenum, as well as the relocated melt and crust volume

This kind of representation of the RPV and core status can be found throughout this work. The light blue lines mark the borders of the different objects and nodes that have been simulated inside the RPV. There are two types of objects on display, characterized by two scales, which are shown on the right. Solid objects like the vessel wall and the fuel rods are characterized by temperature using the upper scale with values from 0 (black) to 2500 °C (yellow). All other objects containing fluids are characterized by the void fraction using the lower scale with values from 0 (dark blue) to 1 (white). As a

reference point for geodetic height, the elevation of 0.0 m was set to the middle of the hot and cold legs where they are connected to the RPV.

Figure 4.6 shows the temperature development in the lower plenum wall, broken down into three lines showing the different temperature evolutions of the outer and inner wall of the RPV as well as in the central wall area. For comparison the melt temperature in the lower plenum is shown as well (please note the different intervals on the ordinates), and in addition the volumes of melt and crust in the lower plenum are displayed. It can be seen that the inner and central vessel wall reach a temperature of 1500 – 1600 °C before the RPV fails. The outer vessel wall temperature does not exceed 1100 °C, which means that the RPV wall does not completely melt but will fail by creep rupture.

At the time of RPV failure, there are about 14.5 m³ of melt with a temperature of more than 1800 °C present in the lower plenum, and an additional volume of 2 m³ of crust enclosing the melt pool. Unfortunately, AIDA gives the volume of the melt instead of its weight, while ECORE does the opposite. When the RPV failure occurs at 21740 s in Node 12 of 40, the AIDA module stops and so should the simulation as a whole. But since the AIDA module does not predict the RPV failure reliably, the simulation is continued as if the RPV was still intact in order to observe the progress of the accident scenario in case the RPV failure had not occurred yet.

5 Reflooding

The main question to be answered in this work was the question whether or not a partially degraded PWR core can be saved by some form of water injection into the primary system, when the process of core melting has already begun. Therefore, a core melting accident scenario was created, which was done by assuming an MBLOCA scenario and a failure of the LPI as soon as the flooding pool is empty.

For the simulation of this so-called „reflooding“, it was assumed that the operator notices the failure of the LPI at some point and manages to re-establish some form of water injection, e.g. from fire pumps or existing injection systems like the ECCS, manually.

5.1 Implementation of the reflooding injection in the simulation model

To simulate the reflooding injection of the HPI and LPI systems, both are characterized by a table giving the mass flow rate depending on the system pressure for one pump respectively. From those tables, a GCSM function generator (FUNGEN) generates a mass flow signal taking into account the current pressure in the primary system. To activate the injection, a set signal has to be given. Two of those set signals had to be implemented, one for the automatic injection after SCRAM (emergency shut-down protocol of the reactor), and one for the reflooding injection. An OR function combines these two set signals into one to activate the LPI or the HPI system respectively. This process is shown exemplarily in figure 5.1, with emphasis on the fact that both the LPI and HPI system consists of four identical pumps.

In order to assess all possible reflooding options, both the LPI and the HPI system were equipped with a potential reflooding start signal. In addition, a system of hypothetical middle pressure pumps (MPI) was implemented. Reason for this and the characteristics of the system will be explained in section 5.4.2. The actual GCSM signals implemented in the input can be found in appendix A6, while the signal type description can be looked up in the ATHLET User's Manual [24].

5.2 Assumptions and boundary conditions

Since the LPI was assumed to fail as soon as the flooding pool is empty in order to generate a core melting sequence, the obvious assumption for a reflooding was to

5 Reflooding

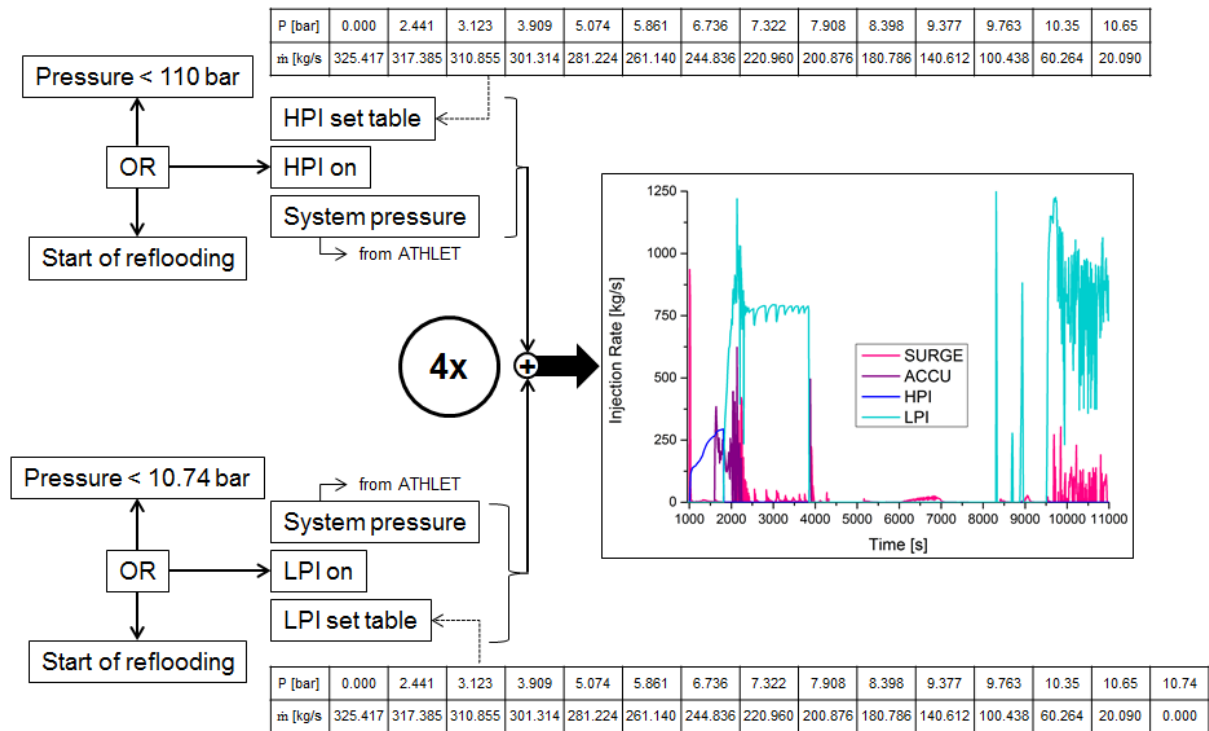


Figure 5.1: Schematic of the reflooding implementation, linked to the usual ECCS representation

re-establish the sump circulation. Since the ATHLET-CD simulations do not include the containment or any characteristics of the systems environment, the water had to be subjected to boundary conditions, like a constant temperature of $40\text{ }^{\circ}\text{C}$. No heat-up due to the waters circulation could be simulated, and the environmental pressure was set to a constant value of 0.1 MPa .

5.3 Reflooding configurations

Depending on the location of the injection, different reflooding configurations are created in the core, which can be seen in figures 5.2 and 5.3.

If the reflooding injection is located in the cold legs of the primary system, the injected water flows through the downcomer to the lower plenum of the RPV and is then divided into the six core channels, flooding them from below. When the water is evaporated in the core area, the created steam rises to the upper core area and either circles through the hot legs (intact loops) or leaves the system through the leak. This is the so-called „bottom flooding condition“, where water and steam flow into the same direction. A conceptual picture can be seen in figure 5.2.

If the reflooding injection is located in the hot legs instead, the water reaches the top of the core first where part of it continues to quench the core from the top in the so-called „top flooding condition“. The other part drains through the reflector bypass into the lower plenum and quenches the core from below. Injection into the

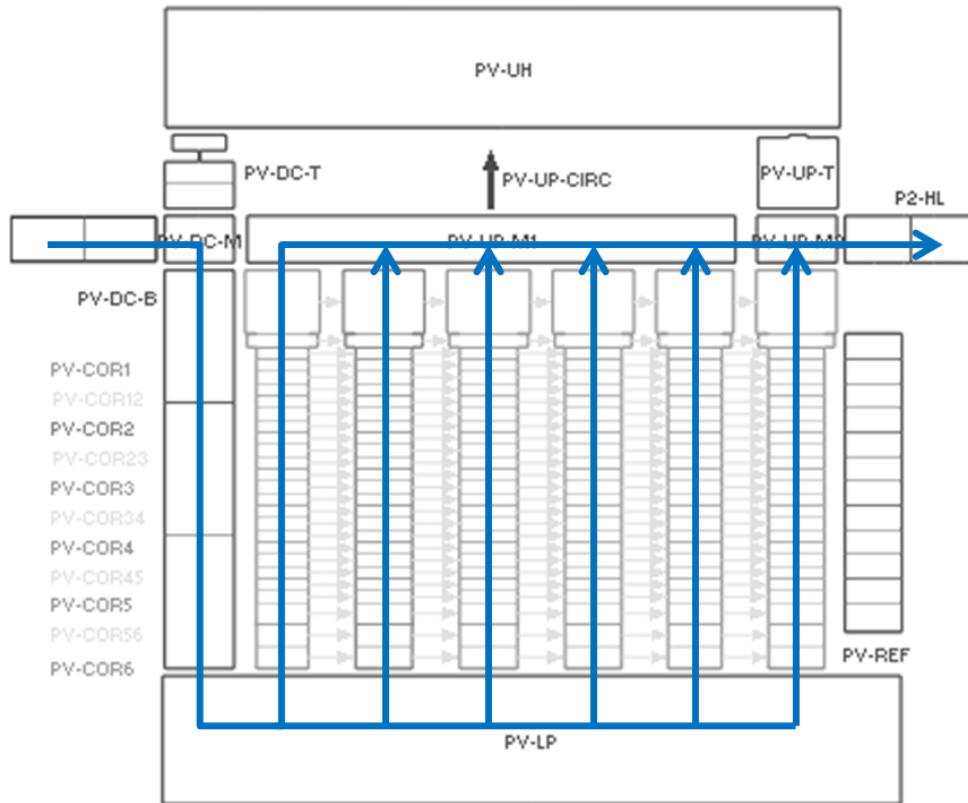


Figure 5.2: Flow paths of the water injected into the cold legs of the primary system

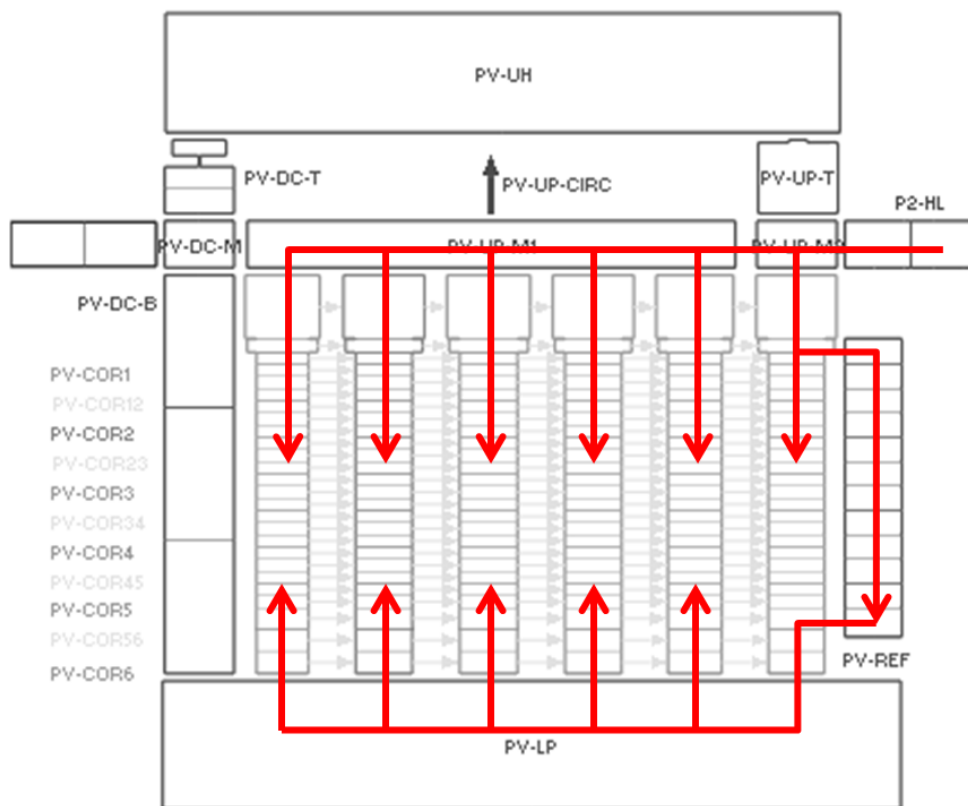


Figure 5.3: Flow paths of the water injected into the hot legs of the primary system

5 Reflooding

hot legs thus creates a combined top and bottom flooding, and the steam produced by evaporation creates a strong counter-current flow in the hot legs. A conceptual picture can be seen in figure 5.3.

During a combined injection into both the hot and the cold legs, both flooding conditions exist in parallel.

5.4 Parametric studies

With the shown assumptions and boundary conditions, different reflooding studies were performed. In each study, a certain variable was changed while all the other variables were held constant, in order to assess the variable's impact on the outcome of the simulation.

5.4.1 Study A: Variation of the beginning of reflooding

First of all, the time of the reflooding was assessed. This should account for the progressing degradation of the core, i.e. the aim was to investigate up to which state of degradation a flooding would successfully lead to a coolable condition. To account for the core melting not being linear, the starting points were linked to the amount of molten core material present in the core, given by the parameter AMISUL. Table 5.1 shows the 10 conducted simulations and the reflooding starting times.

Table 5.1: Simulations conducted with varying reflooding starting times

	Amount of molten core material (AMISUL)	Corresponding time
A1	10 t	7650.0 s
A2	20 t	9126.0 s
A3	30 t	8303.5 s
A4	40 t	8428.0 s
A5	50 t	8577.0 s
A6	60 t	8833.0 s
A7	70 t	9078.5 s
A8	80 t	9197.0 s
A9	90 t	9352.0 s
A10	100 t	9631.0 s

These simulations were conducted with the LPI being the reflooding system, injecting water in all eight legs with a 50/50 distribution between hot and cold legs of the pump mass flow rate. This lead to a combined top and bottom flooding condition, as described in section 5.3. It has to be noted that in simulations A1 and A2 the lower plenum module AIDA was not yet activated, because no ceramic melt had formed in the core area up to this point. This changes the accident evolution, which is why all the other studies were conducted with 30 t or more of molten core material present.

5.4.2 Study B: Variation of the reflooding system

This study was performed in order to assess the effect of different reflooding systems on the outcome of the reflooding. In typical KONVOI type nuclear power plants (NPPs) four active pump-systems are connected to the primary loops. Two of them are the ECCS, the high and low pressure injection systems (HPI and LPI). The other two are the volume control system (VCS) and the extra borating system (EBS), which is connected to the primary loops by means of the VCS. The two latter systems are not modelled explicitly in the present input, but were implemented as fills with a constant injection rate independent of the system pressure. For the EBS, the assumed mass flow rate was 2 kg/s per pump, while the VCS pumps were assumed to supply 35 kg/s . As for the HPI and LPI, each loop was assumed to have its own pump, making four pumps in total for each system. Since in reality there are only three VCS pumps, this assumption can be counted as optimistic. It has to be noted that the injected water has always been assumed to be borated according to specification, meaning that implicitly the assumption was made that the chemical control system is working uninterrupted during the accident. Also the injection locations in the simulations differ from those in reality, because detailed information about plant specifics was not available. Table 5.2 gives an overview of all the different injection systems used in study B.

Table 5.2: Simulations conducted with varying reflooding systems

	Reflooding System	Max. pressure	Max. mass flow rate
B1	Low Pressure Injection System (LPI)	1.07 MPa	325 kg/s
B2	High Pressure Injection System (HPI)	11 MPa	77 kg/s
B3	Volume Control System (VCS)	independent	35 kg/s
B4	Extra Borating System (EBS)	independent	2 kg/s
B5	Generic Middle Pressure Pump (MPI)	4 MPa	118 kg/s
B6	KSB's WKTR Pump	5.1 MPa	111 kg/s
B7	KSB's WKTB Pump	4 MPa	417 kg/s

In addition to the simulation of existing systems, three hypothetical middle pressure injection systems were simulated, starting with a generic middle pressure pump (MPI), which injects 118 kg/s , while withstanding a pressure of 4 MPa . The other two middle pressure systems are composed of condensate feed pumps from KSB AG (Klein, Schanzlin & Becker - a German pump manufacturer). Their characteristic values given in table 5.2 were taken from KSB's homepage [81] and fitted with a parabolic function of second order to generate the pressure dependent injection rate shown in figure 5.4.

5.4.3 Study C: Variation of the reflooding location

In a typical German KONVOI type NPP, the ECCSs are connected to both the hot and the cold legs. Nevertheless, only the LPI is able to feed into all eight legs at the same time, dividing the mass flow rate of every pump by two. It is possible to switch the LPI to pure hot leg or pure cold leg injection, which can be done with the HPI as

5 Reflooding

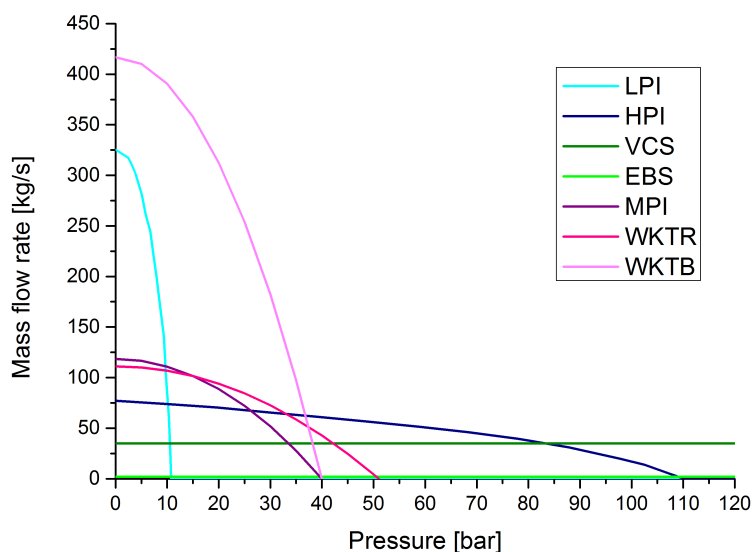


Figure 5.4: Pump curves of the different injection systems; compare with table 5.2

well. For scientific purposes, another case was accounted for, namely the HPI feeding into both the hot and the cold legs at the same time, even though this strategy is not implemented in the German KONVOI type NPPs. Table 5.3 summarizes the three possible reflooding locations.

Table 5.3: Simulations conducted with varying reflooding locations

	Reflooding Location	Resulting pump injection
C1	Cold Legs (CL)	4 x 100 %
C2	Hot Legs (HL)	4 x 100 %
C3	Hot and Cold Legs (HL+CL)	8 x 50 %

5.4.4 Study D: Variation of the number of available pumps

In order to assess the fact that in case of a severe accident not all equipment might be available and functioning, a fourth study has been conducted. Here, the number of available pumps has been reduced, thus accounting for possible pump unavailability.

Table 5.4: Simulations conducted with reduced pump numbers

	Number of pumps	Resulting injection rate
D1	1 x LPI	325.4 kg/s
D2	2 x LPI	650.8 kg/s
D3	3 x LPI	973.2 kg/s
D4	4 x LPI	1301.6 kg/s

5.5 Overview of all conducted simulations

Table 5.5 gives a systematic overview of all parametric simulations, characterized by start of reflooding, reflooding system, reflooding location and whether or not the AIDA module was activated during the course of the accident evolution. Also it is shown, which simulations are discussed in which study (A-D), or have been used in the discussion of the impact of the BLOCKAGE parameters and the AIDA module.

Table 5.5: Reference table for all conducted simulations

Label	Start of reflooding	Reflooding System	Reflooding Location	AIDA	Studies
BaseCase	no reflooding	-	-	YES	A
A1B1C3D4	10 <i>t</i>	LPI	HL+CL	YES	A
A2B1C3D4	20 <i>t</i>	LPI	HL+CL	YES	A
A3B1C1D4	30 <i>t</i>	LPI	CL	YES	C
A3B1C2D4	30 <i>t</i>	LPI	HL	YES	C
A3B1C3D4	30 <i>t</i>	LPI	HL+CL	YES	A, B, C, D, BLOCKAGE
A3B1C3D4**	30 <i>t</i>	LPI	HL+CL	YES	
A3B1C3D4**	30 <i>t</i>	LPI	HL+CL	YES	
A3B1C3D4N	30 <i>t</i>	LPI	HL+CL	NO	
A3B1C3D1*	30 <i>t</i>	LPI	HL+CL	YES	D
A3B1C3D2*	30 <i>t</i>	LPI	HL+CL	YES	D
A3B1C3D3*	30 <i>t</i>	LPI	HL+CL	YES	D
A3B2C1D4	30 <i>t</i>	HPI	CL	YES	
A3B2C2D4	30 <i>t</i>	HPI	HL	YES	
A3B2C3D4	30 <i>t</i>	HPI	HL+CL	YES	B
A3B3C1D4	30 <i>t</i>	VCS	CL	YES	
A3B3C2D4	30 <i>t</i>	VCS	HL	YES	
A3B3C3D4	30 <i>t</i>	VCS	HL+CL	YES	B
A3B4C1D4	30 <i>t</i>	EBS	CL	YES	
A3B4C2D4	30 <i>t</i>	EBS	HL	YES	
A3B4C3D4	30 <i>t</i>	EBS	HL+CL	YES	B
A3B5C1D4	30 <i>t</i>	MPI	CL	YES	
A3B5C2D4	30 <i>t</i>	MPI	HL	YES	
A3B5C3D4	30 <i>t</i>	MPI	HL+CL	YES	B
A3B6C1D4	30 <i>t</i>	WKTR	CL	YES	
A3B6C2D4	30 <i>t</i>	WKTR	HL	YES	
A3B6C3D4	30 <i>t</i>	WKTR	HL+CL	YES	B
A3B7C1D4	30 <i>t</i>	WKTB	CL	YES	
A3B7C2D4	30 <i>t</i>	WKTB	HL	YES	
A3B7C3D4	30 <i>t</i>	WKTB	HL+CL	YES	B

Table 5.6: Reference table for all conducted simulations, continued

Label	Start of reflooding	Reflooding System	Reflooding Location	AIDA	Studies
A4B1C1D4	40 <i>t</i>	LPI	CL	YES	
A4B1C2D4	40 <i>t</i>	LPI	HL	YES	
A4B1C3D4	40 <i>t</i>	LPI	HL+CL	YES	A, B
A4B1C3D4N	40 <i>t</i>	LPI	HL+CL	NO	
A4B2C1D4	40 <i>t</i>	HPI	CL	YES	
A4B2C2D4	40 <i>t</i>	HPI	HL	YES	
A4B2C3D4	40 <i>t</i>	HPI	HL+CL	YES	B
A4B5C1D4	40 <i>t</i>	MPI	CL	YES	
A4B5C2D4	40 <i>t</i>	MPI	HL	YES	
A4B5C3D4	40 <i>t</i>	MPI	HL+CL	YES	B
A4B6C1D4	40 <i>t</i>	WKTR	CL	YES	
A4B6C2D4	40 <i>t</i>	WKTR	HL	YES	
A4B6C3D4	40 <i>t</i>	WKTR	HL+CL	YES	B
A4B7C1D4	40 <i>t</i>	WKTB	CL	YES	
A4B7C2D4	40 <i>t</i>	WKTB	HL	YES	
A4B7C3D4	40 <i>t</i>	WKTB	HL+CL	YES	B
A5B1C1D4	50 <i>t</i>	LPI	CL	YES	
A5B1C2D4	50 <i>t</i>	LPI	HL	YES	
A5B1C3D4	50 <i>t</i>	LPI	HL+CL	YES	A, B, AIDA
A5B1C3D4N	50 <i>t</i>	LPI	HL+CL	NO	AIDA
A5B2C1D4	50 <i>t</i>	HPI	CL	YES	
A5B2C2D4	50 <i>t</i>	HPI	HL	YES	
A5B2C3D4	50 <i>t</i>	HPI	HL+CL	YES	B
A5B5C1D4	50 <i>t</i>	MPI	CL	YES	
A5B5C2D4	50 <i>t</i>	MPI	HL	YES	
A5B5C3D4	50 <i>t</i>	MPI	HL+CL	YES	B
A5B6C1D4	50 <i>t</i>	WKTR	CL	YES	
A5B6C2D4	50 <i>t</i>	WKTR	HL	YES	
A5B6C3D4	50 <i>t</i>	WKTR	HL+CL	YES	B
A5B7C1D4	50 <i>t</i>	WKTB	CL	YES	
A5B7C2D4	50 <i>t</i>	WKTB	HL	YES	
A5B7C3D4	50 <i>t</i>	WKTB	HL+CL	YES	B
A6B1C1D4	60 <i>t</i>	LPI	HL+CL	YES	A
A6B1C2D4N	60 <i>t</i>	LPI	HL+CL	NO	
A7B1C3D4	70 <i>t</i>	LPI	HL+CL	YES	A
A8B1C1D4	80 <i>t</i>	LPI	HL+CL	YES	A
A9B1C1D4	90 <i>t</i>	LPI	HL+CL	YES	A
A10B1C1D4	100 <i>t</i>	LPI	HL+CL	YES	A

5.5 Overview of all conducted simulations

*In study D, the number of LPI pumps available for reflooding was reduced from four to one. D4 represents four pumps, D3 three pumps and so on.

**In section 7.1, the BLOCKAGE values have been changed in order to investigate their effect.

Of the simulations not used in any of the studies, simulations A3B1C3D4N, A4B1C3D4N and A6B1C3D4N have been conducted for the investigation of the impact of AIDA discussed in section 7.2. Since the comparisons to the equivalent simulation with AIDA all showed the same trend, only the comparison of A5B1C3D4 to A5B1C3D4N was discussed.

All the other simulations, which have not been part of a study were performed for study C in order to investigate whether the injection location has a different impact on the simulation depending on the injecting system and the mass of molten core material present. Since it was found to make no difference, only the 30 t simulations with LPI injection are discussed in detail in section 6.4.

6 Discussion of the results

In this chapter, the results of the different studies will be discussed in detail, referring at different points to the BaseCase scenario that has been described in chapter 4. An overview of all the conducted simulations has been given in chapter 5.

6.1 Coolability criteria

To decide, whether a core has reached a coolable condition, coolability criteria had to be developed. They not only had to describe the core status as detailed as possible, but also needed to be applicable to the used simulation tool. In this work, four different criteria have been applied in order to assess the coolability as good as possible and also to decide, which criterion is the most conservative.

6.1.1 Criterion I: Vessel failure

The ultimate criterion to decide whether a core melting accident can be stopped by water injection into the primary system or not, is the failure of the pressure vessel. As long as the RPV stays intact throughout the accident, it does not matter whether the core has relocated to the lower plenum, or what temperature the materials inside the RPV have. In case of RPV failure, coolability could also be established within the containment. However, this is not subject of the present work.

The lower plenum module AIDA used in most of the conducted simulations provides a DAMAGE factor for the lower vessel wall, which equals RPV failure as soon as the factor reaches the value 1. Unfortunately, the AIDA module does only account for creep failure of the vessel's steel wall due to temperature loads charged by the melt pool. The criterion is applied (see section 6.2), but has to be considered carefully for two reasons:

Since the AIDA module needs a lot of user input for the simulation of melt relocation to the lower plenum and RPV failure, its simulation results depend strongly on what the user expects to happen during the core meltdown. For example, it has to be specified in the input, whether or not water will be present in the lower head during the relocation of melt from the core area, and what configuration will result in the lower plenum. Giving that information as input renders the simulation less meaningful and the results unobjective. The second reason for carefully applying RPV failure as coolability criterion is its ultimacy. Whether or not the RPV fails is a yes / no decision, and if it fails, the power plant and its environment are in danger. Therefore it was logical to choose a criterion that emerges before RPV failure is even possible.

6.1.2 Criterion II: Temperature criterion

The first approach to determine coolability independent of vessel integrity was to have a look at the temperature of the core materials during the accident sequence. If the material temperatures in all core sections would fall below the melting point of the corresponding materials, the core would be solid and must thus be coolable.

In one of the earlier studies [82], a temperature limit of $1800\text{ }^{\circ}\text{C}$ was applied, since this is the roughly approximated melting temperature of the cladding material. Looking at the temperature development in the whole core led to the realization that even if one or two nodes remain at higher absolute temperatures, the core can be labelled as coolable if the average temperature does not rise anymore.

$$TF = \frac{1}{132} \cdot \left| \frac{\Sigma (TB)_{t_2} - \Sigma (TB)_{t_1}}{t_2 - t_1} \right| \leq 0.076 \frac{K}{s} \quad (6.1)$$

An ATHLET-CD simulation gives one fuel temperature (TB) per node, making $6 \times 22 = 132$ values per time step. The TB-values are summarized for each time step, and their difference for two consecutive time steps is divided by the time step size and the number of nodes, resulting in a value for the temperature fluctuation (TF), as given in equation 6.1. The resulting curve fluctuates heavily, but approaches the time axis in the course of the accident, and when the variation in the value TF is smaller than 0.076 K/s (10 K/s for the whole core divided by the 132 nodes), the core area is assumed to be quenched.

The same kind of analysis would have to be conducted for the material that has been relocated to the lower plenum, using the melt temperature TMELT instead of the sum of the fuel temperatures TB. The application of a temperature criterion of this kind is rather difficult, because it always contains a generalization or assumption chosen by the user. For example the value of 10 K/s has simply been assumed without any scientific background to it. For this reason, the temperature criterion was not applied in the end.

6.1.3 Criterion III: Geometry criterion

A different approach to define coolability is to say that the core is safe when its geometry stops changing. This means that all melting and relocating has stopped, even though there might still be melt present in melt pools surrounded by crust. This criterion is hard to apply, because a melt pool that has not changed for a given time might still change at a later time and it is impossible to simulate the accident scenario forever. So for the successful application of this criterion, a time value must be chosen after which it is assumed that the geometry does not start changing again.

All simulations presented in this thesis were conducted from 0 s to 30000 s , with the accident starting at 1000 s . The accident evolution is thus investigated for the first

eight hours, and since some of the simulations needed up to one month to complete, it was decided to not simulate the accident evolution any further.

Another issue with this kind of criterion is that the ATHLET-CD simulation does not give geometry changes as a parameter, thus leaving the user with the task to assess the geometry manually. Since this would take a lot of time and is strongly dependent on the user, the application of this criterion was not pursued any further.

6.1.4 Criterion IV: Heat removal criterion

A core is assumed to be coolable when the total amount of heat produced in the core can be removed at every point in time. The heat produced in the core consists of the heat produced by chemical reactions (like metal oxidation) and the decay heat of the fission products. On the other hand, heat can be removed from the core by radiation to surrounding structures if the core is not covered by water.

The heat removal is done only by the water present in or pumped into the core region. This can result in convective heat transfer to either water, steam or - in the case of a partially covered core - a mixture of these two and boiling heat transfer.

This criterion might bear some difficulties in application, because its confirmation would have to be done for each node in the core separately to ensure that inhomogeneities in heat release and / or removal are taken into account. Fortunately, the ATHLET-CD code calculates some integral power values (in W) over the whole core, which can be used to establish a global power balance [27]:

- TOTNPOW - Power of all fuel rods
- SQOXID - Heat generated by chemical reactions (oxidation, nitride formation)
- SQFLUI - Heat flow to fluid
- SQLOSS - Heat losses to structures

From these values, the summarized power factor SUMPOW was calculated as follows:

$$SUMPOW = TOTNPOW + SQOXID - SQFLUI - SQLOSS \quad (6.2)$$

If $SUMPOW$ is zero, the amount of energy produced in the core is dissipated immediately by the surrounding water and / or steam, and the core has reached a stable condition, as long as the water injection can be kept up. If $SUMPOW$ is negative, the amount of energy dissipated is higher than what is produced in the core area, which means that the core is losing energy thus cooling down. On the other hand, if $SUMPOW$ takes on a positive value, then the amount of power produced by the core cannot be dissipated and the core is not coolable.

6.2 Study A: Variation of the beginning of reflooding

Study A was conducted in order to find the point of no return in the accident evolution, where a water injection cannot stop the accident progression any more.

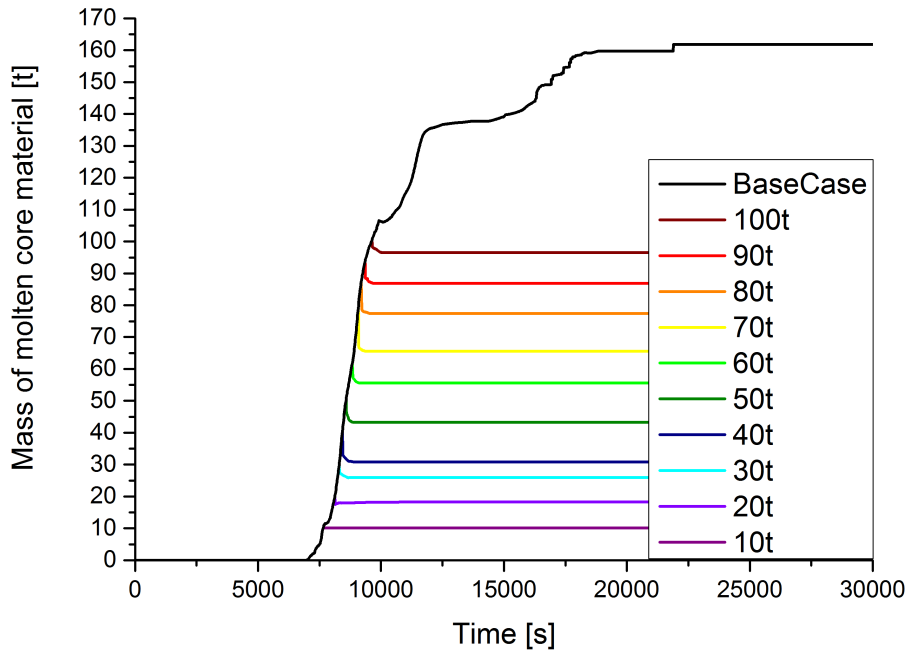


Figure 6.1: Mass of molten core material obtained in study A

Figure 6.1 shows the cumulative mass of molten core material (AMISUL). While in the BaseCase scenario without reflooding almost the whole core inventory is molten (162 t of 181 t), all conducted reflooding scenarios in study A show a stop of further core melting after reflooding. However, this is not equivalent with a quenched core, because the parameter AMISUL does not reflect the current mass of melt present in the core, but summarizes all the masses that have been molten up to some point during the accident. Figure 6.2 shows the melt mass present at each time during the accident, and it can clearly be seen that only in case of simulation A1B1C3D4 (Reflooding after 10 t of core material have been molten) the melt mass decreases to zero. In all other simulations, a small amount of up to 2 t of core materials stays molten inside the core area.

Exemplarily, simulation A3B1C3D4 (reflooding after 30 t) shall be explained and analyzed in greater detail. Figure 6.3 shows the core status at the beginning of reflooding (8300 s) on the left, and the core status at the time of the vessel failure signal (25613 s) on the right. At the beginning of reflooding, 30 t of core material have been molten, and the rods in core section 1, 2 and 3 have failed in node 19 after extensive ballooning of the cladding. The degradation is strongest in rod 3, where nodes 16 to 19 have already melted away. Below the empty nodes, the molten material has canded down the fuel rods and formed crusts outside the cladding, leading to local blockages in the flow paths. Nevertheless, due to relocation of molten core material from the core area to the lower plenum shortly after the start of reflooding, the core area can be quenched completely. This can be verified in the right picture of figure 6.3, because by then the

6.2 Study A: Variation of the beginning of reflooding

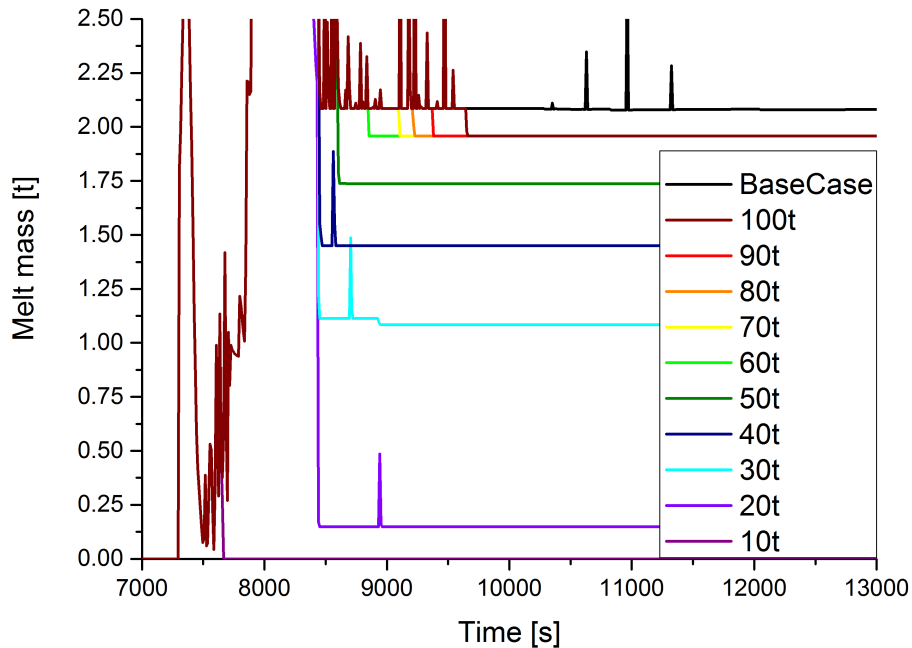


Figure 6.2: Mass of melt present at each time during the accident in study A

RPV is full of water with a void value of close to zero and the fuel temperatures have dropped to $1530\text{ }^{\circ}\text{C}$ or less.

Vessel failure is calculated by the AIDA module, because the module clearly does not account for melt-water interaction during relocation and for the heat transfer from the melt pool to the overlaying water. This is obvious, because the void in the lower plenum is 0.0 while the melt pool has a temperatures of approximately $1000\text{ }^{\circ}\text{C}$, which should evaporate the overlaying water but does not. Also, the crust formed between the melt pool and the vessel wall shows a temperature of up to $2000\text{ }^{\circ}\text{C}$, being too high for the material to remain solid, while the temperature of the liquid melt pool has long fallen below its solidification temperature while the material remains liquid in the simulation.

A few nodes in the core area remain at constant high temperatures, and the reason for those nodes not being coolable was found in the way blockages of fluid flow due to crusts are treated by the ATHLET-CD code, which has been described in section 2.5. During the core melting, the model applies the porosity criteria given in table 2.2 and successively disables radial and axial flow paths for water and steam, as well as the heat transfer from fuel and cladding materials to the surroundings. In figure 6.4 the porosity evolution for the nodes of rod 3 is shown, as well as the porosity limits applied by the BLOCKAGE model, according to table 2.2. It can be seen that in most of the nodes, the porosity never decreases to 0.3, which is the porosity limit for open porosity where the BLOCKAGE model is activated. On the other hand, there are five nodes, in which the porosity decreases below 0.3, leading to the activation of the BLOCKAGE model. Four of these nodes show a porosity lower than 0.25 %, which means that the radial and axial flows as well as the convective heat transfer to the surrounding fluid have been turned off, thus leaving the concerned nodes without an option for heat transfer. Even when the porosity increases again due to re-melting and relocation of

6 Discussion of the results

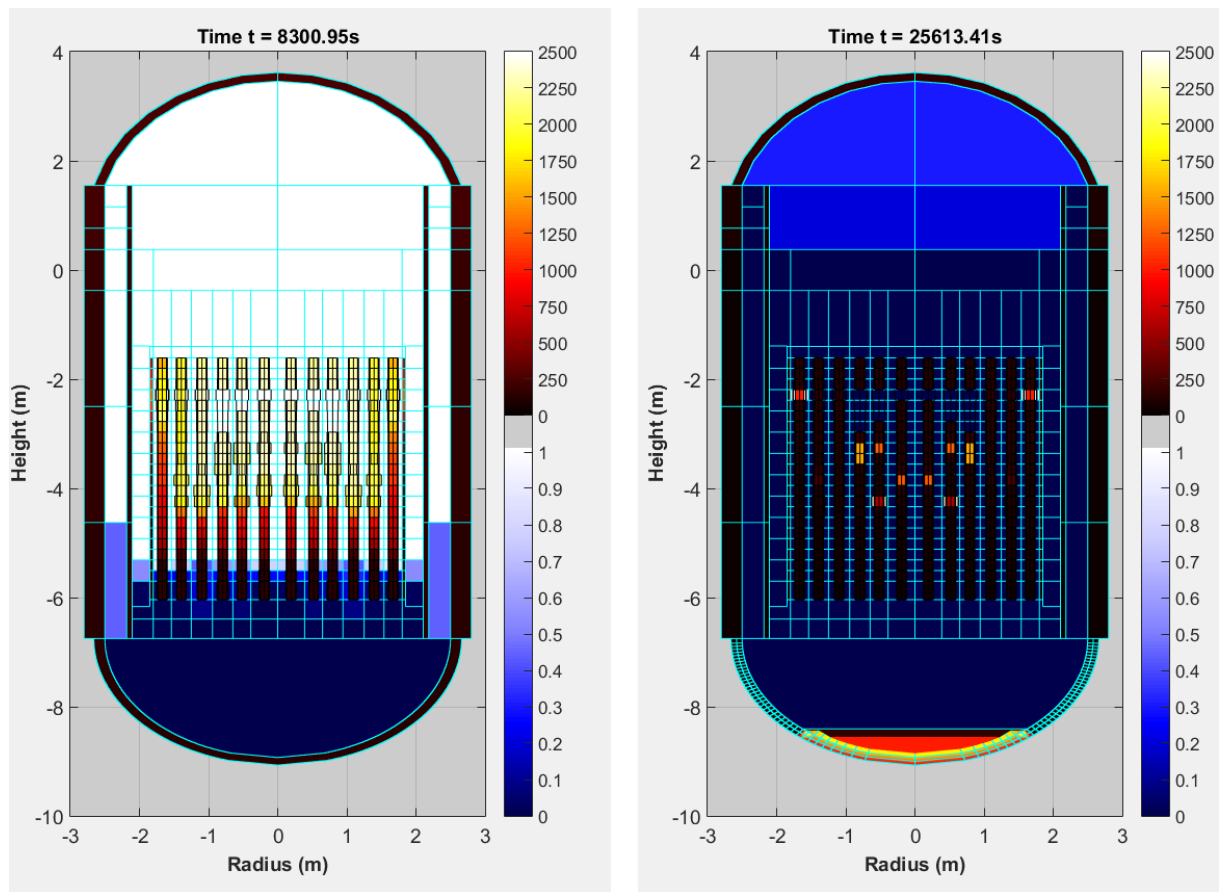


Figure 6.3: Comparison of the core status at the time of the beginning of reflooding (left) and at the time of vessel failure (right) for simulation A3B1C3D4.

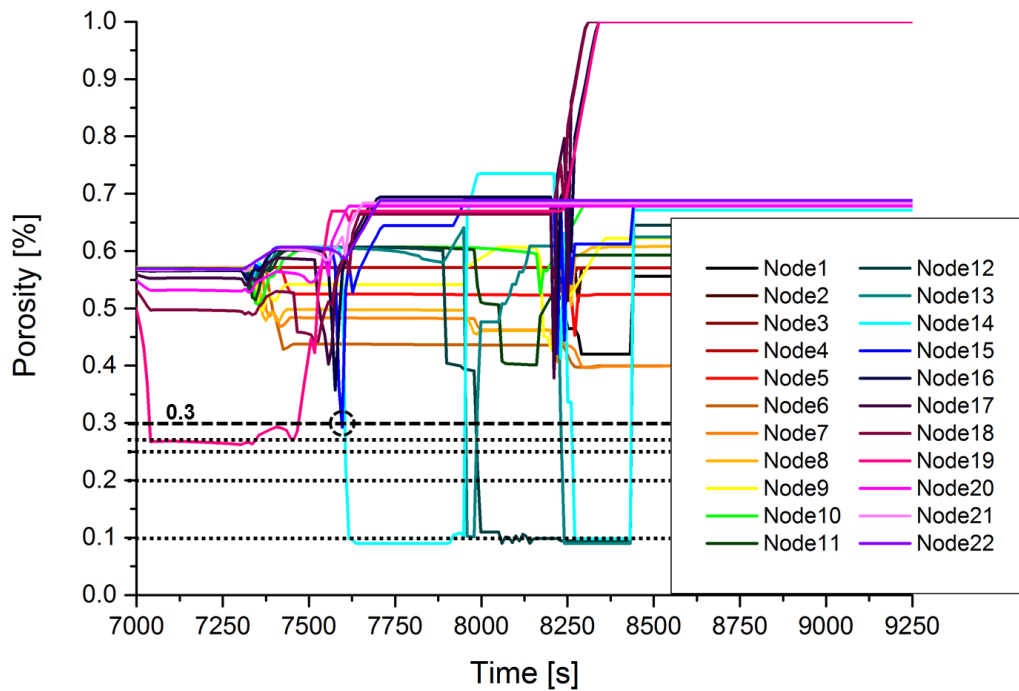


Figure 6.4: Porosity evolution in Rod 3 during simulation A3B1C3D4

the crust, the expected cooling of the nodes does not take place.

Of the five nodes discussed, one (Node 22) is completely depleted of material, reaching a porosity of 1.0 around the time the relocation to the lower plenum is started. In the other four nodes, small amounts of ceramic melt remain present, as can be seen in figure 6.5. Node 12 holds 1.25 kg, node 13 160.91 kg, node 14 197.26 kg and node 15 23.61 kg, making a total of 383.02 kg of ceramic melt mass that is not quenched and successively heats up to more than 3000 °C, as proven by figure 6.6.

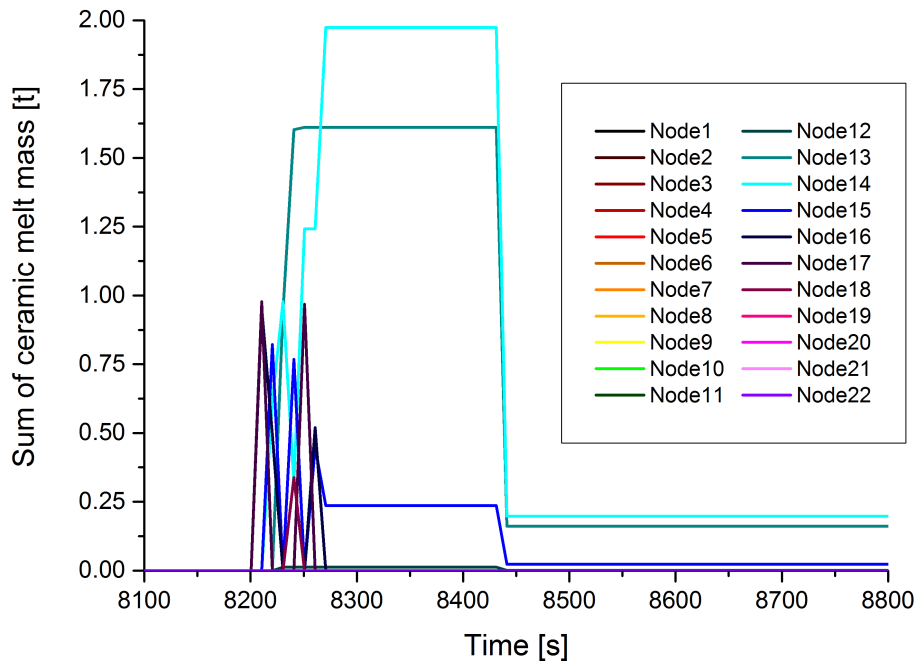


Figure 6.5: Current amount of ceramic melt mass present in the nodes of rod 3 during simulation A3B1C3D4

This behavior can be explained, if it is assumed that the BLOCKAGE model can only disable flow paths and heat transfer, but not re-enable them when the porosity increases again due to clogging or relocation of material out of the affected node. This assumption has yet to be verified, since the input manual for the ATHLET-CD code [27] only contains the values given in table 2.2 without explaining or describing anything else about the BLOCKAGE model. Nevertheless, the observed behaviour of ceramic melt mass in the simulation is clearly not realistic.

Consequently, the application of a temperature criterion for coolability is difficult, because every node in every simulation would have to be treated separately resulting in a serious amount of work. This is why in the end, criterion IV (see section 6.1.4) was applied.

Figure 6.7 shows the summarized power factor SUMPOW for the simulations of study A. The results show that simulations A1B1C3D4 (10 t) and A2B1C3D4 (20 t) as well as simulation A4B1C3D4 (40 t) reach a stable condition, where the SUMPOW values fluctuate slightly around zero after the quenching of the core is complete. The simulations A5B1C3D4 (50 t) to A10B1C3D4 (100 t) show SUMPOW values higher than zero and have thus not reached a coolable condition, because the produced energy

6 Discussion of the results

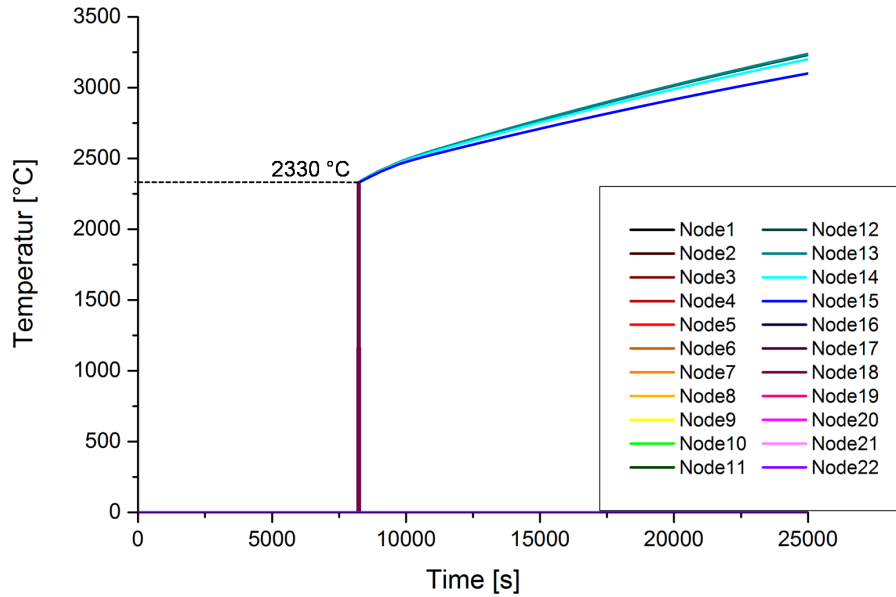


Figure 6.6: Average temperature of ceramic melt mass present in the nodes of rod 3 during simulation A3B1C3D4

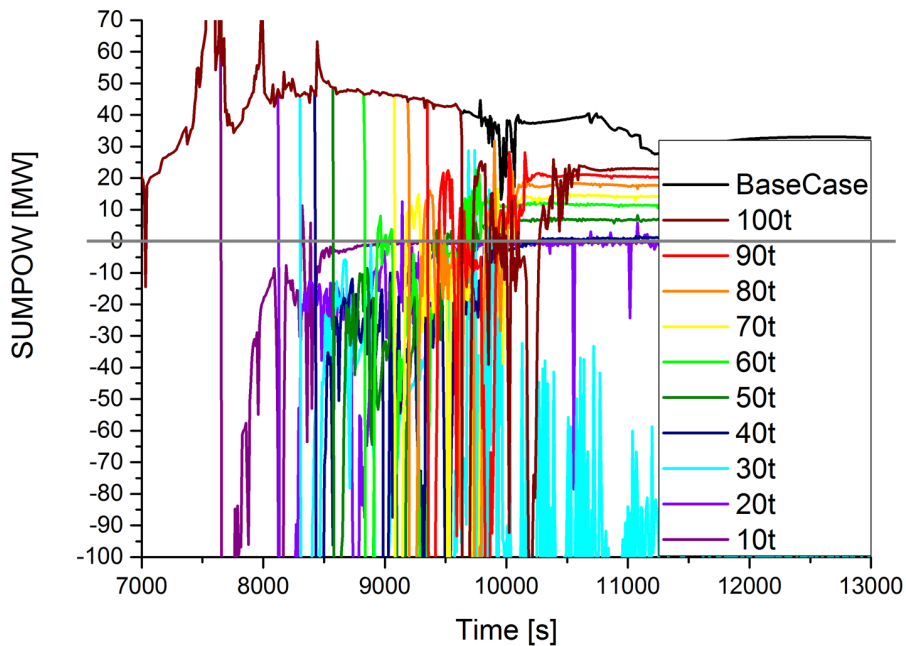


Figure 6.7: Power balance of the reactor for the simulations of study A

in the core cannot be dissipated to the surroundings completely. An exception is simulation A3B1C3D4 (30 t), which shows SUMPOW values that fluctuate heavily around $-100 MW$ indicating a rapid decrease in energy inventory in the core area. It is unclear, why only this one simulation shows this behaviour and where the dissipated energy is taken from, because the core is clearly quenched at 10000 s.

The hydrogen production has to be evaluated since it can be treated as a parameter of cladding oxidation and thus represents the present core state. Hydrogen is generated during the oxidation of the fuel and absorber rod cladding material, which consists

6.2 Study A: Variation of the beginning of reflooding

mainly of zirconium. This oxidation poses two threats simultaneously, because other than producing vast amounts of hydrogen, it is also a highly exothermic reaction releasing even more energy inside the core area than the decay heat. This process is intensified during reflooding as can be seen for example in the „reflood map“ developed at KIT [83], which led to the presumption that reflooding might be counterproductive when the core is heavily damaged and should thus be avoided. The simulations conducted for this work confirm accelerated hydrogen production during reflooding, but the results do not indicate that the reflooding is over-all counterproductive and should be avoided.

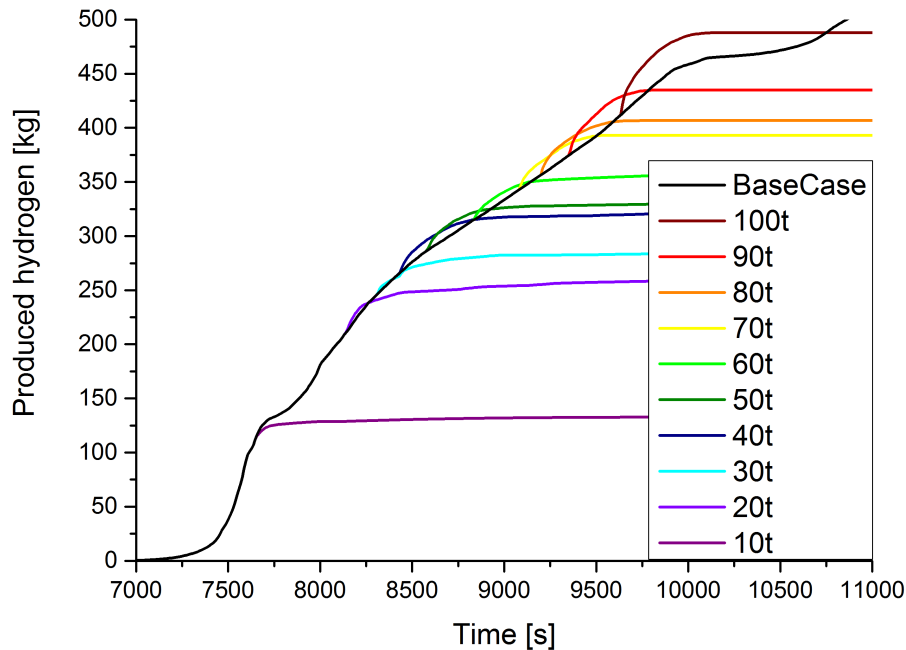


Figure 6.8: Mass of hydrogen produced in study A

Figure 6.8 shows the accumulated amount of hydrogen produced during the accident simulations in study A. Without reflooding, approximately 590 kg of hydrogen will be produced, which corresponds to a zirconium fraction of 40.05% being oxidized. Table 6.1 summarizes the values for the amount of produced hydrogen and the degree of oxidation for all the simulations of study A. A clear trend is visible, the earlier the reflooding takes place, less hydrogen is produced in total corresponding to a smaller fraction of oxidized zirconium and a lower heat generation due to the oxidation. Nevertheless, the reflooding itself speeds up the oxidation for a short time, leading to an instantly higher hydrogen generation rate but ultimately stopping the oxidation. This can be seen in figure 6.8, where the curves for the reflooding simulations rise above the BaseCase simulation without reflooding right after the beginning of reflooding, but turn to a constant value afterward.

This accelerated oxidation due to the initiation of reflooding is reflected in the hydrogen production rates shown in the top picture of figure 6.9, where the peak oxidation rate obviously correlates to the beginning of reflooding leading to the shift in the position of the peaks.

The same is true for the chemical reaction heat generated by zirconium oxidation, as displayed in the bottom picture of figure 6.9. The peak values range from about

6 Discussion of the results

Table 6.1: Hydrogen produced and fraction of zirconium oxidized in the simulations of study A

Simulation	Produced hydrogen	Degree of oxidation
A1B1C3D4	133.0 kg	9.02 %
A2B1C3D4	282.2 kg	16.90 %
A3B1C3D4	285.3 kg	18.53 %
A4B1C3D4	322.9 kg	21.27 %
A5B1C3D4	330.6 kg	21.73 %
A6B1C3D4	357.6 kg	23.63 %
A7B1C3D4	393.2 kg	26.19 %
A8B1C3D4	406.7 kg	27.17 %
A9B1C3D4	435.0 kg	29.18 %
A10B1C3D4	488.1 kg	32.97 %

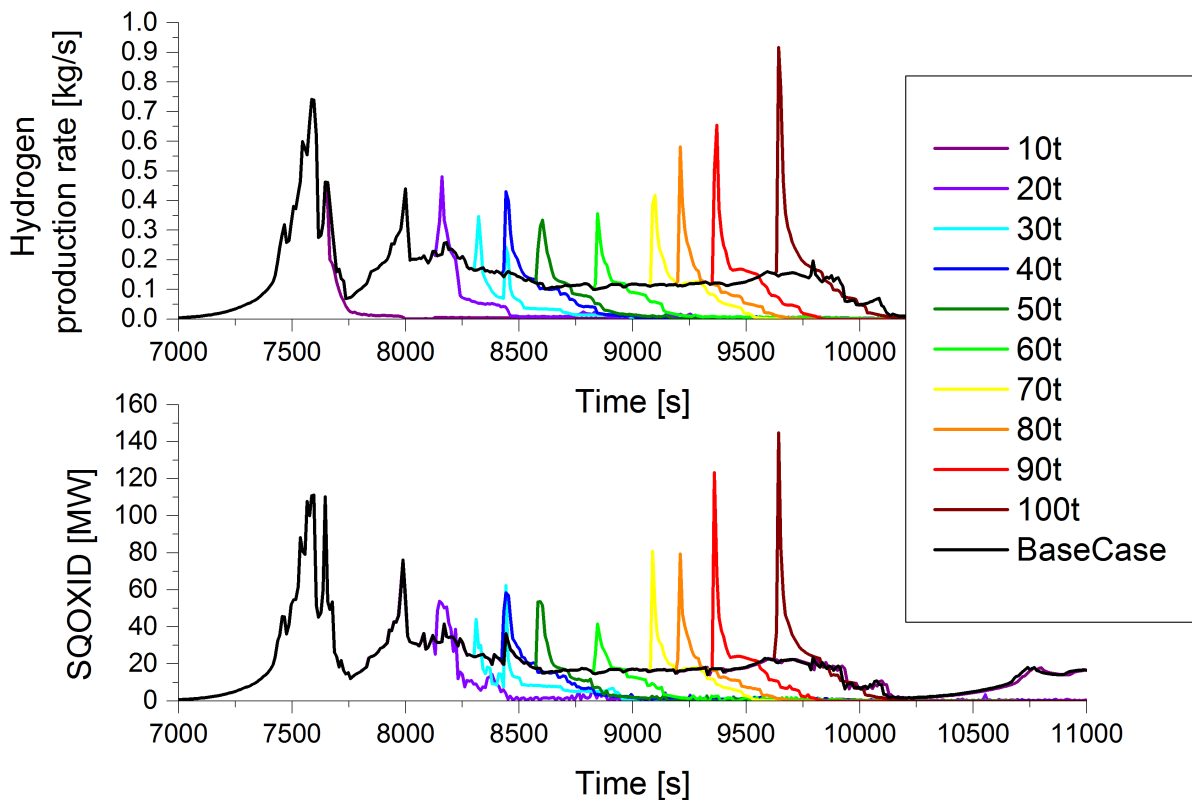


Figure 6.9: Hydrogen production rate and exothermic heat release during oxidation (SQOXID) in study A

40 MW in simulation A6B1C3D4 (60 t) up to nearly 150 MW in simulation A10B1C3D4 (100 t). This heat has to be dissipated from the core in addition to the 40 MW of decay heat at that time, thus counteracting the core cooling efforts.

Another phenomenon observed arises from the massive evaporation that takes place, when the water injected into the primary circuits by the reflooding system (in this case the LPI) hits the melting core with temperatures beyond 2000 °C. The evaporation

6.3 Study B: Variation of the reflooding system

leads to a pressure increase from around 260 kPa before the start of reflooding to 3.04 MPa in 90 s after the start of reflooding. Unfortunately, the LPI pumps can only withstand a counter pressure of up to 1.07 MPa , and thus are unable to inject further against the pressure after only 20 s of water injection. This behaviour can be observed in figure 6.10, where the leak and injection mass flow rates are displayed against the pressure and void near the leak position.

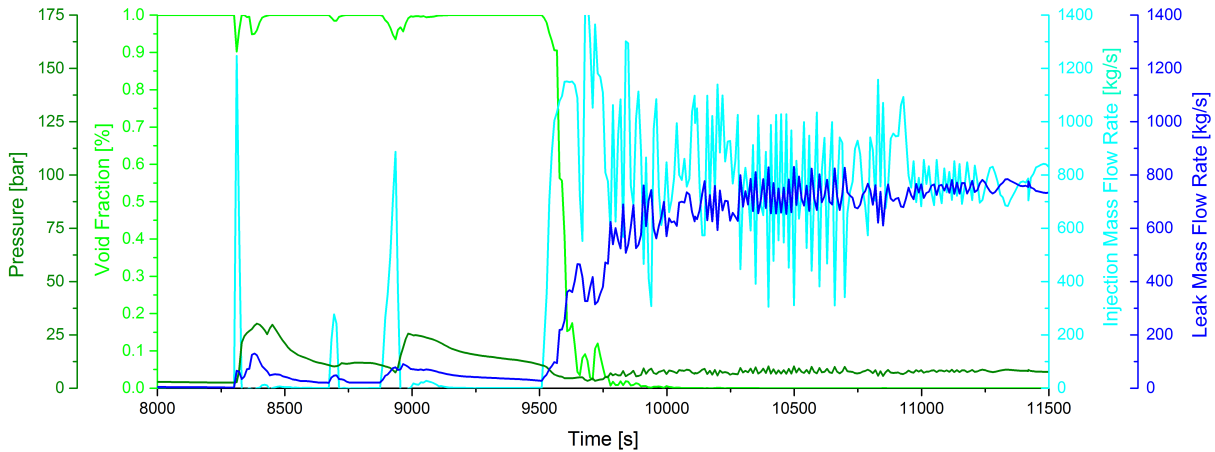


Figure 6.10: Comparison of the leak and injection mass flow rates with the pressure and void near the leak position for simulation A3B1C3D4 (30 t).

Since the LPI injection rate drops to zero after a first injection of roughly 18.5 t of water, the pressure decreases again, until it reaches 1.07 MPa after 360 s , and the LPI is able to inject water again. Now the process, which will be called „self-blocking effect“, repeats itself twice, until at 9518 s the LPI is able to inject continuously, quenching the core in the process. This pressure dependent injection behaviour of the LPI leads to nearly 20 minutes of potential reflooding time remaining unused, because the pressure is too high for the LPI pumps to inject water into the primary circuits. If other pumps were available, which could provide higher pressures than the LPI, those 20 minutes could be used to effectively quench the core and thus preventing further damage to the core, possibly even preventing vessel failure. These considerations led to the conduction of study B.

6.3 Study B: Variation of the reflooding system

There are three different systems connected directly to the primary circuit in the KONVOI input that contain pumps: The HPI, the LPI and the VCS. Attached to the VCS is another system using separate pumps: the EBS. Since study A has shown that reflooding a partially degraded PWR core with the regular LPI system leads to injection stops due to pressure peaks, an investigation was conducted to see whether the other potentially available pumps could perform any better. The three reflooding cases marking the transition from coolable to non-coolable conditions, namely A3B1C3D4 (30 t), A4B1C3D4 (40 t) and A5B1C3D4 (50 t), were taken as basis, and in each case the reflooding system was varied according to table 5.2 (p. 59). For the sake of clarity, only the simulations based on A3B1C3D4 (30 t) will be discussed in detail.

6.3.1 High and low pressure injection systems

Since the cause for the injection delay with the LPI was the pressure built-up, the obvious course of action was to investigate a reflooding using the HPI system. The HPI pumps can withstand a pressure of up to 11 MPa and inject up to 77 kg/s per pump, making a maximum injection rate of 308 kg/s in total.

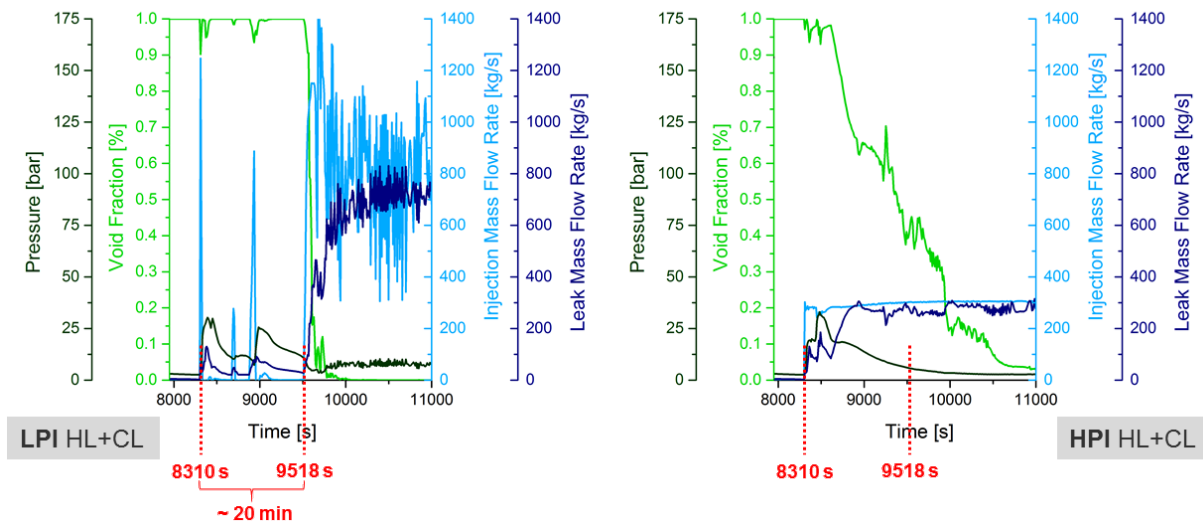


Figure 6.11: Comparison of the leak and injection mass flow rates with the pressure and void near the leak position for simulations A3B1C3D4 (LPI) and A3B2C3D4 (HPI)

Figure 6.11 shows a comparison of the reflooding with the LPI and HPI, in which the injection gap of about 20 min in the LPI reflooding is marked in red. Using the HPI instead of the LPI does not lead to an injection gap at all, because even though the pressure does built up to 2.9 MPa following the start of reflooding, the HPI pumps continue their water injection uninterruptedly.

The void decrease starts immediately after reflooding, and the core is quenched much faster. This can be seen from figure 6.12, where the core status after 5 min of reflooding is shown for both the simulations A3B1C3D4 (LPI) and A3B2C3D4 (HPI). At this time in the reflooding process, the LPI is still shut down because of the pressure built-up in the system, leaving the core materials at temperatures of up to 2000 °C.

At the same time the HPI has already flooded and quenched most of the core, with only a few blocked nodes remaining at high temperatures. But since those nodes are surrounded by cold ones and water, they do not pose a threat to the integrity of the safety barriers any more.

It has to be noted that the lower plenum module AIDA does not account for the heat transfer from the melt pool to the overlaying water, because in both cases the lower plenum is completely filled, thus giving the same results for the melt behaviour in the lower plenum in both simulations.

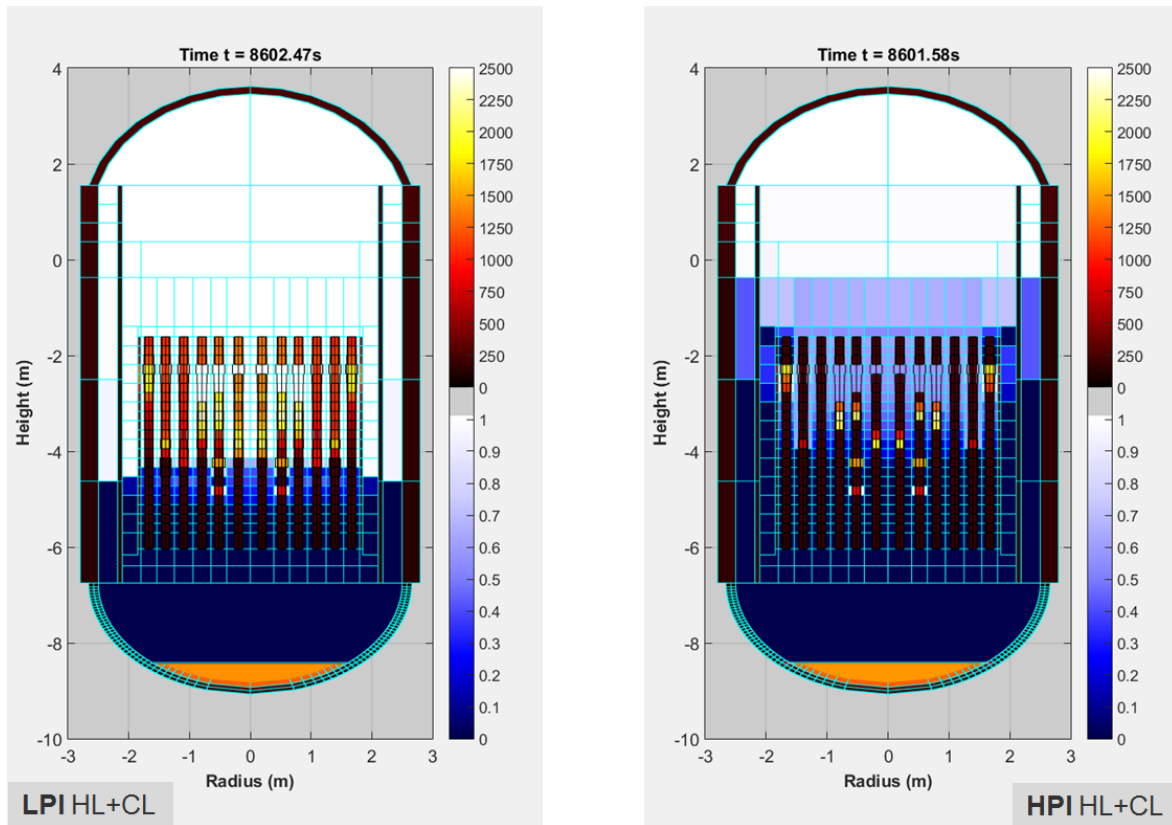


Figure 6.12: Comparison of the core status after 5 minutes of reflooding for simulations A3B1C3D4 (LPI) and A3B2C3D4 (HPI)

6.3.2 Middle pressure injection systems WKTB and WKTR

The next question that came to mind was whether the results might be optimized by using a hypothetical middle pressure injection (MPI) system that can withstand the pressure built-up of 3 MPa while at the same time injecting more water than the HPI. Thus the MPI system was implemented into the simulation, and since the results of the corresponding simulation (A3B5C3D4) were promising, a research for pumps with similar characteristics was undertaken, revealing two available KSB pumps: WKTB and WKTR. Both pumps are condensate feedwater pumps and might actually be available on site of the NPP, even though their use in a severe accident might not have been considered yet.

Figure 6.13 shows the comparison of the reflooding using the WKTB and WKTR pumps as middle pressure reflooding system. This means that each loop was equipped with its own pump, leaving the system with four available pumps. It can be seen that the WKTB pumps with their injection rate of up to 417 kg/s quench the system very fast, withstanding the pressure built-up easily. The WKTR pumps are a lot more similar to the HPI pumps with a slightly higher injection rate, thus showing a similar quenching behaviour as the HPI. Nevertheless, both the WKTB and the WKTR pump system can quench the core in a matter of minutes, as can be seen in figure 6.14. The core status after 5 min is in case of the WKTR nearly the same as with the HPI system, while the WKTB pumps have filled the RPV almost to the top at this point, thanks to their high injection mass flow rate.

6 Discussion of the results

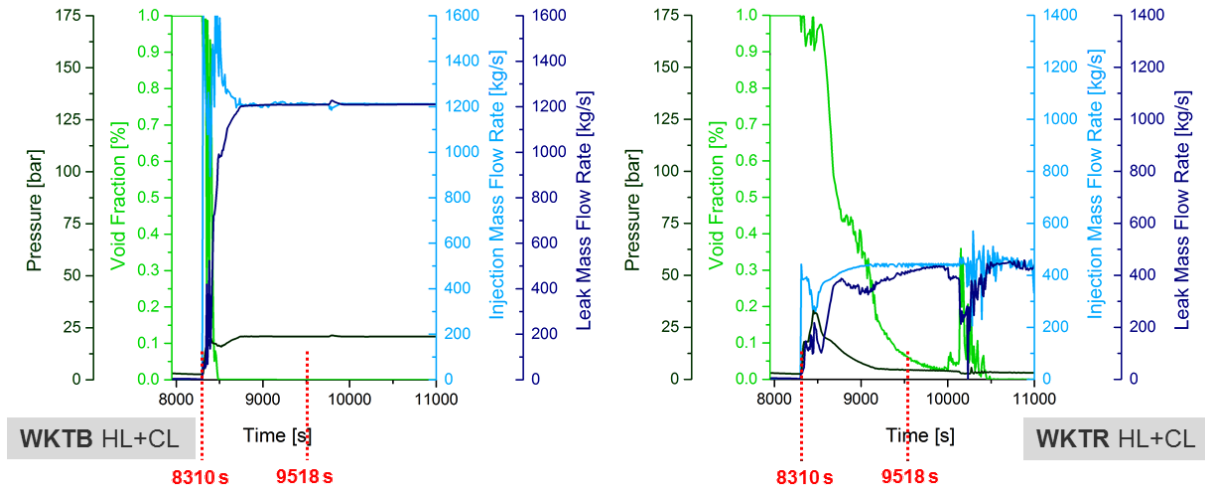


Figure 6.13: Comparison of the leak and injection mass flow rates with the pressure and void near the leak position for simulations A3B6C3D4 (WKTR) and A3B7C3D4 (WKTB)

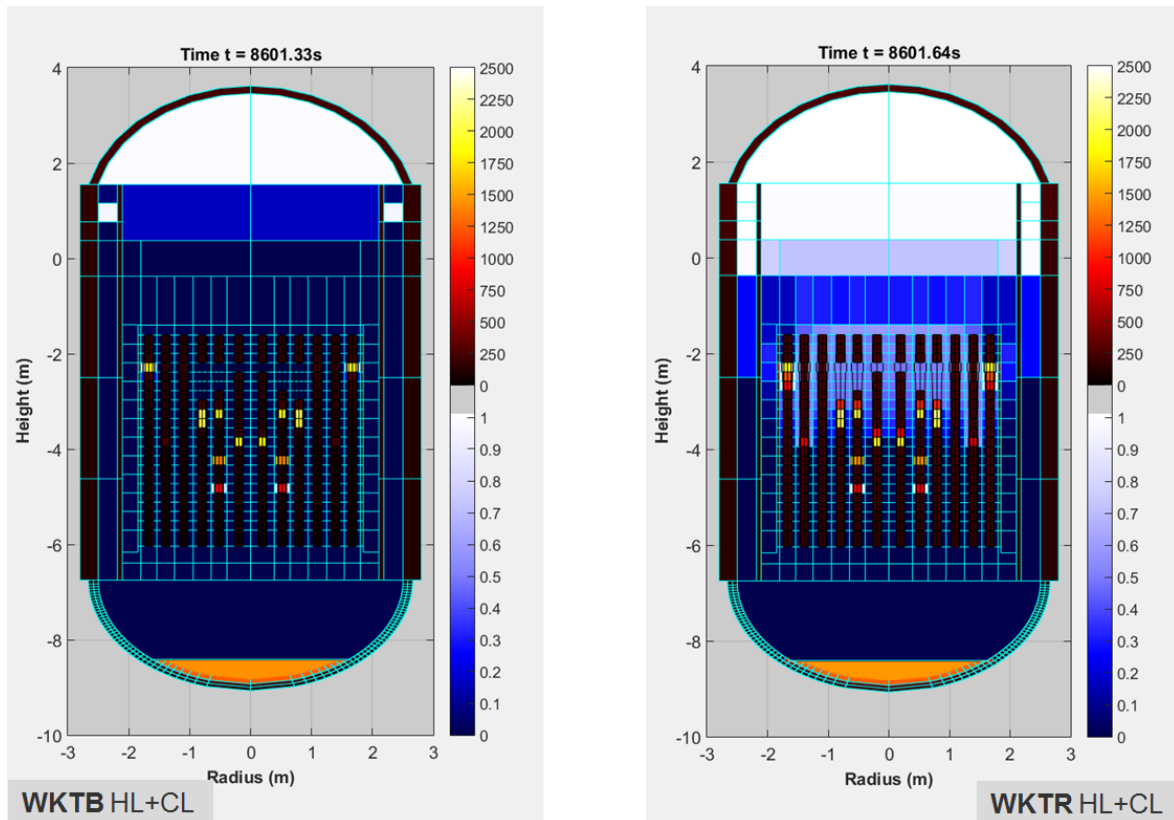


Figure 6.14: Comparison of the core status after 5 minutes of reflooding for simulations A3B6C3D4 (WKTR) and A3B7C3D4 (WKTB)

From efficiency's point of view, it would be very useful for the reflooding, if middle pressure injection pumps were available. Such a system is currently not implemented in German NPPs, but maybe it should be considered to invest into such pumps or to at least equip fire trucks near NPPs with pumps that can withstand the expected pressure built-up during the reflooding.

6.3.3 Volume control and extra borating system

The results of the reflooding using the VCS (A3B3C3D4) and EBS (A3B4C3D4) pumps were unexpected. An injection rate this low was not considered to make much difference in the accident evaluation, but a comparison of the results refuted this expectation. A rough estimation of the energy that can be dissipated by heating water from $40\text{ }^{\circ}\text{C}$ to $2330\text{ }^{\circ}\text{C}$ (see fig. 6.6, p. 72) was done with the formula for the specific evaporation heat:

$$\Delta Q = m \cdot c \cdot \Delta T \quad (6.3)$$

With a value of 2290 K for ΔT and $4200\frac{\text{J}}{\text{kgK}}$ at standard pressure for c , the amount of energy that can be dissipated by the injection of 35 kg/s by the VCS comes to 337 MW , while the result for the injection of 2 kg/s by the EBS gives a value of 19.2 MW . These values indicate that the injection with the VCS should be able to dissipate the decay heat of about 45 MW easily, while the EBS can only dissipate 43% of the decay heat.

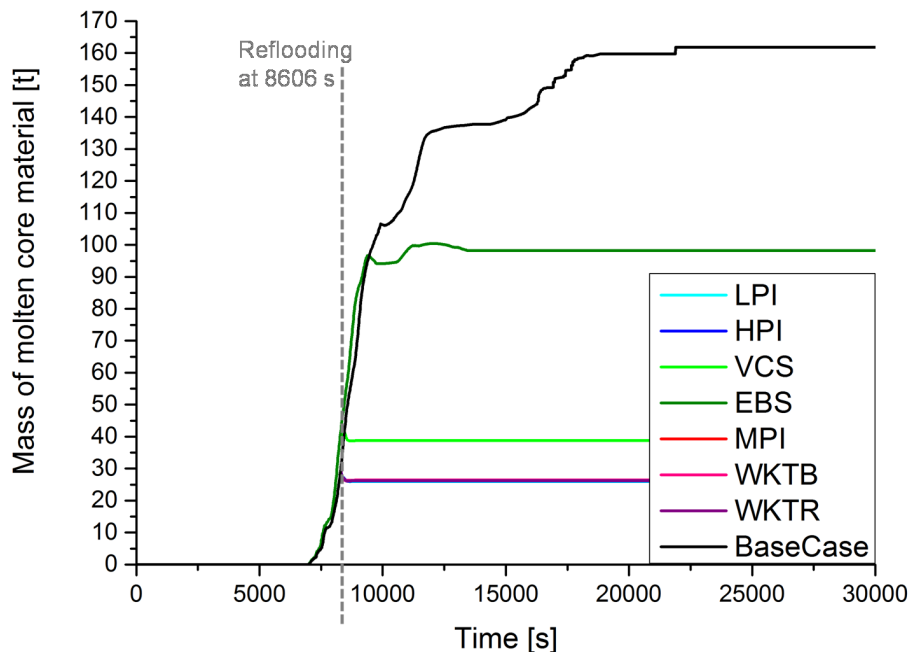


Figure 6.15: Mass of molten core material obtained in study B

Considering the mass of molten core material shown in figure 6.15, the final value in the VCS simulation is 38.79 t and 98.25 t in the EBS simulation. In comparison, the mass of molten core material reaches a value of 156 t in the BaseCase simulation without reflooding. This shows that even a water injection of a few kilos per second could save a considerable amount of core material from melting.

A similar behavior can be observed for the hydrogen production during the evolution of the accident shown in figure 6.16. The final value for the VCS simulation is 325.2 kg and 443.7 kg for the EBS simulation. 590.4 kg of hydrogen were produced in the

6 Discussion of the results

BaseCase simulation, thus proving that the reduced amount of molten core material even in the EBS simulation leads to a reduction in the amount of produced hydrogen as well.

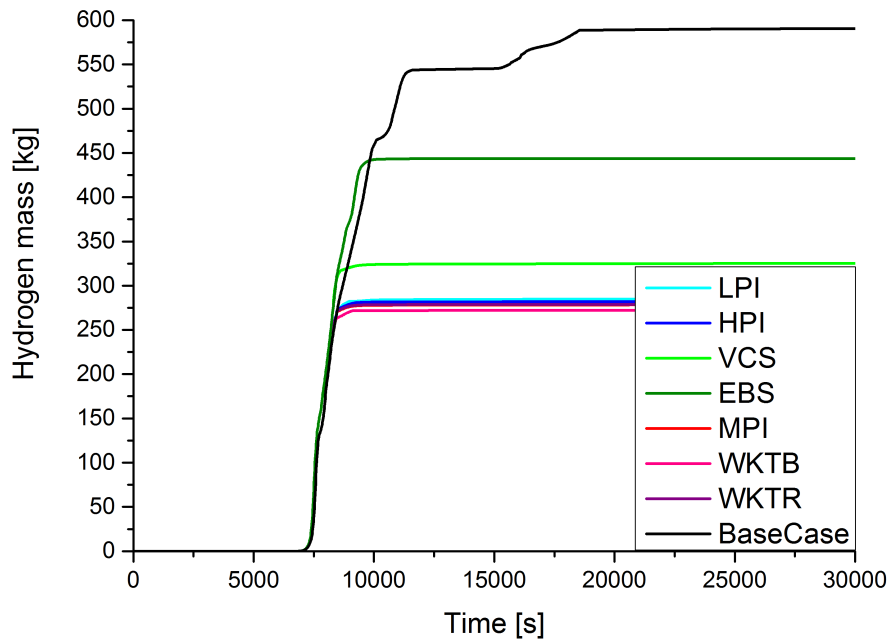


Figure 6.16: Mass of hydrogen produced in study B

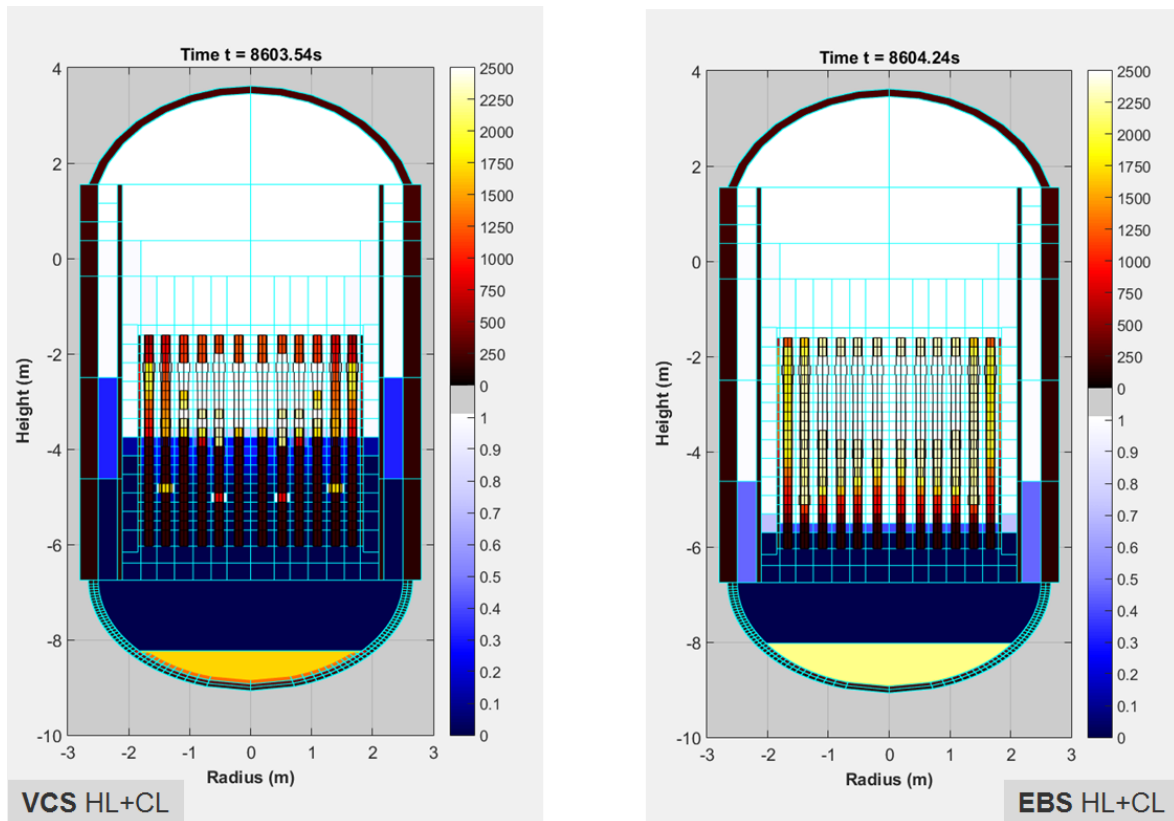


Figure 6.17: Comparison of the core status after 5 minutes of reflooding for simulations A3B3C3D4 (VCS) and A3B4C3D4 (EBS)

6.3 Study B: Variation of the reflooding system

5 minutes into the reflooding, the core status in the VCS simulation looks even slightly better than in the LPI simulation, because the VCS system is modelled with a pressure independent injection mass flow rate (see fig. 6.17), which can be considered realistic since the VCS is designed to work under nominal reactor operation conditions ($\sim 16 \text{ MPa}$). This results in the core being quenched to more than 50 % using the VCS system for the reflooding, while in the LPI simulation (see fig. 6.12), the reflooding is still stuck in the pressure built-up, which counteracts the injection. In the EBS simulation (see fig. 6.17), not much can be seen after only 5 minutes of reflooding. The core status is very similar to the core status without reflooding, and the differences in the accident evolution between the BaseCase simulation and the EBS reflooding become important at a later point in the simulated sequence and can be seen better in the graphs than in the figures picturing the core status at a certain time.

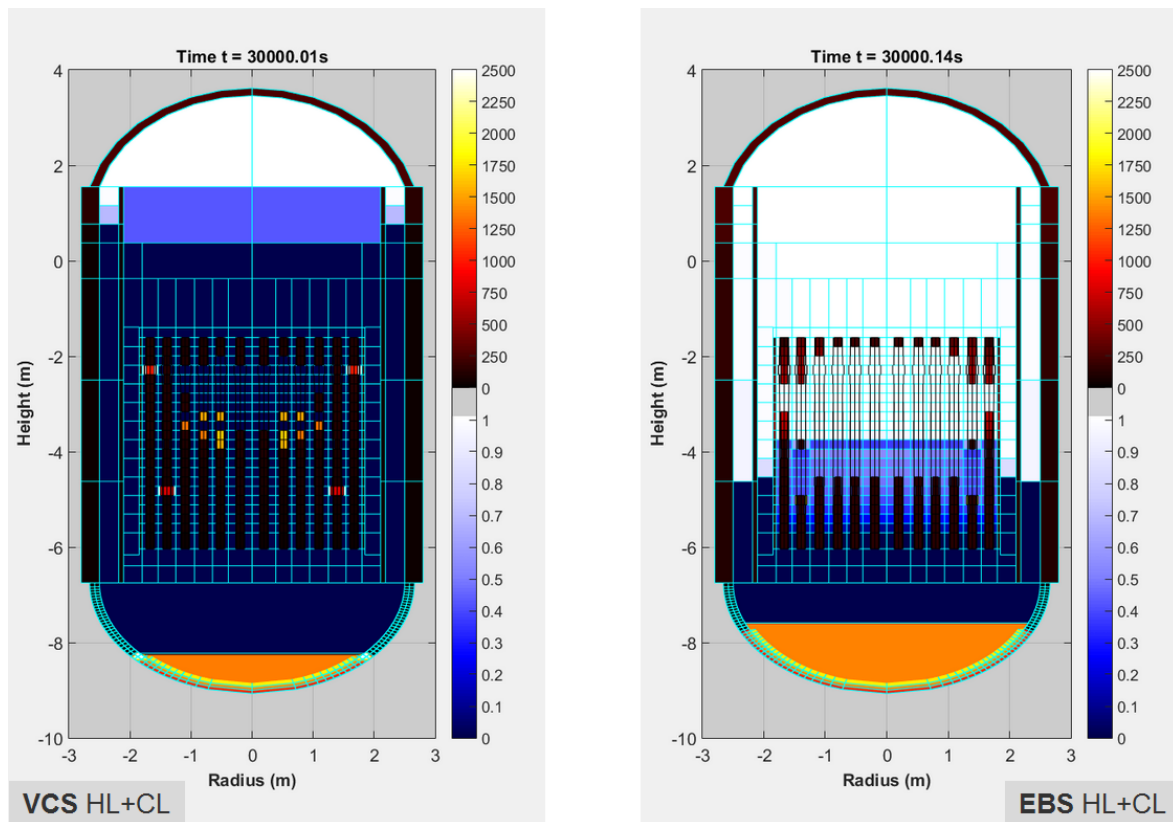


Figure 6.18: Comparison of the core status at the end of the simulation for simulations A3B3C3D4 (VCS) and A3B4C3D4 (EBS)

However, an assessment of the core status at the end of the simulation shown in figure 6.18 is of interest. In the VCS simulation, the RPV is now filled way above core level and the core is quenched with an exception of a few single nodes, which do not pose a threat to the power plant any more, as long as continuous cooling can be maintained. The EBS on the other hand is not able to fill the RPV above core level. This results in further core melting and continuous relocation to the lower plenum. At the end of the simulation, the core is quenched as well, but the amount of material relocated to the lower plenum is nearly four times as high as in the VCS simulation. This result indicates that an injection of 2 kg/s is not enough to stop the core melting process quickly, even though it mitigates the amount of relocated material in comparison to the BaseCase scenario by a factor of 0.57.

6 Discussion of the results

It can be seen however that in both the VCS and EBS simulation, the amount of core material relocated to the lower plenum is higher than in the reflooding with bigger pump systems as shown in figure 6.19. In case of the EBS simulation, roughly 100 t will end up in the lower plenum, leading to a condition that will most likely not be coolable no matter what the external conditions might be. In case of the VCS simulation, the relocated material might form a coolable debris bed, if the melt fragments during its interaction with the water in the lower plenum. For more information and a detailed discussion, see section 7.2.

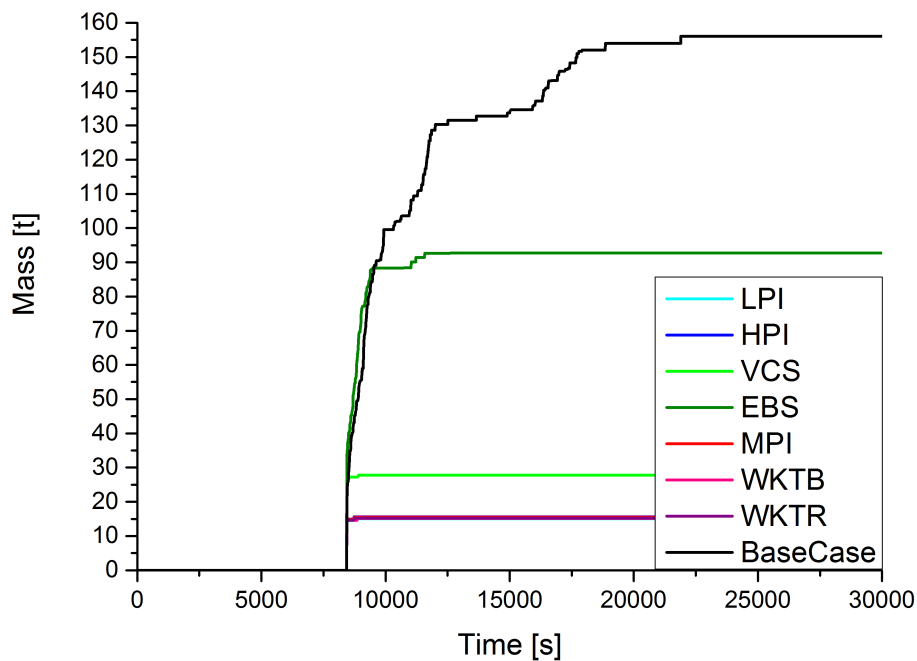


Figure 6.19: Mass relocated to the lower plenum in study B

6.3.4 Results for reflooding after the formation of 40 t or 50 t of melt

The simulations of study B conducted for the reflooding after 40 t and 50 t show basically the same results as the simulations for reflooding after 30 t. All systems with high injection rates (LPI, HPI, MPI, WKTB and WKTR) quench the core more or less fast, while producing similar amounts of hydrogen. The VCS and EBS systems are slower due to their lower injection mass flow rates, but nevertheless save a large amount of core material from melting and relocating to the lower plenum.

A difference between the study conducted for reflooding after 30 t and the studies for reflooding after 40 t and 50 t can be found in the power balance of the reactor. The power balance was calculated as a sum of powers created inside the reactor core and powers lost from the core. For details see section 6.1.4

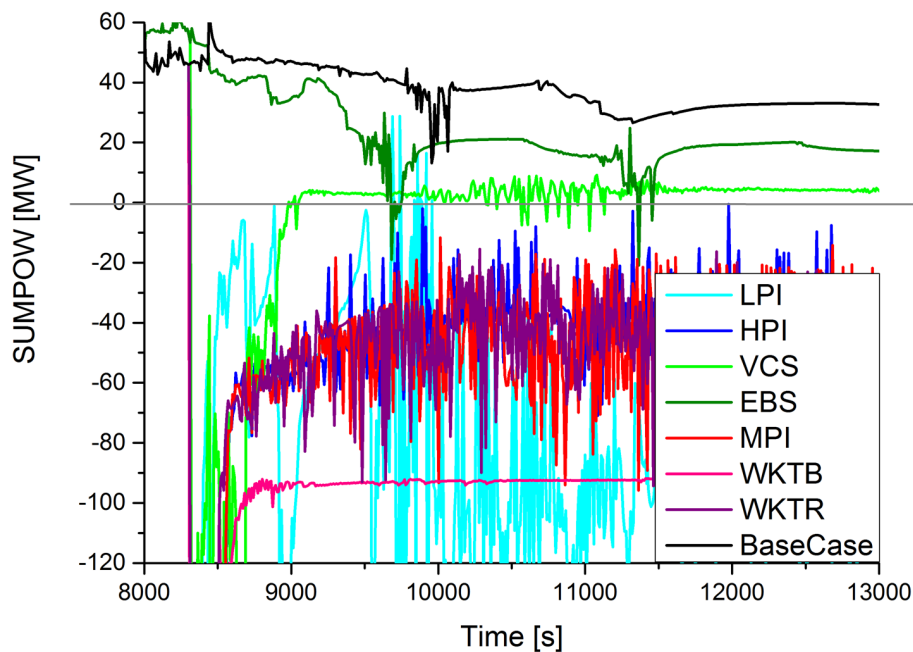


Figure 6.20: Power balance of the reactor in study B for reflooding after 30 t

In the study with reflooding after 30 t, shown in figure 6.20, the VCS system is able to bring the power balance close to zero, meaning that the amount of energy produced inside the core is nearly completely removed to the structures and surrounding fluid, creating a kind of meta-stable cooling condition. In the EBS and BaseCase simulation, the power balance is clearly positive, which indicates an insufficient cooling, because more heat is generated than can be removed. All other simulations show highly negative power balances. This indicates a removal of high amounts of energy from the core, leading to its fast quenching.

A comparison to the study with reflooding after 40 t reveals that the VCS is no longer able to bring the power balance close to zero. In fact it remains at a low positive value, meaning that the core should slowly heat up despite of the water injection. The stronger systems on the other hand all quickly bring the power balance to zero, thus quenching the core and keeping it in a coolable condition afterwards.

6 Discussion of the results

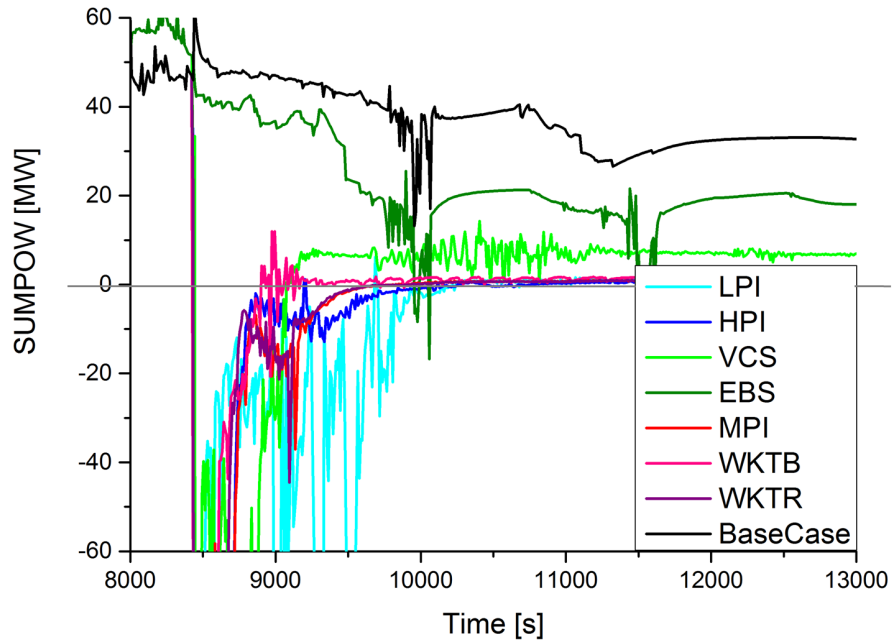


Figure 6.21: Power balance of the reactor in study B for reflooding after 40 t

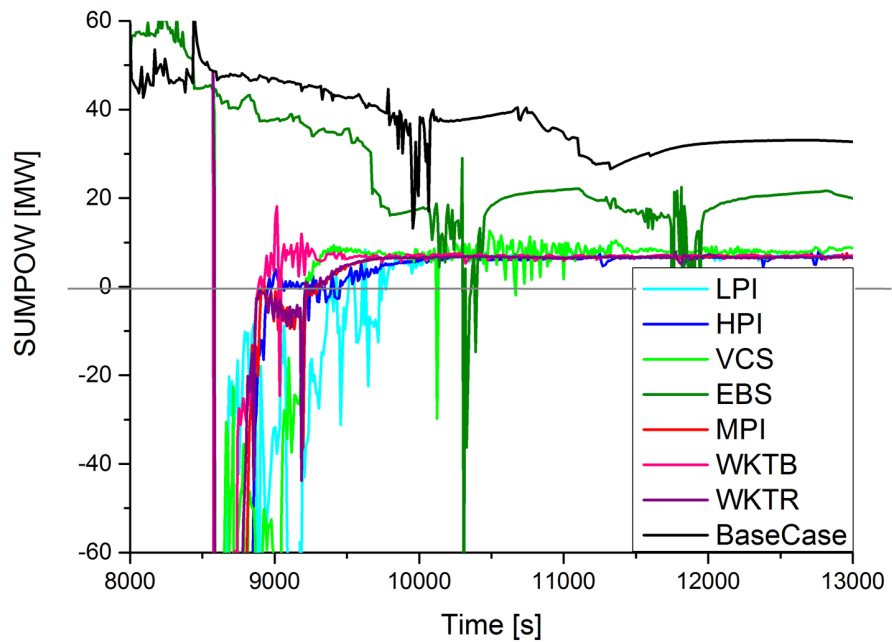


Figure 6.22: Power balance of the reactor in study B for reflooding after 50 t

Power balance studies conducted with reflooding after 50 t prove the alleged trend derived from the studies for reflooding after 30 t and 40 t . In figure 6.22, it can be seen that the VCS produces a power balance of positive value, just as the systems with higher pressure heads do. The reason for this behaviour is that the power balance does not consider the melt in the lower plenum. Thus, the stronger the core degradation is and the more material has been relocated to the lower plenum, the less decay heat is considered necessary to remove from the core area, which is why the VCS now removes as much heat as the bigger systems.

6.4 Study C: Variation of the reflooding location

By default, the LPI inject into both the hot and cold legs at the same time. But with regard to the self-blocking effect, a pure bottom flooding condition might be advantageous because it reduces the counter current flows in the core area and might reduce the pressure built-up in the RPV. It is possible, to switch the LPI from injecting into both the hot and cold legs of each loop to injecting into either only the hot or only the cold legs even though it is not standard procedure. The goal in study C was to investigate whether the injection location and the resulting core flooding conditions have an influence on the outcome of the simulation. These conditions have been described in section 5.3.

6.4.1 Reflooding via the cold legs

Reflooding using only the cold legs leads to a bottom flooding condition. During a bottom flooding, the water enters the core from below, while the produced steam rises to the top of the RPV and leaves the system through the leak in the hot leg. This means that entering water and exiting steam flow in the same direction, thus not creating unnecessary counter-current flow conditions. For this reason, bottom flooding is generally considered to be more effective than top flooding.

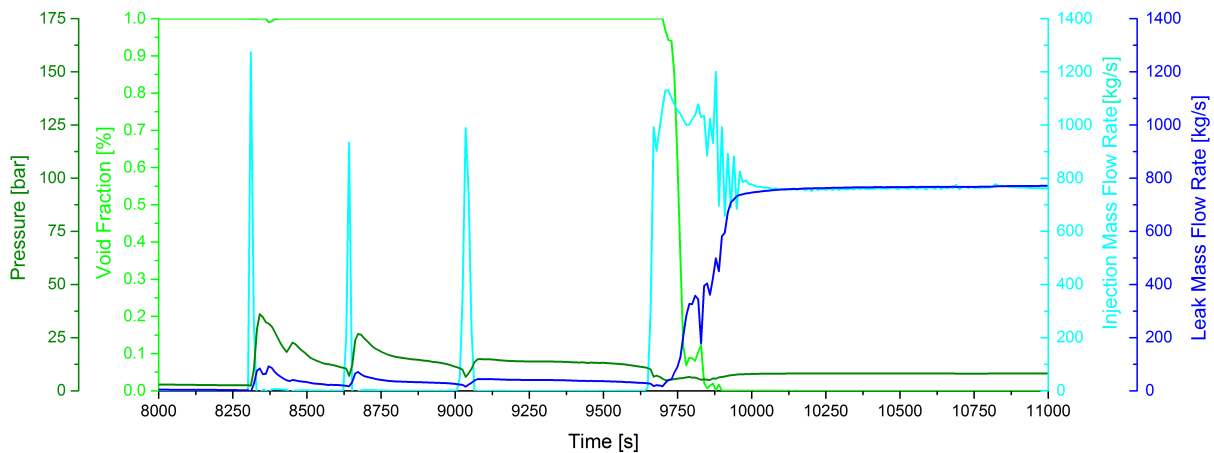


Figure 6.23: Comparison of the leak and injection mass flow rates with the pressure and void near the leak position for simulation A3B1C1D4 (CL)

In figure 6.23 the previously discussed behaviour of the LPI reflooding is clearly visible. The start of the injection leads to a pressure built-up, which shuts the injection down again. This is repeated three times, and it takes 22.5 min until the LPI can start to inject water continuously.

Interestingly, the dead time is even a little higher than with the combined top and bottom flooding condition, achieved by injecting into both the hot and the cold legs of the system, where it took 20 min for the pressure to decrease far enough for the LPI to start working continuously (see figure 6.10). This finding is opposed to the fact that

6 Discussion of the results

the summarized amount of water injected during the peaks is 7 t lower in the bottom flooding simulation than it was in the combined top and bottom flooding simulation. The prolonged shut-down time can thus not be explained by a higher pressure due to a higher amount of injected water.

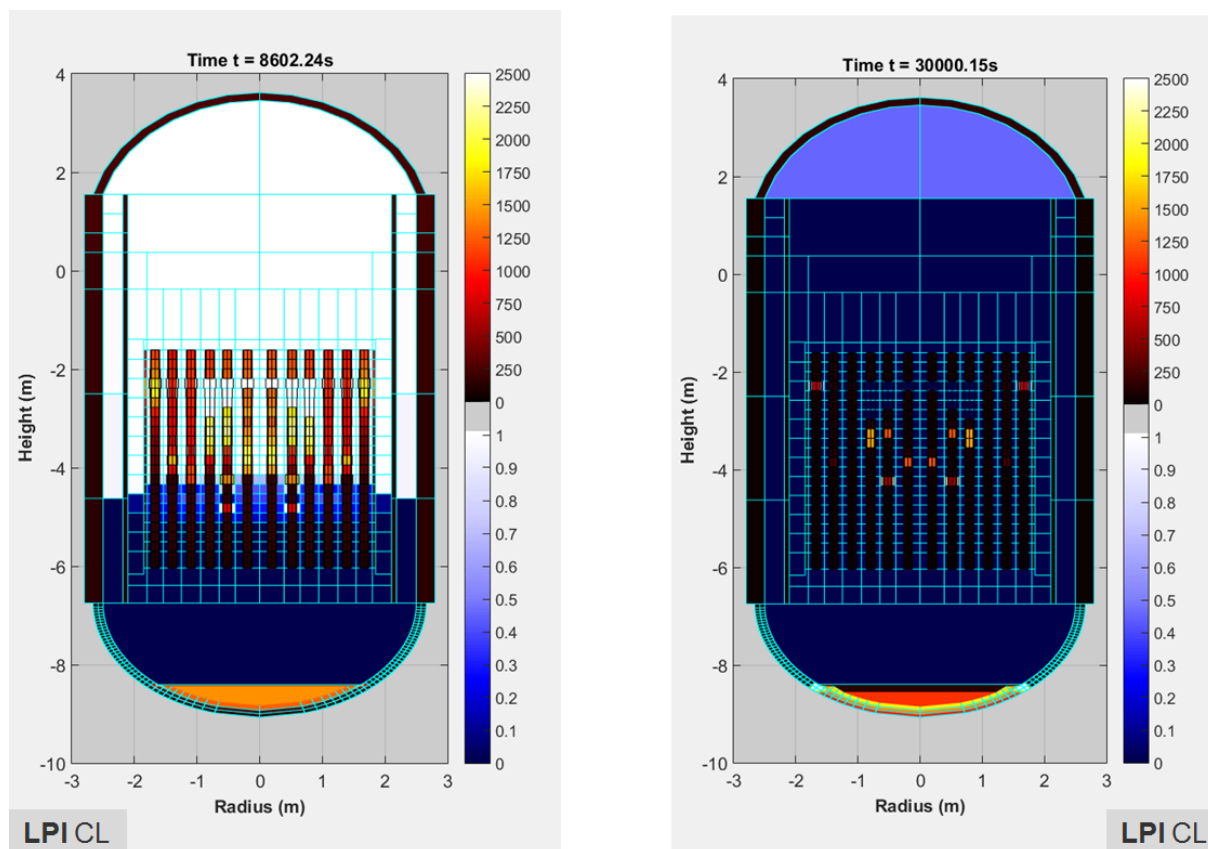


Figure 6.24: Comparison of the core status after 5 minutes of reflooding and at the end of the simulation for simulation A3B1C1D4 (CL)

The core status during the cold leg reflooding shown in figure 6.24 however does not differ significantly from the combined hot and cold leg reflooding shown in study A (see figure 6.3). At the end of the simulation, the resulting core configuration is virtually identical.

6.4.2 Reflooding via the hot legs

Using only the hot legs for the reflooding, leads to a top and bottom flooding condition. This condition is characterized by strong counter current flows inside the core area, because the water flowing down into the core is opposed by steam rising upwards.

This condition is expected to be less effective than the bottom flooding, and the simulation results confirm this expectation. Figure 6.25 shows the reflooding through the hot legs, and it can clearly be seen that it takes more than half an hour (32.8 min to be exact) for the LPI to establish a continuous injection, thus confirming the expectation of top flooding being less efficient than pure bottom flooding.

6.4 Study C: Variation of the reflooding location

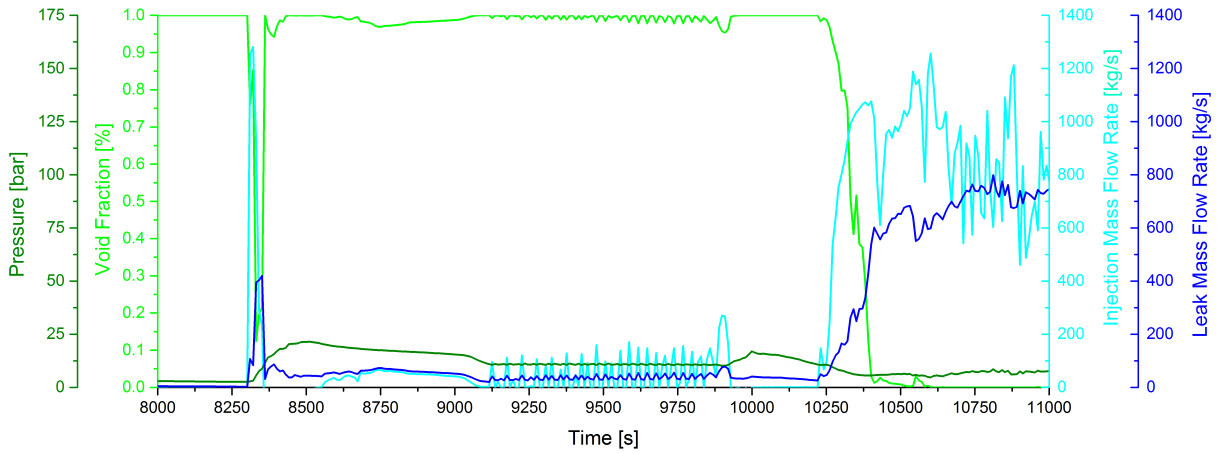


Figure 6.25: Comparison of the leak and injection mass flow rates with the pressure and void near the leak position for simulation A3B1C2D4 (HL)

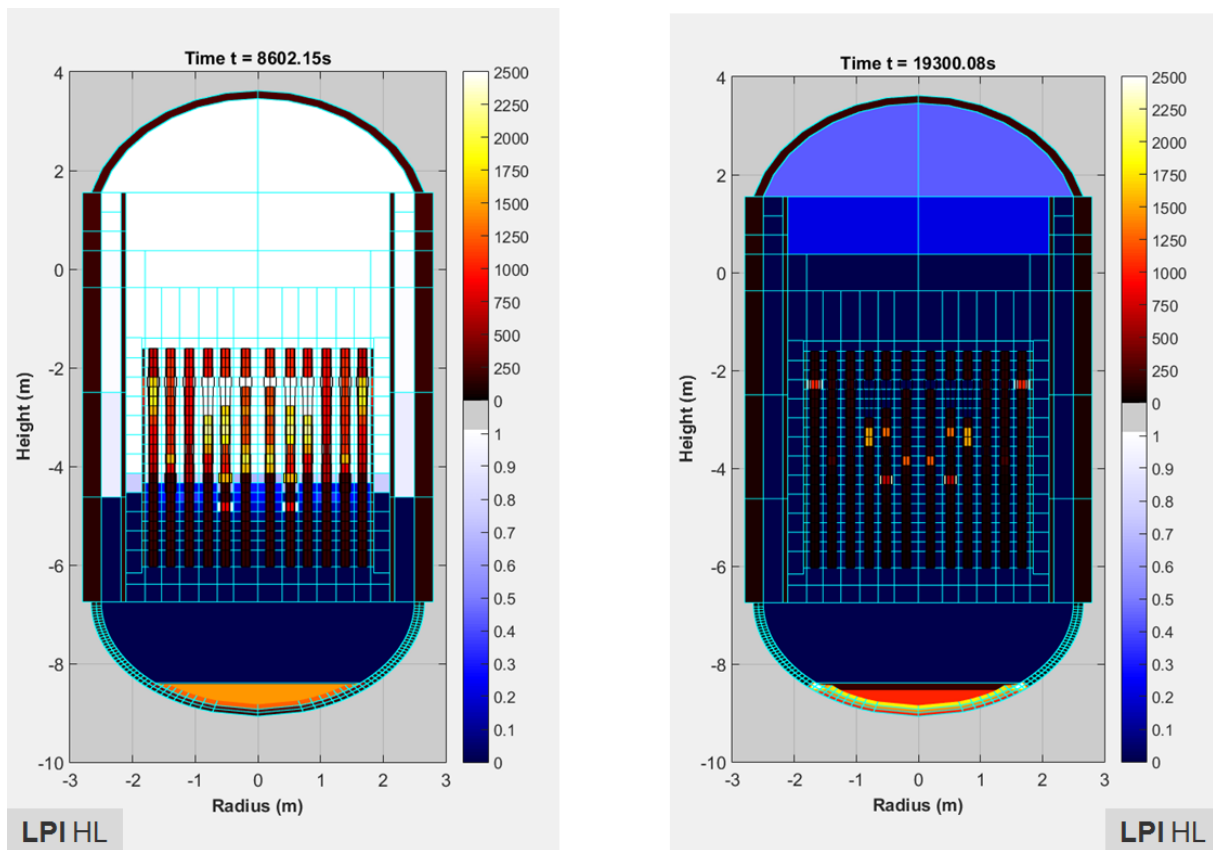


Figure 6.26: Comparison of the core status after 5 minutes of reflooding and at the end of the simulation for simulation A3B1C2D4 (HL)

Nevertheless, the core status both after 5 minutes of reflooding and at the end of the simulation shown in figure 6.26 does not differ significantly from the combined reflooding in study A (see figure 6.3). These results prove that the choice of injection location is a lot less relevant than the choice of reflooding system, which was shown in study B.

6.5 Study D: Variation of the number of available pumps

This study was inspired by the safety principle of redundancy and the underlying assumption that in case of an accident a certain fraction of systems like pumps might not be available. This is the reason why there are always a higher number of safety relevant systems on site than needed. The question arose, whether instead of the usual four pumps three or less pumps might have a chance to quench a partially molten reactor core as well. Another question is, whether a successful quenching can be achieved by a high injection rate (number of pumps) rather than a high pump pressure (type of pump). In study D simulation A3B1C3D4 (reflooding with the LPI after 30 *t*) was taken as basis, where all four LPI pumps are working properly. Derived from this, simulation A3B1C3D3 was conducted with three LPI pumps available, A3B1C3D2 with two and A3B1C3D1 with only one LPI pump.

Figure 6.27 shows the resulting core status at 5 minutes after the start of reflooding for all four simulations. It can be seen that the temperatures in the core are the lower the more pumps are available, even though the water inventory in the core is not significantly different in the four simulations. This is due to the fact that the water mass injected during the first 5 minutes of reflooding varies from 19.10 *t* in case of four available pumps to 14.61 *t* in the simulation where only one pump is available. The water hits the core from the top, where it evaporates quickly thus cooling the fuel rods. In accordance to the different amounts of injected water, the pressure peak height varies from 3.03 *MPa* reached after 80 *sec* of reflooding in case of all four pumps available to 1.91 *MPa* after 30 *sec* of reflooding in the simulation with only one pump available.

At the end of the simulation, the core status of simulation A3B1C3D1 (one pump) is very different from the core status in the other three simulations, shown in figure 6.28. While the other three pump configurations manage to quench the core completely sooner or later, the RPV remains less than half filled in the simulation with only one pump. This effect can be explained by looking at the reflooding evolution in figure 6.30.

From top to bottom, the reflooding evolution is shown for decreasing available pumps number. In simulation A3B1C3D4 (four pumps available) the self-blocking effect of the LPI system is clearly visible, and it takes 20.3 *min* until the LIP can establish a continuous water injection. Using three instead of four pumps for the reflooding expands the self-blocking effect, and in simulation A3B1C3D3 it takes 41.1 *min* until a continuous injection can be established. In simulation A3B1C3D2 only two LPI pumps were assumed to be available, and the time during which the self-blocking controls the reflooding has expanded to 119.5 *min*.

With only one pump available, the self-blocking effect cannot be overcome completely during the simulated 30,000 *s*. Though the pressure built-up is not high enough to shut the LPI pump down completely, it remains with an injection rate of roughly 25 *kg/s* and a system pressure of 1.06 *MPa* throughout the simulation time, showing an equilibrium state between decay heat and dissipated heat by evaporation on the one hand, and between water injection and pressure on the other hand.

6.5 Study D: Variation of the number of available pumps

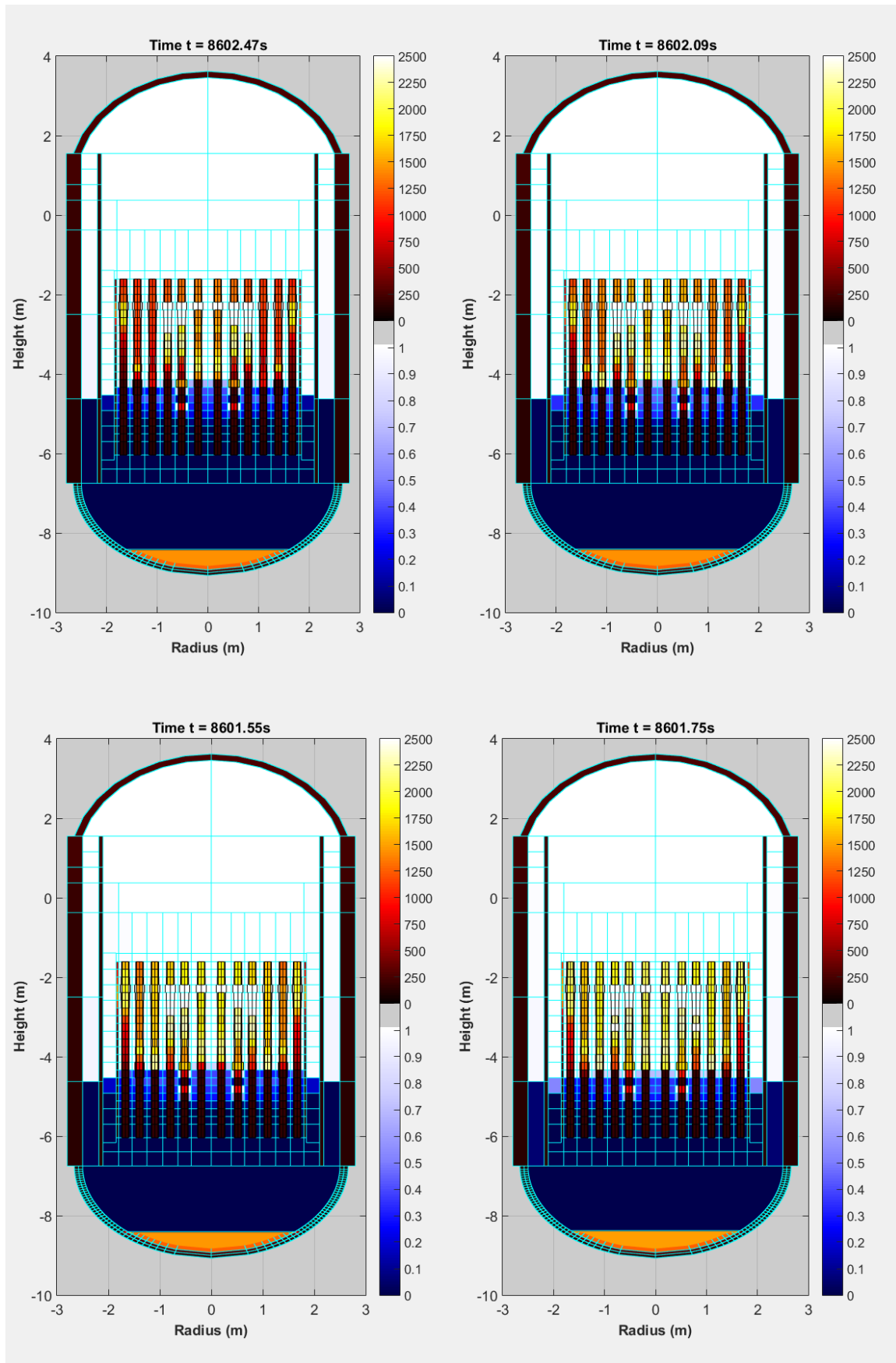


Figure 6.27: Comparison of the core status after 5 minutes of reflooding for the simulations of study D (top left: A3B1C3D4 - four pumps, top right: A3B1C3D3 - three pumps, bottom left: A3B1C3D2 - two pumps, bottom right: A3B1C3D1 - one pump)

6 Discussion of the results

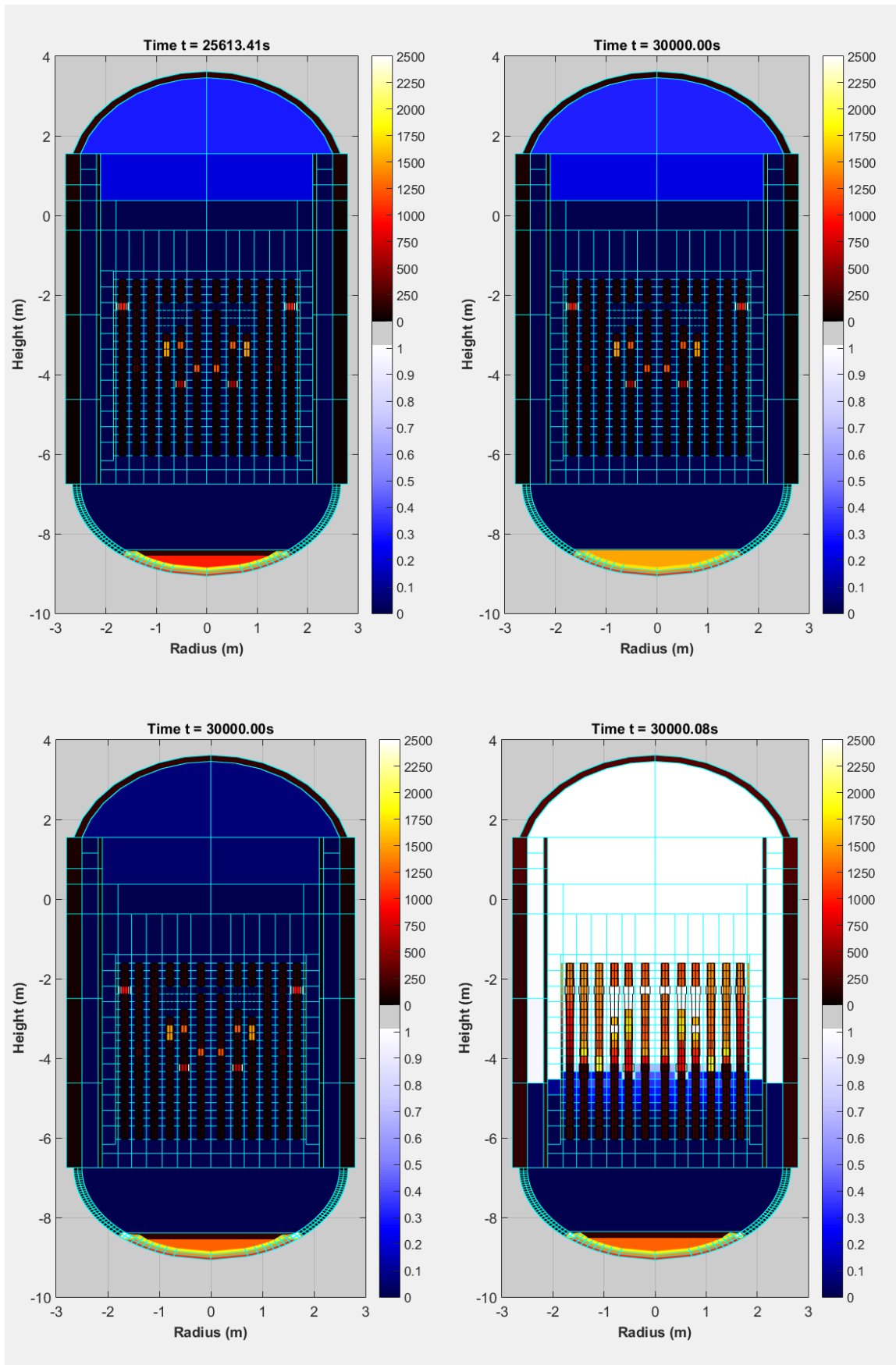


Figure 6.28: Comparison of the core status at the end of the simulations of study D (top left: A3B1C3D4 - four pumps, top right: A3B1C3D3 - three pumps, bottom left: A3B1C3D2 - two pumps, bottom right: A3B1C3D1 - one pump)

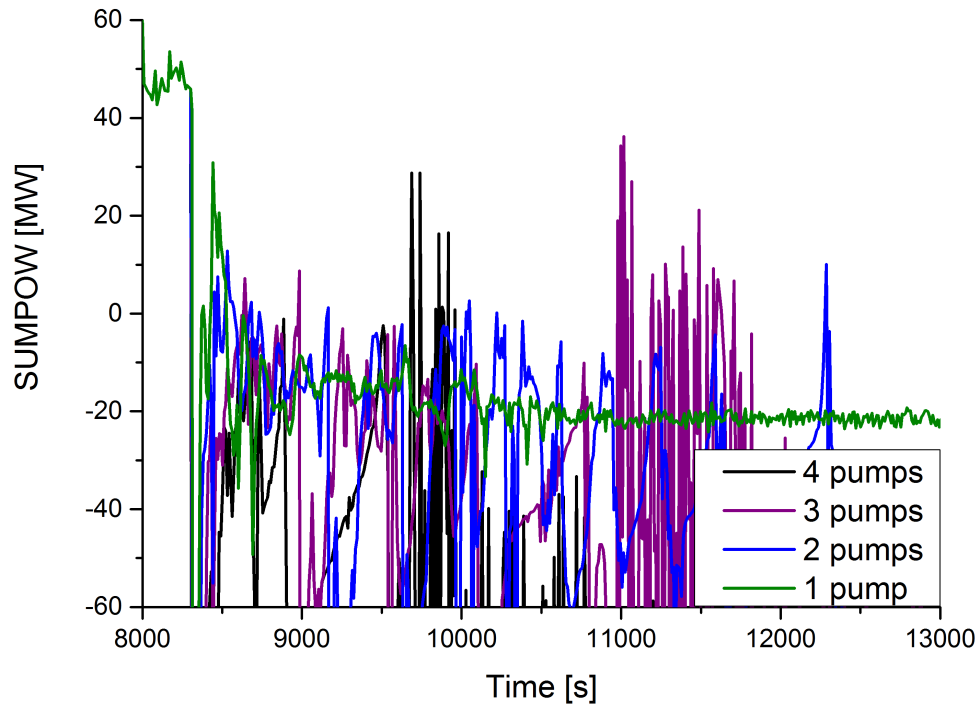


Figure 6.29: Power balance of the reactor in study D for reflooding after 30 t

A look on the power balance shown in figure 6.29 on the other hand reveals that in all four simulations investigated in study D the reactor should be coolable, because SUMPOW is negative, meaning that less energy is produced in the reactor core than is dissipated to the surroundings. This finding led to another conduction of simulation A3B1C3D1, but with a simulation time twice as high as before (60000 s instead of 30000 s). The expectation was to see the self-blocking effect collapse sometime after 30000 s , and the core being quenched completely in the aftermath.

Unfortunately, no collapse of the self-blocking effect could be observed. Pressure and injection rate remain the same, and the injection is blocked further until the end of the extended simulation at 60000 s . The core status after 60000 s on the other hand, is different as shown in figure 6.31. The water level has not improved much, but the steam cooling is taking effect on the temperatures of the fuel remaining inside the core area. After 60000 s , most of the nodes show a temperature below 1000 $^{\circ}C$, meaning that the materials have solidified and should be coolable by now.

Figure 6.32 shows a section of the reflooding evolution, where a small disturbance can be seen. This disturbance happens at the same time as the temperature drop that can be observed throughout the core (see fig. 6.33), as well as the small rise of the water level inside the core area.

During the 1000 s of disturbance, the pressure decreases a little, enabling the LPI to rise its injection rate. The previous balanced cooling condition is thus disrupted, leading to injection peaks nearly four times as high as before. In the time interval between 18500 s and 19500 s , a water mass of 37.02 t is injected into the core compared to the average 29.70 t of water that would have been injected during this time in the previous balanced cooling condition.

6 Discussion of the results

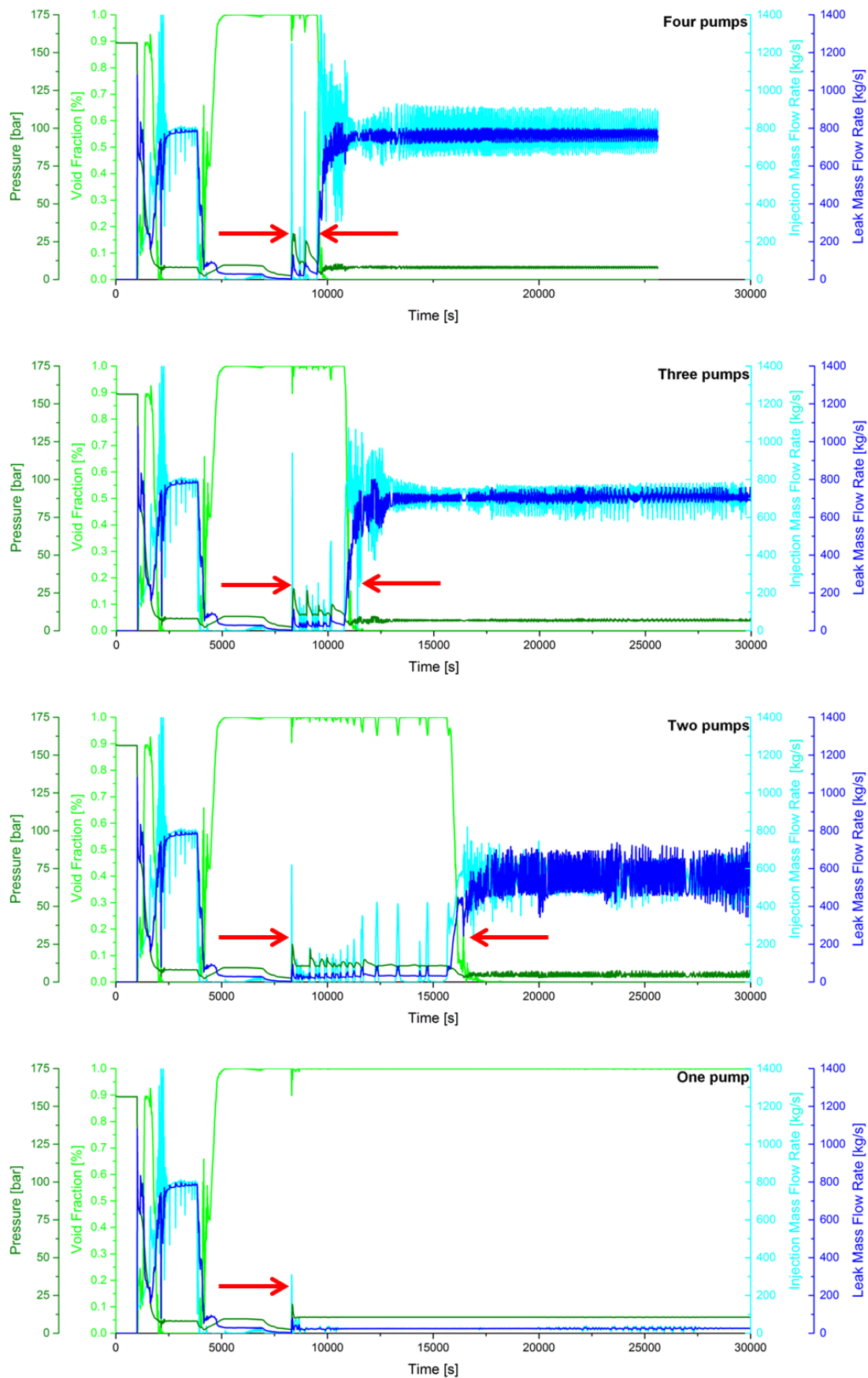


Figure 6.30: Comparison of the reflooding evolution for the simulations of study D (from top to bottom: A3B1C3D4 - four pumps, A3B1C3D3 - three pumps, A3B1C3D2 - two pumps and A3B1C3D1 - one pump)

6.5 Study D: Variation of the number of available pumps

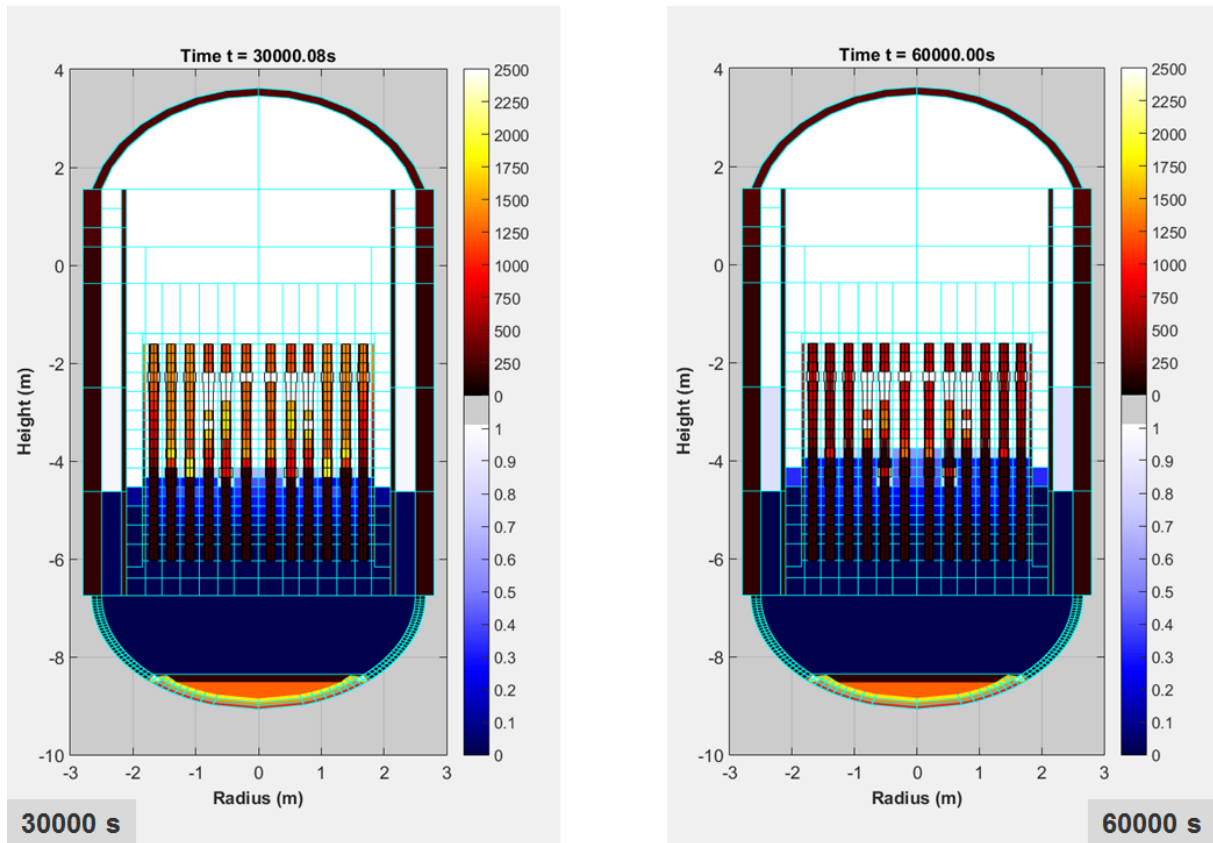


Figure 6.31: Comparison of the core status at the original end of simulation A3B1C3D1 (one pump) and after an additional 30000 s of simulation time

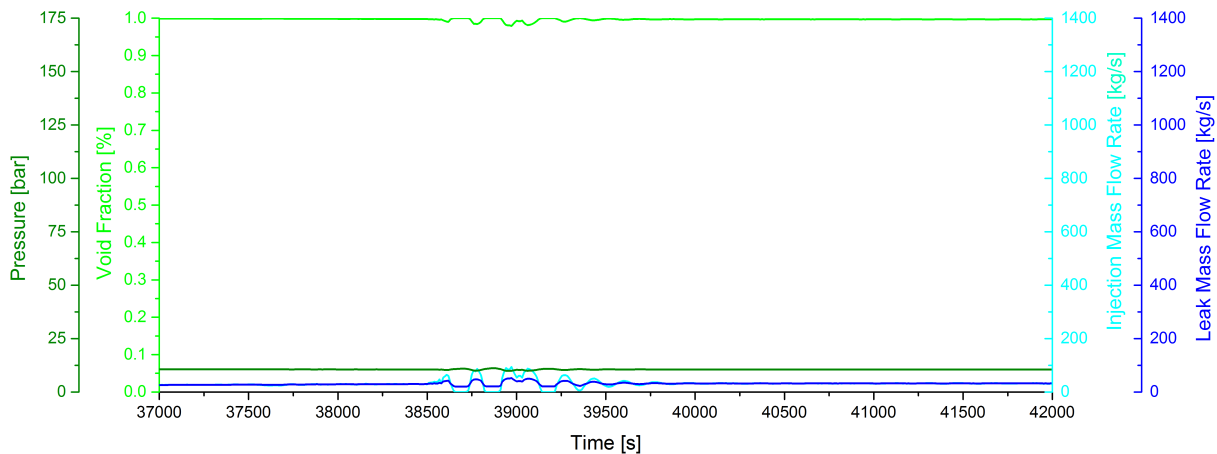


Figure 6.32: Comparison of the leak and injection mass flow rates with the pressure and void near the leak position for simulation A3B1C3D1 (one pump) after an additional 30000 s of simulation time

So an additional amount of 7.32 t of water is injected during the disturbance, which leads to the abrupt cooling of still hot upper core parts. The water levels in the core rise only about 0.3 m over the time interval of the disturbance, while the core temperatures drop rapidly by up to 700 °C.

6 Discussion of the results

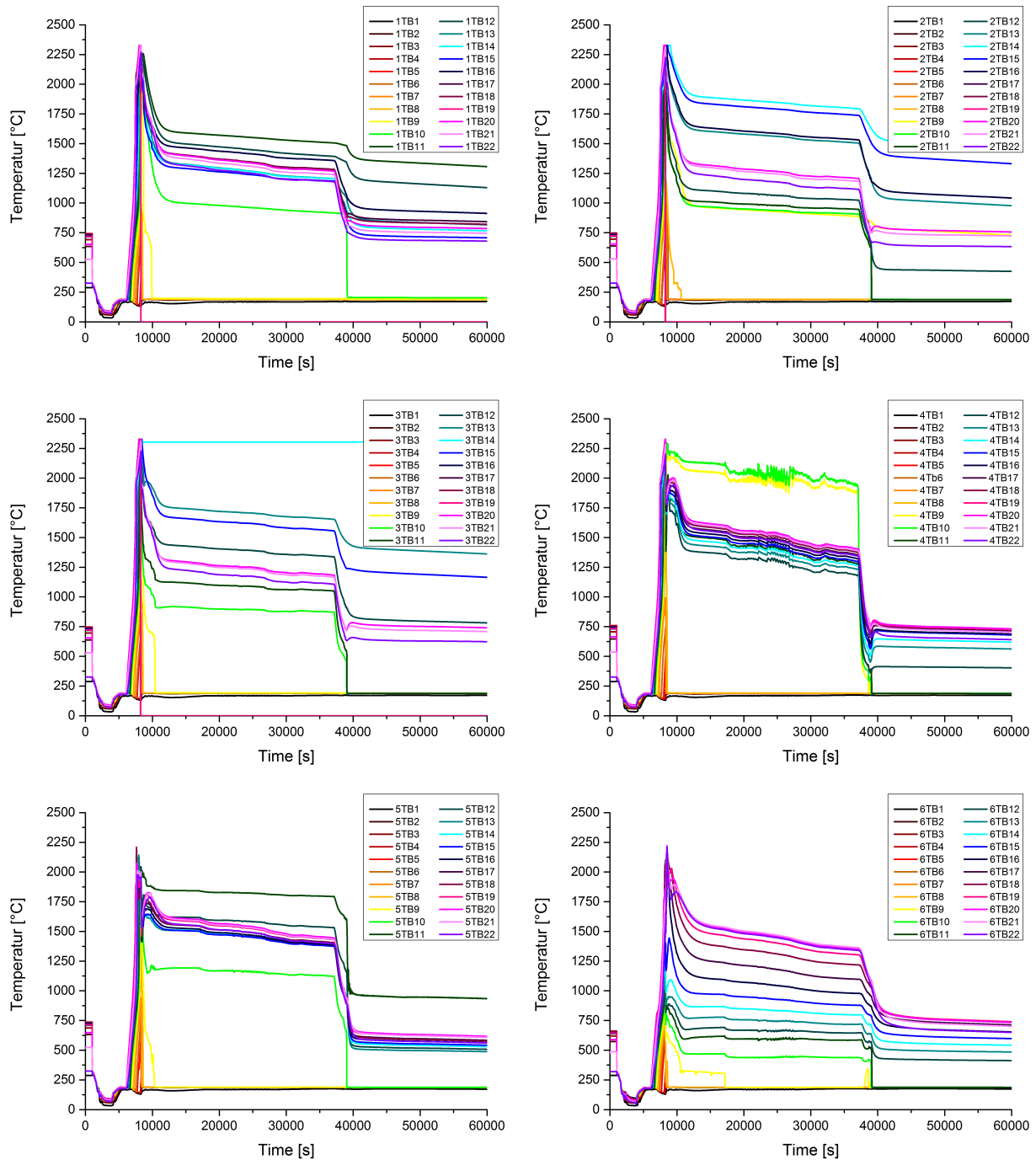


Figure 6.33: Fuel temperature evolution in the six core channels during the extended simulation A3B1C3D1 (one pump)

7 Sensitivity and uncertainty considerations

In this chapter, some considerations shall be made concerning the sensitivities and uncertainties of the conducted simulations with the ATHLET-CD code systems. This is necessary, because not only the user-given input data contains uncertainties and assumptions, but also the simulation tool itself.

It is beyond the scope of this work to give a full overview of all the assumptions and models used in the ATHLET-CD code system, but at least two important factors will be discussed. These two have been chosen, because they had a major impact on the conducted simulations presented in this work.

7.1 The BLOCKAGE input parameters

The BLOCKAGE input parameters are porosity boundaries used in the BLOCKAGE module of the E CORE module for the simulation of melt path blockage during core melting. It is a very coarse modelling approach, where the values for radial and axial coolant flow as well as convective heat transfer to fluid are artificially decreased to zero one after another, after which the radiative heat transfer is strongly increased before the value for melt candling is decreased to zero as well. All shown simulations have been conducted with the default values given in table 2.2, which were taken from the ATHLET-CD User Manual [27]. Unfortunately, no further information on these values or the blockage model itself was available.

From a purely geometrical point of view, the default values seem to be too high. A good value to stop the radial coolant flow would be when the fuel rods are just touching each other due to the enlargement of their diameter due to candling and accumulation of melt (see fig. 7.1). With the geometry values given in table 3.2, the value of the initial porosity is 57.4%, while the porosity value of the touching fuel rods comes to 21.45%.

Opposed to this, the default value used for the stop of radial flow in the BLOCKAGE module is 27%. Only 2% lower, at a porosity value of 25%, the axial flow is turned off as well, even though a quarter of the channel is still open - at least on average. Of course one could argue that the candling is not uniform over the core and that even with a porosity value of 25% a node can be blocked off from coolant ingress. Nevertheless, since no other information on the model or underlying considerations is available, a critical assessment is not possible.

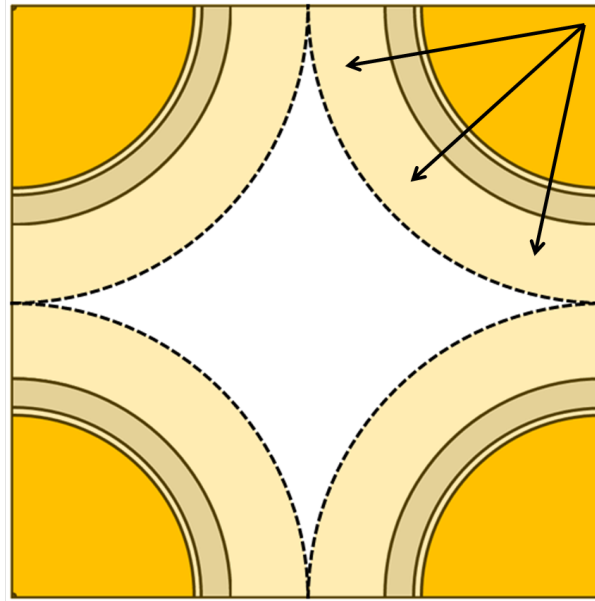


Figure 7.1: Schematic of the enlarged fuel rod diameter due to candling of melt

In order to assess the impact of the BLOCKAGE parameters, simulation A3B1C3D4 (30t, LPI HL+CL) was chosen as basis. Now two more simulations were conducted in which the BLOCKAGE values were raised by 10 % or reduced by 10 % respectively. The resulting values are summarized in table 7.1.

Table 7.1: BLOCKAGE values used in the BLOCKAGE study

Simulation	POPEN	PCLSR	PCLSX	PCONV	BLOCKG
A3B1C3D4	0.30	0.27	0.25	0.20	0.10
A3B1C3D4 + 10 %	0.40	0.37	0.35	0.30	0.20
A3B1C3D4 - 10 %	0.20	0.17	0.15	0.10	0.00

The simulations showed different behaviour of the core melting process, which is mainly due to the changes in the parameters PCLSR and PCLSX, which limit the radial and axial coolant flow. By default they are set to 27 % and 25 % respectively, which means that in the +10% - simulation the radial and axial flows are turned off even sooner at 37 % and 35 %. This leads to an earlier blocking of the fuel channels and a lower cooling capability, since the water is less able to penetrate into the degrading core. On the other hand, the reduction in water ingress results in a reduced oxidation, thus decreasing the heat and hydrogen content produced by the zirconium reaction. Figure 7.4 shows mainly one oxidation peak, which occurs during the start of reflooding. It can be assumed that before reflooding the core was in a steam starvation condition, the ingress of water lead to a massive production of steam, thus enabling the zirconium oxidation.

In the simulation with reduced BLOCKAGE values (-10%), figure 7.2 shows an advanced degradation status of the core compared to the +10% - simulation. This might seem counterintuitive at first since the blocking of the channels occurs later in the simulation and the water should have enhanced penetration capabilities and thus

7.1 The BLOCKAGE input parameters

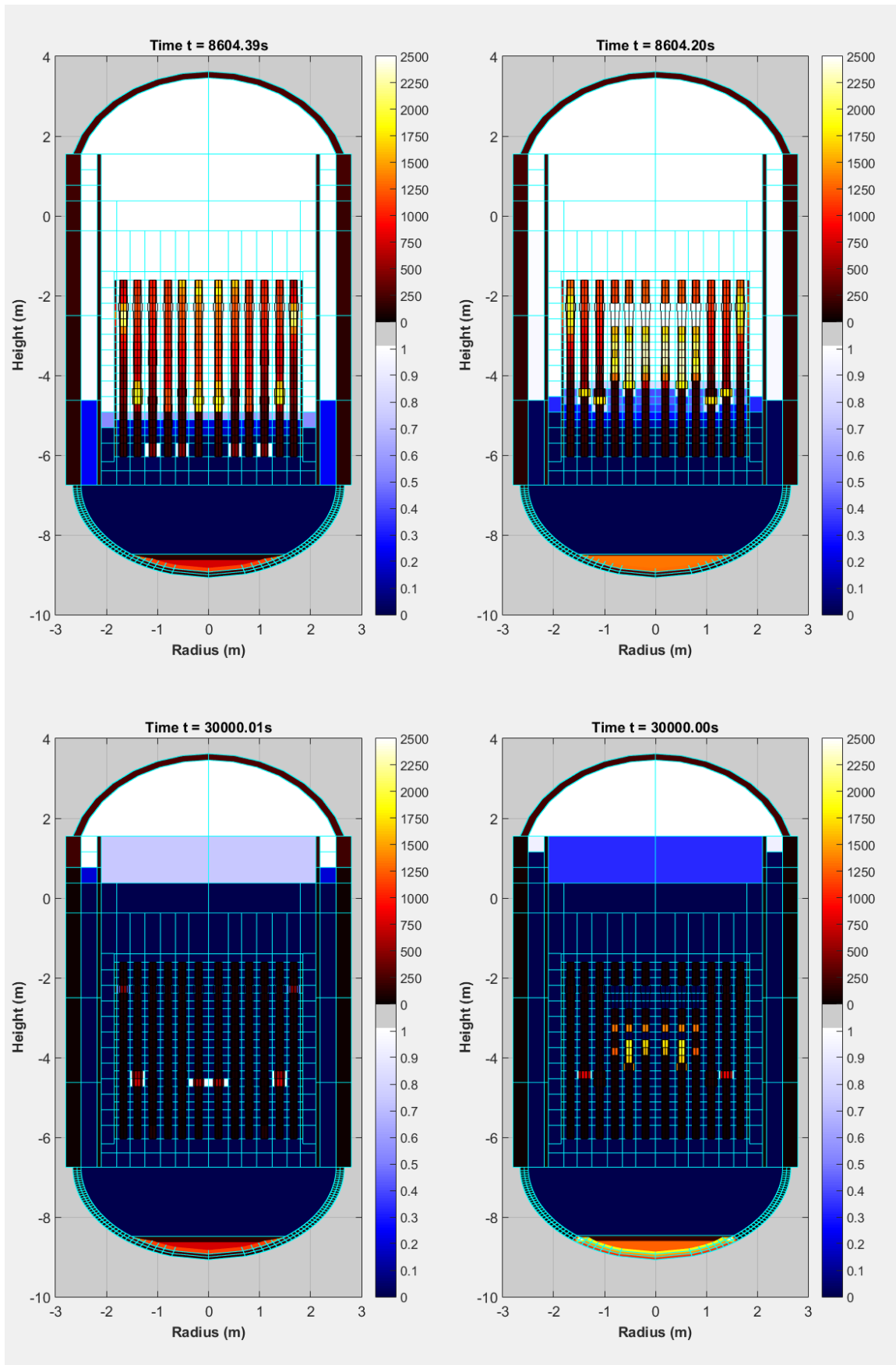


Figure 7.2: Comparison of simulation A3B3C1D4 with 10 % higher BLOCKAGE values on the left and simulation A3B3C1D4N with 10 % lower BLOCKAGE values on the right five minutes into the reflooding (upper row) and at the end of the simulation (lower row)

7 Sensitivity and uncertainty considerations

result in a better cooling. But it has to be taken into account that the reduction of the BLOCKAGE values also results in a higher oxidation and heat release, leading to a faster degradation of the core, even before the start of reflooding.

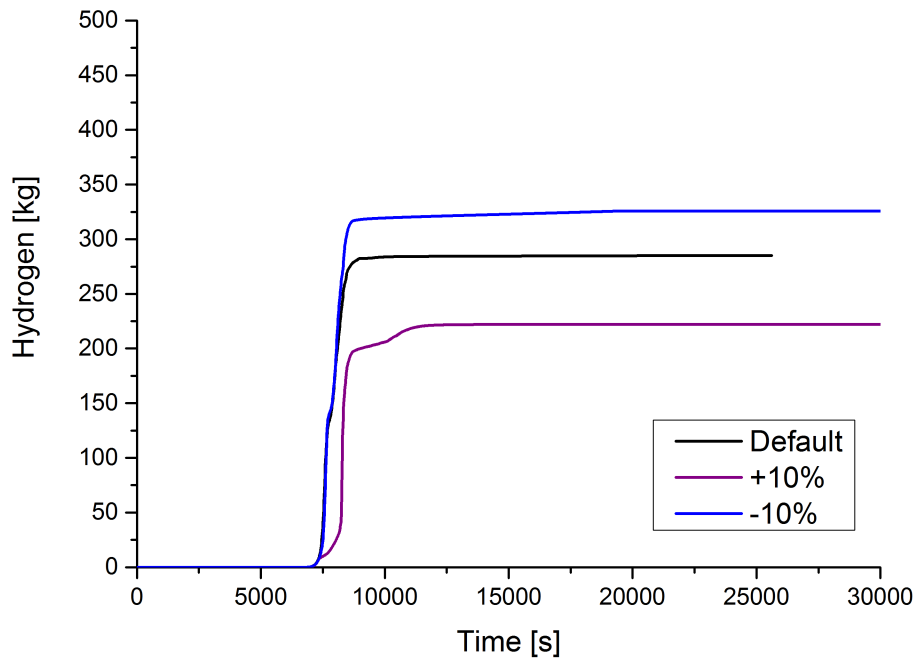


Figure 7.3: Comparison of the hydrogen production during the three simulations investigated in the BLOCKAGE study

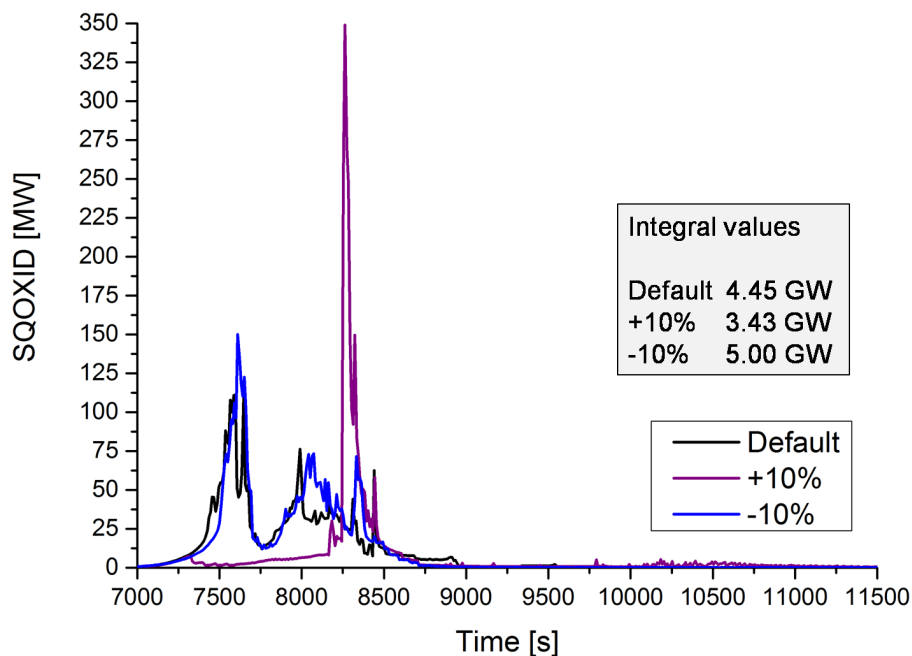


Figure 7.4: Comparison of the oxidation heat produced during the three simulations investigated in the BLOCKAGE study

The comparison of the hydrogen produced during the three simulations in figure 7.3 shows that the difference between the simulations with increased and decreased

BLOCKAGE values is more than 100 kg , the simulation with increased values being the one with the lowest hydrogen production, just as expected.

The comparison of the released oxidation heat in figure 7.4 confirms this result. Although the highest peak for the simulation with increased BLOCKAGE values is more than twice as high as in the other two simulation, the summarized heat release is only 3.43 GW , while in the simulation with default BLOCKAGE values the summarized oxidation heat is 4.45 GW , and 5.00 GW in the simulation with decreased BLOCKAGE values. This does also mean that the amount of heat that has to be dissipated from the core is reduced by 1 GW to 1.5 GW in total, leaving the simulation with increased BLOCKAGE values with the best (but most unrealistic) reflooding result.

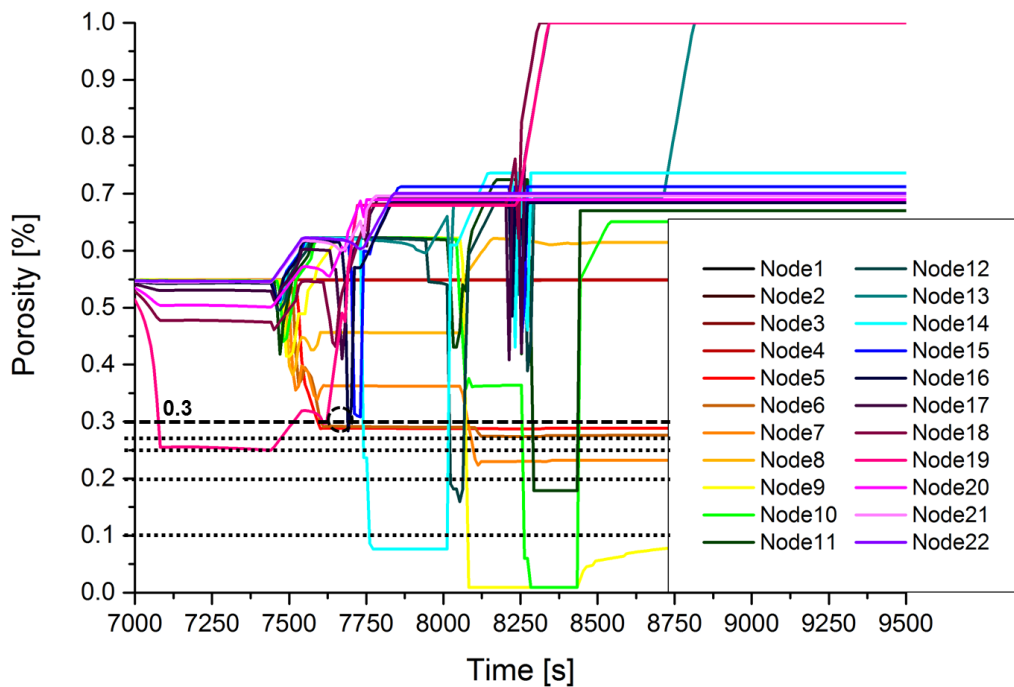


Figure 7.5: Porosity evolution in Rod 3 during the simulation with decreased BLOCKAGE values

Figure 7.6 shows a comparison of the reflooding evolution for the three simulations, and it can clearly be seen that the self-blocking effect of the LPI is stronger, the higher the BLOCKAGE values are. Nevertheless, the coolability of the core increases with increasing BLOCKAGE values, even though the quenching process itself takes longer. This is due to the fact that in the simulation with decreased BLOCKAGE values the porosity can decrease to zero, meaning a complete blocking of certain nodes.

The blocked nodes can be identified by looking at the porosity evolution, exemplarily shown in figure 7.5 for rod 3. The nodes with the lowest porosity are also the ones that remain at the highest temperatures, as can be seen in figure 7.2.

7 Sensitivity and uncertainty considerations

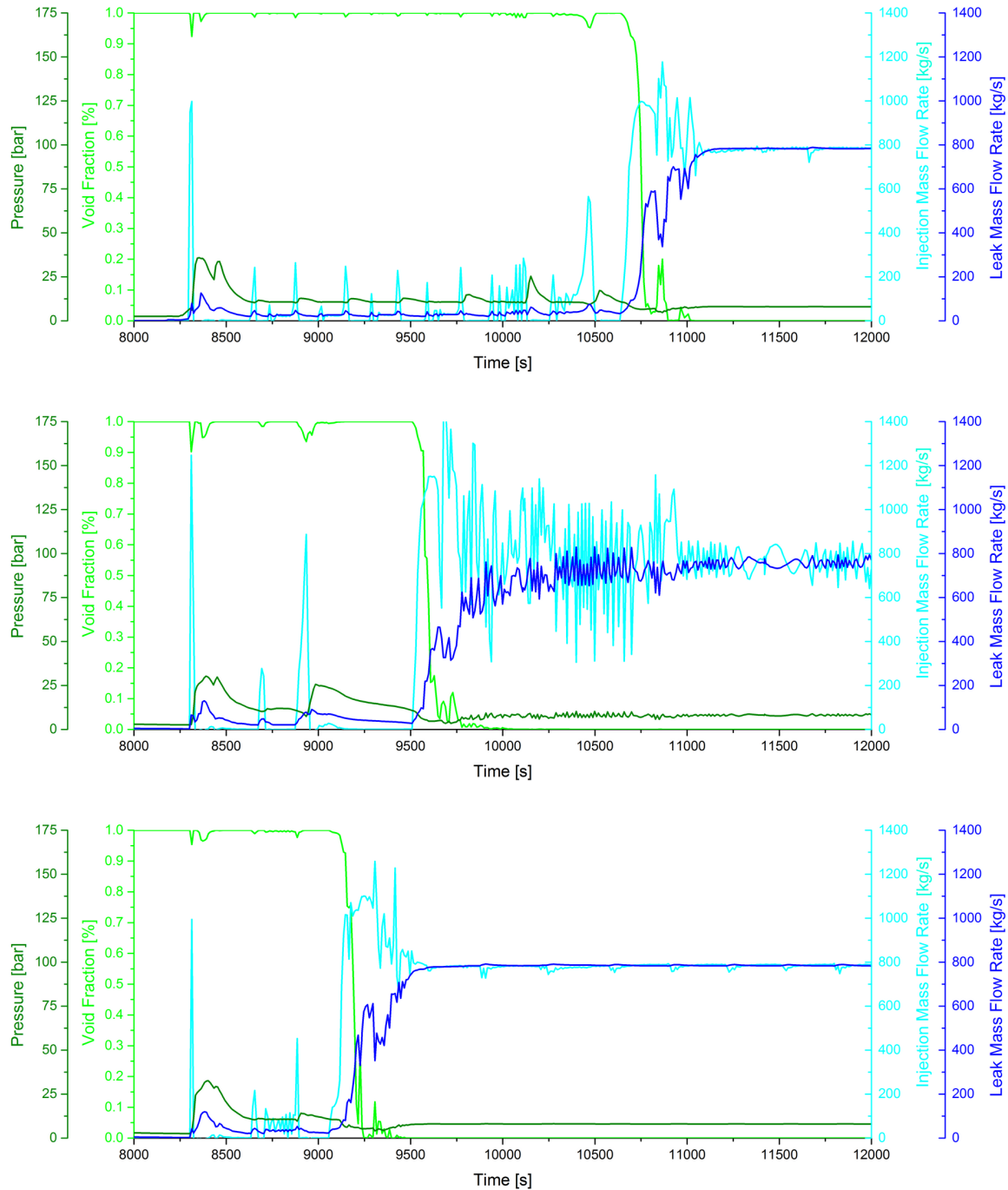


Figure 7.6: Comparison of the reflooding evolution during the three simulations investigated in the BLOCKAGE study with decreasing BLOCKAGE values from top to bottom (default values in the middle)

7.2 The impact of the lower plenum modelling

The AIDA module simulates the relocation to and behaviour of molten core materials in the lower plenum and has been described in section 2.6. Since the ATHLET-CD simulations can be conducted with or without using the AIDA module, the obvious question arose how the simulation is affected by use of the lower plenum module

7.2 The impact of the lower plenum modelling

AIDA. Thus simulation A5B3C1D4 was chosen as basis and the AIDA module was turned off, creating simulation A5B3C1D4N.

Without the AIDA module, the molten core materials candle down the fuel rod structures and accumulate over a not explicitly simulated lower core plate, which marks the lower border of the ECORE module's jurisdiction. Using the AIDA module leads to a relocation of the candling melt to the lower plenum, thus freeing the core area from molten corium and blockades between the fuel rods, leading to a better cooling. On the other hand, molten corium now accumulates in the lower plenum, heating up the lower plenum wall and leading to creep-failure of the RPV. This difference is depicted in the upper row of figure 7.7, where the first relocation has taken place in the simulation using the AIDA module, while in the simulation not using the AIDA module, the molten materials candle down the fuel rods and start forming blockades.

The influence of this behaviour can be seen in the lower row of figure 7.7, where the core area has been quenched to a high extent in the simulation using the AIDA module, because most of the excess material forming blockades between the fuel rods has relocated to the lower plenum. In the simulation not using the AIDA module, the blockades formed between the fuel rods lead to the formation of a molten pool inside the core area, which is surrounded by a frozen crust. This crust shows porosities low enough to make it impenetrable for water, leaving the affected nodes without any form of cooling and thus very high temperatures of around 2000 °C.

In the simulation using the AIDA module, about 36.49 t of molten core materials relocate to the lower plenum, consisting of 20.98 t of ceramic material and 15.52 t of metallic material (10.98 t from the fuel rods and 4.53 t from the control rods). The process starts with the sudden relocation of 21.23 t of molten core materials, the other 15.27 t are relocated slowly over the next 23.3 min. The relocated material forms an oxidic molten pool, which is the configuration that was chosen by input. The other possible configurations are „debris bed“ and „melt stratification“ but using these configurations did not result in numerically stable simulations. The successive wall heat-up leads to failure of the RPV at 21177 s, but since the AIDA module is not able to simulate the fragmentation of the melt when it hits the water in the lower plenum, or the formation and cooling of a debris bed and also does not account for any interaction with the overlaying water, this results are not very useful. This discovery however sparked the idea to use IKE's own MEWA tool for the simulation of the melt behaviour in the lower plenum, for further information see [84].

In summary the use of the lower plenum module AIDA improves the coolability of the core area, because the AIDA module relocates the melt candling down the rods to the lower plenum thus preventing the formation of excessive blockades between the rods. On the other hand, the melt in the lower plenum is likely to destroy the RPV at some point, even if the simulation tool AIDA is very rudimentary and does not give reliable data.

7 Sensitivity and uncertainty considerations

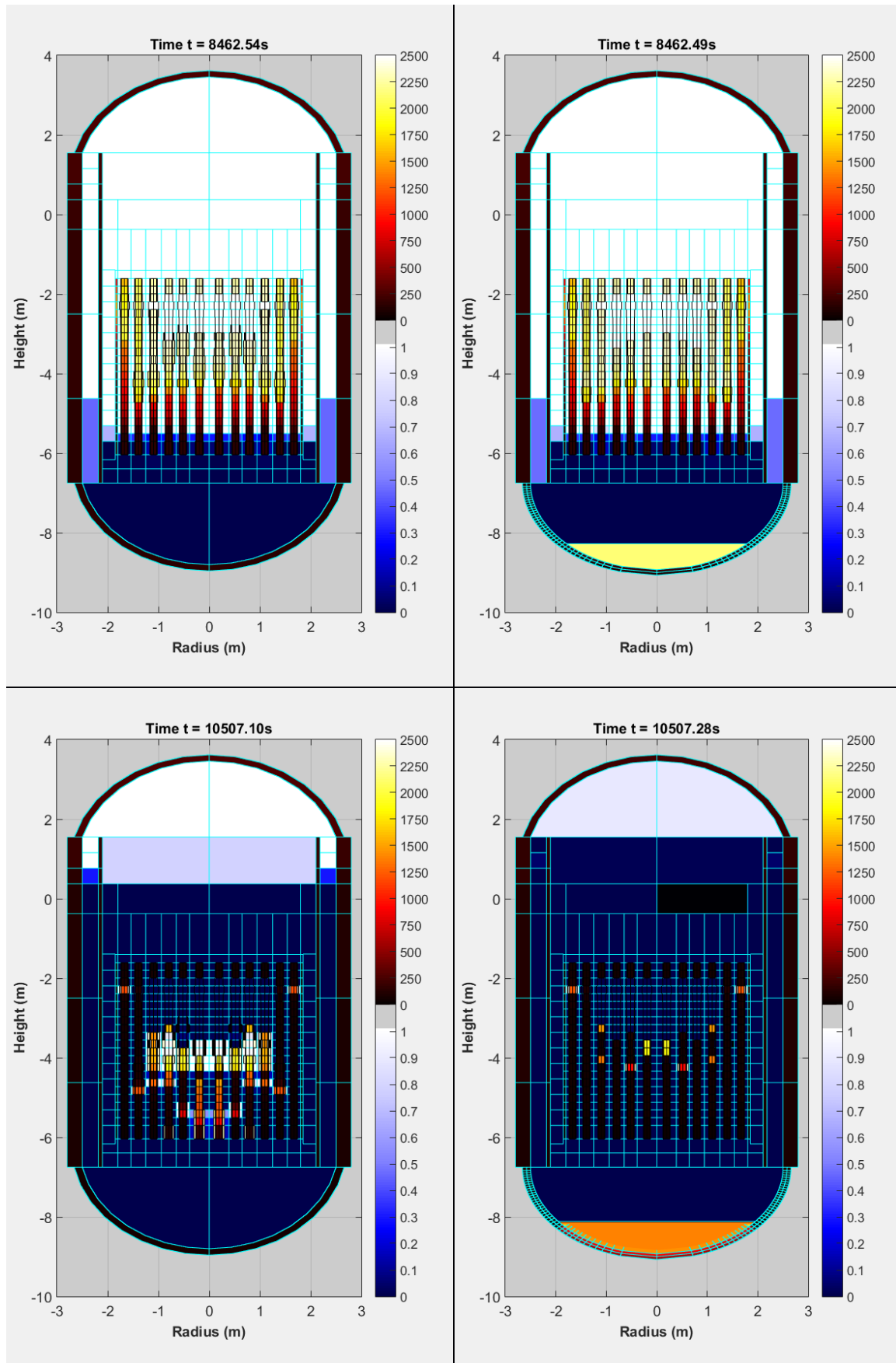


Figure 7.7: Comparison of simulation A5B3C1D4 using the AIDA module on the right and simulation A5B3C1D4N not using the AIDA module on the left at the moment of the first relocation of melt to the lower plenum (upper row) and after 10500 s simulation time (lower row)

8 Summary and Conclusions

The objective of this work was to investigate a late water injection into a partially degraded PWR core and to evaluate whether such a degraded core can be cooled. Simulations with the ATHLET-CD code system have been conducted, assessing a beyond design basis accident sequence in a German KONVOI type PWR. A basic scenario was selected and consisted of a 200 cm^2 leak in the hot leg next to the PSL, combined with the failure of the ECCS as soon as the flooding pool is empty and a switch to sump circulation would be necessary. This failure leads to a core melting accident and in its discourse 156 t of core materials are molten and relocated to a high extend to the lower plenum, eventually leading to the failure of the vessel wall.

Based on this accident simulation, a reflooding scenario was created in order to investigate the effects of a late water injection into a partially degraded PWR core. Four different studies have been carried out, the first being study A in which the reflooding was performed with the LPI injecting 50 % / 50 % into both the hot and the cold legs of the system. The variable in study A was the time at which the reflooding was started, correlating to different amounts of molten core materials present in the core.

From study A, three simulations were judged as „critical“: the reflooding after 30 t , 40 t and 50 t . The simulations with reflooding after 10 t and 20 t were excluded from the analysis, because the lower plenum module AIDA had not been activated due to lack of ceramic melt present in the core. The simulations with even higher amounts of melt ($> 50 \text{ t}$) present before the reflooding is started tend to not give coolable conditions any more.

The second study, study B, investigated the reflooding with different pump systems, namely the LPI and HPI, as well as the VCS and EBS and three hypothetical middle pressure systems: MPI, WKTb and WKTR. The results of the simulations with the LPI system revealed a self blocking effect of the system, because it can only withstand a pressure of up to 1.07 MPa while the water injection creates pressure peaks with up to 3 MPa . The HPI does not show this effect because the pumps can withstand up to 11 MPa , but the injection mass flow rate is rather low.

For scientific reasons, a hypothetical middle pressure system MPI was created, followed by simulations with reflooding systems consisting of KSB's WKTb and WKTR pumps. In these simulations the core was quenched much faster, because the pumps have rather high injection mass flow rates combined with a pressure head of 4 MPa or higher, thus preventing the self blocking effect of the LPI.

The only other system with a direct connection to the primary system is the VCS, which also hosts the EBS pumps. Both systems were modelled with a constant injection rate of 35 kg/s for the VCS and 2 kg/s for the EBS, assuming that the pumps should be able

8 Summary and Conclusions

to withstand the primary system's nominal pressure. It was found that even though both systems cannot quench the core effectively like the LPI or HPI, their usage does make a big difference to the BaseCase simulation without reflooding. Even the EBS is able to save 50 t of core materials from melting compared to the BaseCase simulation, which reduces the load on the lower plenum walls and creates additional time for other mitigation measures as well.

The next question was whether or not the location of the injection makes a difference in the outcome of the simulation, because both the LPI and HPI can be switched from cold leg injection to hot leg injection. A combined injection 50 % / 50 % was investigated as well, because at least the LPI is by design able to do this kind of injection. This investigation was called study C, and included all the analyzed injection systems from study B. It turned out that the reflooding location does not influence the outcome of the simulation too much, even though a reflooding via the cold legs seems to be beneficial because it leads to a bottom flooding condition without the counter-current flow condition found during top flooding.

Study D now investigated scenarios, where not all four redundancies of the LPI pumps were available, to answer the question whether a reduced number of pumps would be able to quench the core as well. The chosen scenario was the reflooding with the LPI system into both the hot and cold legs after 30 t of core materials had been molten. Four simulations were carried out, reducing the number of available pumps by one each.

The results indicate that three or two pumps are able to quench the core as well, even though the self-blocking effect of the LPI system expanded while reducing the number of available pumps. In the simulation with only one pump, the self-blocking effect does not collapse even during a doubled simulation time. Nevertheless the core is quenched by steam cooling at some point, but the mass of melt relocated to the lower plenum has grown by 3 t.

After the four studies had been carried out, two interesting sensitivity questions have been analyzed in order to account for uncertainties on the side of the simulation tool ATHLET-CD. First, the BLOCKAGE input parameters were investigated, by changing the parameters in two separate simulations by + 10 % and – 10 % respectively. The resulting simulations differ strongly from the one conducted with the default BLOCKAGE parameters, and a trend was visible to better core cooling with higher BLOCKAGE parameters, because then the resulting flow paths remain bigger. Blockages should be investigated in more detail, because they play a decisive role in the quenching of a degraded reactor core.

The other investigation focused on the impact of the usage of the AIDA module, because without the AIDA module, no relocation of melt to the lower plenum can be simulated, thus the melt is accumulated in the core area. The simulation not using the AIDA module showed a high amount of blockades in the core area, making it difficult to quench by water. Activation of the AIDA module leads to a relocation of those materials blocking the flow channels to the lower plenum, thus simplifying the core quenching but forming an unquenchable molten pool in the lower plenum.

Summarizing the results as extension of the guidelines for the operators in existing German PWRs it can be said that any amount of water injected into the core will

be better than none, but if a choice can be made, the HPI might be better suited to quench an already melting core, because it leads to more stable reflooding conditions due to its small pressure dependency in the low pressure regime thus creating smaller loads on the structures of the primary system. Also, the quenching starts immediately, because no self-blocking effect is created, opposing the reflooding using the LPI, which is the usual measure currently.

Another suggestion derived from the simulation results is that it might be useful to provide an MPI system as ECCS. Pumps with useful specifications are available on most plant sides, e. g. as condensate feedwater pumps. It might also be useful to equip fire-trucks on the plant site and in the vicinity of the NPP with pumps that can withstand the pressure built-up of up to 4 MPa .

The results obtained in this study can be used to improve the Severe Accidents Management Guidelines. Since the guidelines themselves are specific for each nuclear power plant and classified, the results obtained here are difficult to be applied directly. They should rather be seen as recommendations for authorities, as to where lay improvement potential for those SMAGs. Potential improvements have to be connected with a future experimental and analytical program and further numerical simulations with validated codes in order to evaluate the question, which measures have to be taken to cool a partially degraded PWR core in a more detailed manner.

Appendix

The appendices are referred to on the following pages:

- Appendix A1
Input data for the AIDA module on page 28
- Appendix A2
Input data for the GCSM signals used by the AIDA module on page 28
- Appendix A3
Input data for the ECORE module on page 40
- Appendix A4
GMCS input for the emergency cooling preparation signal (ECPS) on page 41
- Appendix A5
GCSM input for the reactor control systems observation values on page 43
- Appendix A6
Input data for the GCSM signals used for the reflooding simulation on page 55

A1 Input data for the AIDA module

The following code is the complete user input for the lower plenum module AIDA. A description of all the parameters can be found in the ATHLET-CD User's Manual [27].

```

----- AIDA
@
@      IPRI      ICB      INTEK      DTMAX
@          0          1          1          -1.0
@
@
S----- COUPLING WITH AIDA
AIDA      LIBRARY      -      -      -      -
      15  1.0000D+00  0.0000D+00  0.0000D+00  0.0000D+00  0.0000D+00
@
S----- DEGREE OF SUBCOOLING
DTSUB      ADDER      TSLH      TLH      -      -
      0  1.0000D+00  1.0000D+00  -1.0000D+00  0.0000D+00  0.0000D+00
@
S----- SURROUNDING TEMPERATURE (K)
TENVK      ADDER      ENVTEMP      -      -      -
      0  1.0000D+00  1.0000D+00  2.7315D+02  0.0000D+00  0.0000D+00
@
S----- TEMPERATURE LOWER HEAD STRUCTURES (K)
TSTRK      ADDER      TSTR      -      -      -
      0  1.0000D+00  1.0000D+00  2.7315D+02  0.0000D+00  0.0000D+00
@
S----- POWER TO LOWER HEAD FLUID
QAIDA      LAG      AIDA      -      -      -
      0  1.0000D+00  1.0000D+00  0.0000D+00  0.0000D+00  0.0000D+00
@
S----- AVERAGE LH INNER WALL SURFACE TEMPERATURE
TAVELH      NPA      AIDA      -      -      -
      2  1.0000D+00  0.0000D+00  0.0000D+00  0.0000D+00  0.0000D+00
@
S----- TEMPERATURE AT LH INNER WALL SURFACE
TINLH      NPA      AIDA      -      -      -
      3  1.0000D+00  0.0000D+00  0.0000D+00  0.0000D+00  0.0000D+00
@
S----- TEMPERATURE AT LH INNER WALL SURFACE (C)
TINLHC      ADDER      TINLH      -      -      -
      0  1.0000D+00  1.0000D+00  -273.15  0.0000D+00  0.0000D+00
@
S----- TEMPERATURE AT LH OUTER WALL SURFACE
TOUTLH      NPA      AIDA      -      -      -
      4  1.0000D+00  0.0000D+00  0.0000D+00  0.0000D+00  0.0000D+00
@
S----- TEMPERATURE AT LH OUTER WALL SURFACE (C)
TOUTLHC      ADDER      TOUTLH      -      -      -
      0  1.0000D+00  1.0000D+00  -273.15  0.0000D+00  0.0000D+00
@
S----- LOWER HEAD PRESSURE
PINLH      NPA      AIDA      -      -      -
      1  1.0000D+00  0.0000D+00  0.0000D+00  0.0000D+00  0.0000D+00
@
S----- OUTER PRESSURE
POUT      ADDER      -      -      -      -
      0  1.0000D+00  1.0000D+05  0.0000D+00  0.0000D+00  0.0000D+00
@

```

Figure A.1: Input for the AIDA module, part I

```

@
C---- AIDA @AJT für AIDA
@
@   ICOUP      IMOD      NZATH      NLATH      SIGNAL
@       1        1         40         10      'DEFAULT'
@
@   SIG2      SIG3      SIG4      SIG5
@   'PLH'     'DTSUB'   'TENVK'  'TSTRK'
@   SIG6      SIG7      SIG8      SIG9
@   'DEFAULT' 'DEFAULT'  'DEFAULT' 'DEFAULT'
@
@   AIDA SPECIFIC INPUT DATA
@----- GEOMETRY
@   RIRPV      THW      CONFIG
@   2.18       0.127   'A12'
@
@
@ Initial Configuration
@
@ Configuration A - Oxidic Melt Pool
@
@ A11: water in lower head, external cooling
@ A12: water in lower head, no external cooling
@ A21: No water in lower head, external cooling
@ A22: No water in lower head, no external cooling
@
@ Configuration B - Debris Bed (Oxidic melt with overlying particles)
@
@
@ B11: water in lower head, external cooling
@ B12: water in lower head, no external cooling
@ B21: No water in lower head, external cooling
@ B22: No water in lower head, no external cooling
@
@ Configuration C - Melt Stratification
@
@ C11: water in lower head, external cooling
@ C12: water in lower head, no external cooling
@ C21: No water in lower head, external cooling
@ C22: No water in lower head, no external cooling
@ C31: overlying debris, external cooling (not yet available)
@ C32: overlying debris, no external cooling (not yet available)
@ C41: overlying debris, no water in lower head, external cooling (not yet available)
@ C42: overlying debris, no water in lower head, no external cooling (not yet available)
@
@
@ THE FOLLOWING DATA ARE NEEDED IF CONFIG(1:1) = B OR C
@   SMASS      FRATE      PBED      DP      COSPHI
@
@----- PARAMETER
@   NCOUP      NCODN      HTCU      NHTGAP   DGAP      HTCR
@   2          3          10000.    2         2.0E-3    10000.
@   SFAK      PCRUST      PBETA     CS        CBED      HTCC
@   1.5       0.2         2.        1.        1.        100.
@
@----- DAMAGE
@
@   IDAM      HSW
@   1         30.
@

```

Figure A.2: Input for the AIDA module, part II

A2 Input data for the GCSM signals used by the AIDA module

The following code shows the GCSM control signals used by the lower plenum module AIDA. A description of the GCSM signals can be found in the ATHLET User's Manual [24].

```

@
@ LOWER HEAD VARIABLES (FOR AIDA)
@
S----- PLH
@   YNAME      VARTYPE      OBJECTNAME      MODELNAME      SPVO
   PLH         PRESSURE     PV-LP           -              0.0

@
S----- TLH
@   YNAME      VARTYPE      OBJECTNAME      MODELNAME      SPVO
   TLH         FLUIDTEMP    PV-LP           -              0.0

S----- TSLH
@   YNAME      VARTYPE      OBJECTNAME      MODELNAME      SPVO
   TSLH        SATTEMP      PV-LP           -              0.0

S----- T LOWER CORE SUPPORT PLATE
@   YNAME      VARTYPE      OBJECTNAME      MODELNAME      SPVO
   TSTR        HCOTEMP      HPV-LCP         -              0.122
@
@

```

Figure A.3: Input for the GCSM control signals used by the AIDA module

A3 Input data for the ECOPE module

The following code is the complete user input for the ECOPE module including the input for ROD1 (the innermost core ring). ROD2 to ROD6 are modeled with the same values except for the core ring size and numbers of fuel and control rods modeled in the core sections. These values can be found in table 3.1. A description of all the parameters can be found in the ATHLET-CD User's Manual [27].

```

@
@ CONTROL WORD *****
@
C---- ECOPEMOD
@
@ IBWR      NEKT      NANT      NDIVCO      IOPE
@ 0         1         0         1         1 @732@
@ IWLST     ISTOFF
@ 4         0
@ NROTOT    QTOT      PRZERO
@ 57900    3.765D+09  1.0
@
@ ACTIVE LENGTH: 3.9 M, TOTAL LENGTH 4.43 M|
@ UPPER AND LOWER PLUG LENGTH: 33.8 CM, 19 CM
@
@ SBCORE     SECORE     STU       STO
@ 1.050     4.950     0.338    0.190
@ RR0D0     RCLIO      RPEL     PITCH     IQUA
@ 4.75D-3   4.11D-3   4.025D-3 12.9D-3   0
@ EPS       HAC       PROD0    DTFAIL    ITFBK
@ 0.70D+0   10.0D+3     3.2D6    1.0D2     1
@ TAM       TAL
@ 2.25D+3   2.80D+3     @ ALPHA-ZR
- * --- EMISSIVITY
@ EPSKU     EPSKO     EPSKL     EPSKR     EPSW
@ 0.7D0     0.7D0     0.7D0     0.7D0     0.7D0
@ EPSUU     EPSUO     EPSUL     EMISML
@ 0.7D0     0.7D0     0.7D0     0.7D0
----- RODOXID
@ IOXMOD    OXXLIMI    OXIDIN    TFLOWR    ROXLIM
@ 16        1.0D-1     1.0D0     1.0D10    1.0D-0
----- MFRODB
@ IPROD     TC00      VPLENU    POROS0    IDOURB
@ 1         5.93D02   1.00D-5   0.017D0   0
@ IBLOW     TBEGIN    DELOXY
@ 0         5.0D2     2.5D-3
@ IBURN     BURN
@ 0         9.9D1
@ IWUEZ     ITERM     ISHAT     IRUB
@ 1         0         0         0
@ IDTRU     ITH       JTH
@ 0         1         1
----- RODLIQCAN
@ ILIQI     IREMLT    IEUTEC    IDOUSL    IACUO
@ 1         1         0         0         0
@ XZRMIN
@ 0.2D0
@ DDTAL     TALLOW    TALHIG    DELTSL
@ 300.D-6   2.300D3   2.500D3   5.0D1 @ RECOMM. VALUES
@ IOXML     OXLM0     dhzrp     ALAMSL    EPSMLT    ROXXLM
@ 16        1.0D-5    22.50D04  3.00D01   0.70D0    1.0D0
@ WSLMAX     BUSL     DELSL     COUR
@ 0.060D0   0.125D0   1.0D-03   0.1D0
@ TCOMP     TCOMPL    DTSLUO    DTACUO
@ 2.600D+3  2.80D+3   0.5D+02   0.3D+02 @ RECOMM. VALUES
@ DHZRO2     DHUO     ALAMUO    ANYUO
@ 2.25D5     1.0D5     2.0D+01   4.D-3
@ WSLUO     BUSLUO    DSLUO
@ 0.030D-0  2.50D-01  -1.0D-03 @ RECOMM. VALUES
@ IPLST     DTSL     DTKR     DTVLPL
@ 0         1.000D9   1.0D+09   1.D+9

```

Figure A.4: Input for the ECOPE module, part I

Appendix

```

----- CRODPWR
@ NCRTOT   IWWER   IWLCR   IDOUCR   icontr
  2328      0       3       0       1
@ CRSTAB   CRHU    CRBA    CRAIC
6.16D-3  5.55D-3  4.65D-3  4.00D-3
@ CRHAC    CRTAM   CRTAL
500.0D0  1073.0D0  1453.0D0
----- CROXID
  16       1.0D0   1.0D0   20000.0
----- CRLIQCAN
@ CRTVER   CRDTSL
1523.0D0  50.0D0
@ CROXM0   DHAIC   ALAMCR
1.0D-4    9.56D4   50.0D0
@ CRWSL    CRBUSL  CRDELS
0.030    0.2D0   1.0D-3
@ IPLCR    DTCRSL  DTCRKR
  0      1.0D9  1.0D9
@
----- HEATINPAR
@
@ STEMLR   TEMPL   TEMPR   TEMPS
0.0D0     99.99   99.99   99.99
@
----- HEATINPTAB
@
@ HTCOND   DENS     HTCAP    @ (I)
'HTCONDUO2' 'DENSUO2' 'HTCAPUO2' @ 1 FUEL
'HTCONDZR'  'DENSZR'  'HTCAPZR'  @ 2 CLADDING
'HTCONDZRO2' 'DENSZRO2' 'HTCAPZRO2' @ 3 CLADDING, OXIDISED
'HTCONDST'  'DENSST'  'HTCAPST'  @ 4 STEEL FUEL PLUG
'HTCONDABS' 'DENSABS' 'HTCAPABS'  @ 5 ABSORBER MATERIAL
'HTCONDCL'  'DENSCL'  'HTCAPCL'  @ 6 ABSORBER ROD CLADDING
'EMISSI'    'EMISSI'  @ 7 EMISSIVITY
'VISCOSFR'  @ 8 VISCOSITY U-O-ZR MELT
'VISCOSCR'  @ 9 VISCOSITY ABSORBER MELT
'VRATE'     @ 10 ?? OXIDATION DIFFUSION
@
----- BLOCKAGE
@ popen  pclsr  pclsx  pconv  blockg
  0.30   0.27   0.25   0.20   0.10
@
----- RHEATTRANS
@ IRADHT  ARADHT  BRADHT
  1       1.0     0.5
@
----- MTLP-SIG
@ AMTLP  IDMTLP
@ MTLP  0 zum aktivieren AIDA: IDMTLP = 1
@ MTLP  1
@
----- HECUNAMER
@
@ POSCOR
'RIGHT'
@
@ AHECNR   SHECLR   SHECRR   SHEATR   @ (I)
'HPV-REF1' 0.00    0.338   0.00    @ 1 LOWER PLUG
'HPV-REF2' 0.00    3.90    0.338   @ 2 ACTIVE LENGTH
'HPV-REF3' 0.00    0.19    4.238   @ 3 UPPER PLUG
@

```

Figure A.5: Input for the Ecore module, part II

```

@
----- NAMES
@
@   ACORE
   'ROD1'
   'ROD2'
   'ROD3'
   'ROD4'
   'ROD5'
   'ROD6'
@
@   #####
K----- ROD1
@
@   PRODR      RODFRA      CRFRA      RSEC
   1.0440     2700.0D0     96.0D0     0.38D0
@
@   ANEUTR     AHTCNA     APRDIN
   'POWER'    'DUMMY'    'DUMMY'
@
----- TFONAM
@
@   ATFNAM
   'PV-COR1'
@
----- HECUNAMEBT
@
@   AHECNB     POSCOB     SHECBB     SHECBE     DISHCB
   'ADIABAT'  'LEFT'     0.0D0     0.0D0     0.0D0
@
@   AHECNT     POSCOT     SHECTB     SHECTE     DISHCT
   'ADIABAT'  'LEFT'     0.0D0     0.0D0     0.0D0
@
----- HEATCONDAX
@
@   SGCXTB     SGCXHB     SGCXTT     SGCXHT
   'DUMMY'    'DUMMY'    'DUMMY'    'DUMMY'
@
----- POWERZ
@
@   POWT%STI   POWT%NAM
   0.0D0      'PROFZ'
@
----- OXLAY
@
@   SOXLAY     OXLAY
   0.0        5.D-6
@
----- HTCINP
@
@   SOHTC     HTCALF
   0.0D0     4.0D4
@
----- HTCCONTTB
@
@   ICHFO
   1
@
@   #####

```

Figure A.6: Input for the ECOPE module, part III

A4 GMCS input for the emergency cooling preparation signal (ECPS)

```

@ NOTKUEHLVORBEREITUNGSSIGNAL
@
S----- PRESSURE LESS 110 BAR
@ YNAME      CONTYPE      X1NAME      X2NAME      X3NAME      X4NAME
  CSIG01     SWITCH        PSIG02      -           -           -
@ IOPT       GAIN          A1          A2          A3          A4
  1          1.           110.D5     180.D5     0.          0.
@ Y0         EPSCON        IPEXO
  0.0       1.0          0
@
S----- LEVEL PRESSURIZER LESS 2.28 M
@ YNAME      CONTYPE      X1NAME      X2NAME      X3NAME      X4NAME
  CSIG02     SWITCH        PSIG03      -           -           -
@ IOPT       GAIN          A1          A2          A3          A4
  1          1.           1.382      10.         0.          0.
@ Y0         EPSCON        IPEXO
  0.0       1.0          0
@
S----- SWITCH OF PRESSURE CONT.
@ YNAME      CONTYPE      X1NAME      X2NAME      X3NAME      X4NAME
  NODELAY    OR           BREAK       -           -           -
@ IOPT       GAIN          A1          A2          A3          A4
  0          1.0         0.0        0.0        0.          0.
@
S----- PRESSURE CONT.
@ YNAME      CONTYPE      X1NAME      X2NAME      X3NAME      X4NAME
  SPCONTAIN  FUNGEN      RUN.TIME    NODELAY     -           PCONTAIN
@ IOPT       GAIN          A1          A2          A3          A4
  -1         1.           0.          0.          0.          0.
@
S----- PRESSURE DIFF. CONT.-ATM.
@ YNAME      CONTYPE      X1NAME      X2NAME      X3NAME      X4NAME
  CSIG05     ADDER       SPCONTAIN  -           -           -
@ IOPT       GAIN          A1          A2          A3          A4
  0          1.D-2       1.          -1.D5     0.          0.
@
S----- PRESSURE DIFF. CONT.-ATM. GREATER 30 MBAR
@ YNAME      CONTYPE      X1NAME      X2NAME      X3NAME      X4NAME
  CSIG03     SWITCH        CSIG05     -           -           -
@ IOPT       GAIN          A1          A2          A3          A4
  0          1.           30.         0.          0.          0.
@
S----- PRESSURE AND LEVEL
@ YNAME      CONTYPE      X1NAME      X2NAME      X3NAME      X4NAME
  CSIG06     AND          CSIG01     CSIG02     -           -
@ IOPT       GAIN          A1          A2          A3          A4
  0          1.           0.          0.          0.          0.
@
S----- PRESSURE AND PRESSURE DIFFERENCE
@ YNAME      CONTYPE      X1NAME      X2NAME      X3NAME      X4NAME
  CSIG07     AND          CSIG01     CSIG03     -           -
@ IOPT       GAIN          A1          A2          A3          A4
  0          1.           0.          0.          0.          0.
@
S----- LEVEL AND PRESSURE DIFF.
@ YNAME      CONTYPE      X1NAME      X2NAME      X3NAME      X4NAME
  CSIG08     AND          CSIG02     CSIG03     -           -
@ IOPT       GAIN          A1          A2          A3          A4
  0          1.           0.          0.          0.          0.
@
S----- NOTKUEHLVORBEREITUNGSSIGNAL
@ YNAME      CONTYPE      X1NAME      X2NAME      X3NAME      X4NAME
  CSIG09     OR           CSIG06     CSIG07     CSIG08     -
@ IOPT       GAIN          A1          A2          A3          A4
  0          1.           0.          0.          0.          0.
@

```

Figure A.7: Input for the GCSM signals used for the simulation of the emergency cooling preparation signal

A5 GCSM input for the reactor control systems observation values

```

-
@    PROCESS SIGNALS
@
S---- PROBLEM TIME
@    YNAME      VARTYPE      OBJECTNAME      MODELNAME      SPVO
    RUN.TIME   TIME          -              -              0.
@
S---- PRESSURE UPPER PLENUM
@    YNAME      VARTYPE      OBJECTNAME      MODELNAME      SPVO
    PSIG02     PRESSURE    PV-UP-M1       -              0.
@
S---- LEVEL PRESSURIZER
@    YNAME      VARTYPE      OBJECTNAME      MODELNAME      SPVO
    PSIG03     LIQLEVEL   P0-PRESS       -              0.
@
S---- LEEL ACCU HOT IL
@    YNAME      VARTYPE      OBJECTNAME      MODELNAME      SPVO
    PSIG04     LIQLEVEL   P0-1ACCUH     -              0.
@
S---- LEVEL STEAM GENERATOR IL TOP
@    YNAME      VARTYPE      OBJECTNAME      MODELNAME      SPVO
    PSIG05     LIQLEVEL   S1-SG-DCT     -              0.
@
S---- PRESSURE STEAMDOME S1
@    YNAME      VARTYPE      OBJECTNAME      MODELNAME      SPVO
    PSIG06     PRESSURE    S1-SG-DOM     -              0.
@
S---- LEVEL STEAM GENERATOR IL BOTTOM
@    YNAME      VARTYPE      OBJECTNAME      MODELNAME      SPVO
    PSIG07     LIQLEVEL   S1-SG-DCB     -              0.
@
S---- LEVEL STEAM GENERATOR BL TOP
@    YNAME      VARTYPE      OBJECTNAME      MODELNAME      SPVO
    PSIG08     LIQLEVEL   S2-SG-DCT     -              0.
@
S---- LEVEL STEAM GENERATOR BL BOTTOM
@    YNAME      VARTYPE      OBJECTNAME      MODELNAME      SPVO
    PSIG09     LIQLEVEL   S2-SG-DCB     -              0.
@
S---- LEVEL ACCU HOT BL
@    YNAME      VARTYPE      OBJECTNAME      MODELNAME      SPVO
    PSIG10     LIQLEVEL   P0-2ACCUH     -              0.
@
S---- PRESSURE STEAM DOME S2
@    YNAME      VARTYPE      OBJECTNAME      MODELNAME      SPVO
    PSIG11     PRESSURE    S2-SG-DOM     -              0.
@
@%%%%%%%%%%%%%%%%%%%%%%%%%%%%%%%%%%%%%%%%%%%%%%%%%%%%%%%%%%%%%%%%%%%%%%%%
@
@ LOWER HEAD VARIABLES (FOR AIDA)
@
S---- PLH
@    YNAME      VARTYPE      OBJECTNAME      MODELNAME      SPVO
    PLH        PRESSURE    PV-LP          -              0.0
@
S---- TLH
@    YNAME      VARTYPE      OBJECTNAME      MODELNAME      SPVO
    TLH        FLUIDTEMP PV-LP          -              0.0

S---- TSLH
@    YNAME      VARTYPE      OBJECTNAME      MODELNAME      SPVO
    TSLH       SATTEMP    PV-LP          -              0.0

S---- T LOWER CORE SUPPORT PLATE
@    YNAME      VARTYPE      OBJECTNAME      MODELNAME      SPVO
    TSTR       HCOTEMP    HPV-LCP        -              0.122
@

```

Figure A.8: Input for the GCSM process signals used as observation values on which the reactor control system is based

A6 Input data for the GCSM signals used for the reflooding simulation

The following code shows the GCSM control signals used for the reflooding simulation. A description of the GCSM signals can be found in the ATHLET User's Manual [24].

```

@
@   REFLOODING
@
S---- RESTART OF HPI PUMP IN LOOP 1/1 (INTACT)
@   YNAME      CONTYPE      X1NAME      X2NAME      X3NAME      X4NAME
@   HPI11ON    SWITCH       RUN.TIME    -           -           -
@   IOPT       GAIN         A1          A2          A3          A4
@   0          1.          %thpi11%   0.          0.          0.
@
S---- RESTART OF HPI PUMP IN LOOP 1/2 (INTACT)
@   YNAME      CONTYPE      X1NAME      X2NAME      X3NAME      X4NAME
@   HPI12ON    SWITCH       RUN.TIME    -           -           -
@   IOPT       GAIN         A1          A2          A3          A4
@   0          1.          %thpi12%   0.          0.          0.
@
S---- RESTART OF HPI PUMP IN LOOP 1/3 (INTACT)
@   YNAME      CONTYPE      X1NAME      X2NAME      X3NAME      X4NAME
@   HPI13ON    SWITCH       RUN.TIME    -           -           -
@   IOPT       GAIN         A1          A2          A3          A4
@   0          1.          %thpi13%   0.          0.          0.
@
S---- RESTART OF HPI PUMP IN LOOP 2 (BROKEN)
@   YNAME      CONTYPE      X1NAME      X2NAME      X3NAME      X4NAME
@   HPI2ON     SWITCH       RUN.TIME    -           -           -
@   IOPT       GAIN         A1          A2          A3          A4
@   0          1.          %thpi2%    0.          0.          0.
@
-----
@
S---- RESTART OF LPI PUMP IN LOOP 1/1 (INTACT)
@   YNAME      CONTYPE      X1NAME      X2NAME      X3NAME      X4NAME
@   LPI11ON    SWITCH       RUN.TIME    -           -           -
@   IOPT       GAIN         A1          A2          A3          A4
@   0          1.          %tlpi11%   0.          0.          0.
@
S---- RESTART OF LPI PUMP IN LOOP 1/2 (INTACT)
@   YNAME      CONTYPE      X1NAME      X2NAME      X3NAME      X4NAME
@   LPI12ON    SWITCH       RUN.TIME    -           -           -
@   IOPT       GAIN         A1          A2          A3          A4
@   0          1.          %tlpi12%   0.          0.          0.
@
S---- RESTART OF LPI PUMP IN LOOP 1/3 (INTACT)
@   YNAME      CONTYPE      X1NAME      X2NAME      X3NAME      X4NAME
@   LPI13ON    SWITCH       RUN.TIME    -           -           -
@   IOPT       GAIN         A1          A2          A3          A4
@   0          1.          %tlpi13%   0.          0.          0.
@
S---- RESTART OF LPI PUMP IN LOOP 2 (BROKEN)
@   YNAME      CONTYPE      X1NAME      X2NAME      X3NAME      X4NAME
@   LPI2ON     SWITCH       RUN.TIME    -           -           -
@   IOPT       GAIN         A1          A2          A3          A4
@   0          1.          %tlpi2%    0.          0.          0.
@

```

Figure A.9: Input for the GCSM signals used for the reflooding simulation, part I

A6 Input data for the GCSM signals used for the reflooding simulation

```

@
S----- RESTART OF EBS PUMP IN LOOP 1/1 (INTACT)
@ YNAME      CONTYPE      X1NAME      X2NAME      X3NAME      X4NAME
  EBS11ON    SWITCH      RUN.TIME    -           -           -
@ IOPT       GAIN        A1          A2          A3          A4
  0          1.         %tebs11%   0.         0.         0.
@
S----- RESTART OF EBS PUMP IN LOOP 1/2 (INTACT)
@ YNAME      CONTYPE      X1NAME      X2NAME      X3NAME      X4NAME
  EBS12ON    SWITCH      RUN.TIME    -           -           -
@ IOPT       GAIN        A1          A2          A3          A4
  0          1.         %tebs12%   0.         0.         0.
@
S----- RESTART OF EBS PUMP IN LOOP 1/3 (INTACT)
@ YNAME      CONTYPE      X1NAME      X2NAME      X3NAME      X4NAME
  EBS13ON    SWITCH      RUN.TIME    -           -           -
@ IOPT       GAIN        A1          A2          A3          A4
  0          1.         %tebs13%   0.         0.         0.
@
S----- RESTART OF EBS PUMP IN LOOP 2 (BROKEN)
@ YNAME      CONTYPE      X1NAME      X2NAME      X3NAME      X4NAME
  EBS2ON     SWITCH      RUN.TIME    -           -           -
@ IOPT       GAIN        A1          A2          A3          A4
  0          1.         %tebs2%    0.         0.         0.
@
-----
@
S----- RESTART OF VCS PUMP IN LOOP 1/1 (INTACT)
@ YNAME      CONTYPE      X1NAME      X2NAME      X3NAME      X4NAME
  VCS11ON    SWITCH      RUN.TIME    -           -           -
@ IOPT       GAIN        A1          A2          A3          A4
  0          1.         %tvcs11%   0.         0.         0.
@
S----- RESTART OF VCS PUMP IN LOOP 1/2 (INTACT)
@ YNAME      CONTYPE      X1NAME      X2NAME      X3NAME      X4NAME
  VCS12ON    SWITCH      RUN.TIME    -           -           -
@ IOPT       GAIN        A1          A2          A3          A4
  0          1.         %tvcs12%   0.         0.         0.
@
S----- RESTART OF VCS PUMP IN LOOP 1/3 (INTACT)
@ YNAME      CONTYPE      X1NAME      X2NAME      X3NAME      X4NAME
  VCS13ON    SWITCH      RUN.TIME    -           -           -
@ IOPT       GAIN        A1          A2          A3          A4
  0          1.         %tvcs13%   0.         0.         0.
@
S----- RESTART OF VCS PUMP IN LOOP 2 (BROKEN)
@ YNAME      CONTYPE      X1NAME      X2NAME      X3NAME      X4NAME
  VCS2ON     SWITCH      RUN.TIME    -           -           -
@ IOPT       GAIN        A1          A2          A3          A4
  0          1.         %tvcs2%    0.         0.         0.
@

```

Figure A.10: Input for the GCSM signals used for the reflooding simulation, part II

Appendix

```

@
S---- MASS FLOW RATE OF HPI INJECTION INTO HOT LEG OF LOOP 1/1 (INTACT)
@ YNAME          CONTYPE          X1NAME          X2NAME          X3NAME          X4NAME
  GHPI11HR       FUNGEN           PSIG02          HPI11ON         TABG1R         TABG1S
@ IOPT           GAIN             A1              A2              A3              A4
  0              %fhpi11h%       0.              0.              0.              0.
@
S---- MASS FLOW RATE OF HPI INJECTION INTO HOT LEG OF LOOP 1/2 (INTACT)
@ YNAME          CONTYPE          X1NAME          X2NAME          X3NAME          X4NAME
  GHPI12HR       FUNGEN           PSIG02          HPI12ON         TABG1R         TABG1S
@ IOPT           GAIN             A1              A2              A3              A4
  0              %fhpi12h%       0.              0.              0.              0.
@
S---- MASS FLOW RATE OF HPI INJECTION INTO HOT LEG OF LOOP 1/3 (INTACT)
@ YNAME          CONTYPE          X1NAME          X2NAME          X3NAME          X4NAME
  GHPI13HR       FUNGEN           PSIG02          HPI13ON         TABG1R         TABG1S
@ IOPT           GAIN             A1              A2              A3              A4
  0              %fhpi13h%       0.              0.              0.              0.
@
S---- TOTAL MASS FLOW RATE OF HPI INJECTION INTO HOT LEG OF LOOP 1(INTACT)
@ YNAME          CONTYPE          X1NAME          X2NAME          X3NAME          X4NAME
  GHPI11HR       ADDER           GHPI11HR       GHPI12HR       GHPI13HR       -
@ IOPT           GAIN             A1              A2              A3              A4
  0              1.              0.33333333    0.33333333    0.33333333    0.
@
S---- MASS FLOW RATE OF HPI INJECTION INTO HOT LEG OF LOOP 2 (BROKEN)
@ YNAME          CONTYPE          X1NAME          X2NAME          X3NAME          X4NAME
  GHPI2HR        FUNGEN           PSIG02          HPI2ON         TABG1R         TABG1S
@ IOPT           GAIN             A1              A2              A3              A4
  0              %fhpi2h%       0.              0.              0.              0.
@
-----
S---- MASS FLOW RATE OF HPI INJECTION INTO COLD LEG OF LOOP 1/1 (INTACT)
@ YNAME          CONTYPE          X1NAME          X2NAME          X3NAME          X4NAME
  GHPI11CR       FUNGEN           PSIG02          HPI11ON         TABG1R         TABG1S
@ IOPT           GAIN             A1              A2              A3              A4
  0              %fhpi11c%       0.              0.              0.              0.
@
S---- MASS FLOW RATE OF HPI INJECTION INTO COLD LEG OF LOOP 1/2 (INTACT)
@ YNAME          CONTYPE          X1NAME          X2NAME          X3NAME          X4NAME
  GHPI12CR       FUNGEN           PSIG02          HPI12ON         TABG1R         TABG1S
@ IOPT           GAIN             A1              A2              A3              A4
  0              %fhpi12c%       0.              0.              0.              0.
@
S---- MASS FLOW RATE OF HPI INJECTION INTO COLD LEG OF LOOP 1/3 (INTACT)
@ YNAME          CONTYPE          X1NAME          X2NAME          X3NAME          X4NAME
  GHPI13CR       FUNGEN           PSIG02          HPI13ON         TABG1R         TABG1S
@ IOPT           GAIN             A1              A2              A3              A4
  0              %fhpi13c%       0.              0.              0.              0.
@
S---- TOTAL MASS FLOW RATE OF HPI INJECTION INTO COLD LEG OF LOOP 1(INTACT)
@ YNAME          CONTYPE          X1NAME          X2NAME          X3NAME          X4NAME
  GHPI11CR       ADDER           GHPI11CR       GHPI12CR       GHPI13CR       -
@ IOPT           GAIN             A1              A2              A3              A4
  0              1.              0.33333333    0.33333333    0.33333333    0.
@

```

Figure A.11: Input for the GCSM signals used for the reflooding simulation, part III

A6 Input data for the GCSM signals used for the reflooding simulation

```

@
S----- MASS FLOW RATE OF HPI INJECTION INTO COLD LEG OF LOOP 2 (BROKEN)
@ YNAME          CONTYPE          X1NAME          X2NAME          X3NAME          X4NAME
  GHPI2CR        FUNGEN            PSIG02          HPI2ON          TABG1R          TABG1S
@ IOPT           GAIN              A1              A2              A3              A4
  0              %fhp12c%         0.              0.              0.              0.
@
-----
@
S----- MASS FLOW RATE OF LPI INJECTION INTO HOT LEG OF LOOP 1/1 (INTACT)
@ YNAME          CONTYPE          X1NAME          X2NAME          X3NAME          X4NAME
  GLPI11HR       FUNGEN            PSIG02          LPI11ON         TABG2R          TABG2S
@ IOPT           GAIN              A1              A2              A3              A4
  0              %flpi11h%        0.              0.              0.              0.
@
S----- MASS FLOW RATE OF LPI INJECTION INTO HOT LEG OF LOOP 1/2 (INTACT)
@ YNAME          CONTYPE          X1NAME          X2NAME          X3NAME          X4NAME
  GLPI12HR       FUNGEN            PSIG02          LPI12ON         TABG2R          TABG2S
@ IOPT           GAIN              A1              A2              A3              A4
  0              %flpi12h%        0.              0.              0.              0.
@
S----- MASS FLOW RATE OF LPI INJECTION INTO HOT LEG OF LOOP 1/3 (INTACT)
@ YNAME          CONTYPE          X1NAME          X2NAME          X3NAME          X4NAME
  GLPI13HR       FUNGEN            PSIG02          LPI13ON         TABG2R          TABG2S
@ IOPT           GAIN              A1              A2              A3              A4
  0              %flpi13h%        0.              0.              0.              0.
@
S----- TOTAL MASS FLOW RATE OF LPI INJECTION INTO HOT LEG OF LOOP 1(INTACT)
@ YNAME          CONTYPE          X1NAME          X2NAME          X3NAME          X4NAME
  GLPI1HR        ADDER            GLPI11HR        GLPI12HR        GLPI13HR        -
@ IOPT           GAIN              A1              A2              A3              A4
  0              1.              0.33333333     0.33333333     0.33333333     0.
@
S----- MASS FLOW RATE OF LPI INJECTION INTO HOT LEG OF LOOP 2 (BROKEN)
@ YNAME          CONTYPE          X1NAME          X2NAME          X3NAME          X4NAME
  GLPI2HR        FUNGEN            PSIG02          LPI2ON          TABG2R          TABG2S
@ IOPT           GAIN              A1              A2              A3              A4
  0              %flpi2h%         0.              0.              0.              0.
@
-----
@
S----- MASS FLOW RATE OF LPI INJECTION INTO COLD LEG OF LOOP 1/1 (INTACT)
@ YNAME          CONTYPE          X1NAME          X2NAME          X3NAME          X4NAME
  GLPI11CR       FUNGEN            PSIG02          LPI11ON         TABG2R          TABG2S
@ IOPT           GAIN              A1              A2              A3              A4
  0              %flpi11c%        0.              0.              0.              0.
@
S----- MASS FLOW RATE OF LPI INJECTION INTO COLD LEG OF LOOP 1/2 (INTACT)
@ YNAME          CONTYPE          X1NAME          X2NAME          X3NAME          X4NAME
  GLPI12CR       FUNGEN            PSIG02          LPI12ON         TABG2R          TABG2S
@ IOPT           GAIN              A1              A2              A3              A4
  0              %flpi12c%        0.              0.              0.              0.
@
S----- MASS FLOW RATE OF LPI INJECTION INTO COLD LEG OF LOOP 1/3 (INTACT)
@ YNAME          CONTYPE          X1NAME          X2NAME          X3NAME          X4NAME
  GLPI13CR       FUNGEN            PSIG02          LPI13ON         TABG2R          TABG2S
@ IOPT           GAIN              A1              A2              A3              A4
  0              %flpi13c%        0.              0.              0.              0.
@

```

Figure A.12: Input for the GCSM signals used for the reflooding simulation, part IV

Appendix

```

@
S----- TOTAL MASS FLOW RATE OF LPI INJECTION INTO COLD LEG OF LOOP 1(INTACT)
@  YNAME      CONTYPE      X1NAME      X2NAME      X3NAME      X4NAME
@  GLPI1CR    ADDER        GLPI11CR    GLPI12CR    GLPI13CR    -
@  IOPT       GAIN         A1          A2          A3          A4
@  0          1.          0.3333333  0.3333333  0.3333333  0.
@
S----- MASS FLOW RATE OF LPI INJECTION INTO COLD LEG OF LOOP 2 (BROKEN)
@  YNAME      CONTYPE      X1NAME      X2NAME      X3NAME      X4NAME
@  GLPI2CR    FUNGEN      PSIG02     LPI2ON     TABG2R     TABG2S
@  IOPT       GAIN         A1          A2          A3          A4
@  0          %f1pi2c%   0.          0.          0.          0.
@
-----
@
S----- MASS FLOW RATE OF EBS INJECTION INTO HOT LEG OF LOOP 1/1 (INTACT)
@  YNAME      CONTYPE      X1NAME      X2NAME      X3NAME      X4NAME
@  GEBS11HR   FUNGEN      PSIG02     EBS11ON    TABG3R     TABG3S
@  IOPT       GAIN         A1          A2          A3          A4
@  0          %f1ebs11h% 0.          0.          0.          0.
@
S----- MASS FLOW RATE OF EBS INJECTION INTO HOT LEG OF LOOP 1/2 (INTACT)
@  YNAME      CONTYPE      X1NAME      X2NAME      X3NAME      X4NAME
@  GEBS12HR   FUNGEN      PSIG02     EBS12ON    TABG3R     TABG3S
@  IOPT       GAIN         A1          A2          A3          A4
@  0          %f1ebs12h% 0.          0.          0.          0.
@
S----- MASS FLOW RATE OF EBS INJECTION INTO HOT LEG OF LOOP 1/3 (INTACT)
@  YNAME      CONTYPE      X1NAME      X2NAME      X3NAME      X4NAME
@  GEBS13HR   FUNGEN      PSIG02     EBS13ON    TABG3R     TABG3S
@  IOPT       GAIN         A1          A2          A3          A4
@  0          %f1ebs13h% 0.          0.          0.          0.
@
S----- TOTAL MASS FLOW RATE OF EBS INJECTION INTO HOT LEG OF LOOP 1(INTACT)
@  YNAME      CONTYPE      X1NAME      X2NAME      X3NAME      X4NAME
@  GEBS1HR    ADDER        GEBS11HR   GEBS12HR   GEBS13HR   -
@  IOPT       GAIN         A1          A2          A3          A4
@  0          1.          0.3333333  0.3333333  0.3333333  0.
@
S----- MASS FLOW RATE OF EBS INJECTION INTO HOT LEG OF LOOP 2 (BROKEN)
@  YNAME      CONTYPE      X1NAME      X2NAME      X3NAME      X4NAME
@  GEBS2HR    FUNGEN      PSIG02     EBS2ON     TABG3R     TABG3S
@  IOPT       GAIN         A1          A2          A3          A4
@  0          %f1ebs2h%  0.          0.          0.          0.
@
-----
@
S----- MASS FLOW RATE OF EBS INJECTION INTO COLD LEG OF LOOP 1/1 (INTACT)
@  YNAME      CONTYPE      X1NAME      X2NAME      X3NAME      X4NAME
@  GEBS11CR   FUNGEN      PSIG02     EBS11ON    TABG3R     TABG3S
@  IOPT       GAIN         A1          A2          A3          A4
@  0          %f1ebs11c% 0.          0.          0.          0.
@
S----- MASS FLOW RATE OF EBS INJECTION INTO COLD LEG OF LOOP 1/2 (INTACT)
@  YNAME      CONTYPE      X1NAME      X2NAME      X3NAME      X4NAME
@  GEBS12CR   FUNGEN      PSIG02     EBS12ON    TABG3R     TABG3S
@  IOPT       GAIN         A1          A2          A3          A4
@  0          %f1ebs12c% 0.          0.          0.          0.
@

```

Figure A.13: Input for the GCSM signals used for the reflooding simulation, part V

A6 Input data for the GCSM signals used for the reflooding simulation

```

@
S----- MASS FLOW RATE OF EBS INJECTION INTO COLD LEG OF LOOP 1/3 (INTACT)
@ YNAME          CONTYPE          X1NAME          X2NAME          X3NAME          X4NAME
  GEBS13CR       FUNGEN           PSIG02          EBS13ON        TABG3R          TABG3S
@ IOPT           GAIN             A1              A2              A3              A4
  0              %feps13c%       0.              0.              0.              0.
@
S----- TOTAL MASS FLOW RATE OF EBS INJECTION INTO COLD LEG OF LOOP 1(INTACT)
@ YNAME          CONTYPE          X1NAME          X2NAME          X3NAME          X4NAME
  GEBS1CR        ADDER           GEBS11CR       GEBS12CR       GEBS13CR       -
@ IOPT           GAIN             A1              A2              A3              A4
  0              1.              0.3333333     0.3333333     0.3333333     0.
@
S----- MASS FLOW RATE OF EBS INJECTION INTO COLD LEG OF LOOP 2 (BROKEN)
@ YNAME          CONTYPE          X1NAME          X2NAME          X3NAME          X4NAME
  GEBS2CR       FUNGEN           PSIG02          EBS2ON        TABG3R          TABG3S
@ IOPT           GAIN             A1              A2              A3              A4
  0              %feps2c%       0.              0.              0.              0.
@
-----
@
S----- MASS FLOW RATE OF VCS INJECTION INTO HOT LEG OF LOOP 1/1 (INTACT)
@ YNAME          CONTYPE          X1NAME          X2NAME          X3NAME          X4NAME
  GVCS11HR      FUNGEN           PSIG02          VCS11ON       TABG4R          TABG4S
@ IOPT           GAIN             A1              A2              A3              A4
  0              %fvcs11h%     0.              0.              0.              0.
@
S----- MASS FLOW RATE OF VCS INJECTION INTO HOT LEG OF LOOP 1/2 (INTACT)
@ YNAME          CONTYPE          X1NAME          X2NAME          X3NAME          X4NAME
  GVCS12HR      FUNGEN           PSIG02          VCS12ON       TABG4R          TABG4S
@ IOPT           GAIN             A1              A2              A3              A4
  0              %fvcs12h%     0.              0.              0.              0.
@
S----- MASS FLOW RATE OF VCS INJECTION INTO HOT LEG OF LOOP 1/3 (INTACT)
@ YNAME          CONTYPE          X1NAME          X2NAME          X3NAME          X4NAME
  GVCS13HR      FUNGEN           PSIG02          VCS13ON       TABG4R          TABG4S
@ IOPT           GAIN             A1              A2              A3              A4
  0              %fvcs13h%     0.              0.              0.              0.
@
S----- TOTAL MASS FLOW RATE OF VCS INJECTION INTO HOT LEG OF LOOP 1(INTACT)
@ YNAME          CONTYPE          X1NAME          X2NAME          X3NAME          X4NAME
  GVCS1HR       ADDER           GVCS11HR       GVCS12HR       GVCS13HR       -
@ IOPT           GAIN             A1              A2              A3              A4
  0              1.              0.3333333     0.3333333     0.3333333     0.
@
S----- MASS FLOW RATE OF VCS INJECTION INTO HOT LEG OF LOOP 2 (BROKEN)
@ YNAME          CONTYPE          X1NAME          X2NAME          X3NAME          X4NAME
  GVCS2HR       FUNGEN           PSIG02          VCS2ON        TABG4R          TABG4S
@ IOPT           GAIN             A1              A2              A3              A4
  0              %fvcs2h%     0.              0.              0.              0.
@
-----
@
S----- MASS FLOW RATE OF VCS INJECTION INTO COLD LEG OF LOOP 1/1 (INTACT)
@ YNAME          CONTYPE          X1NAME          X2NAME          X3NAME          X4NAME
  GVCS11CR      FUNGEN           PSIG02          VCS11ON       TABG4R          TABG4S
@ IOPT           GAIN             A1              A2              A3              A4
  0              %fvcs11c%     0.              0.              0.              0.
@

```

Figure A.14: Input for the GCSM signals used for the reflooding simulation, part VI

Appendix

```

@
S----- MASS FLOW RATE OF VCS INJECTION INTO COLD LEG OF LOOP 1/2 (INTACT)
@ YNAME          CONTYPE          X1NAME          X2NAME          X3NAME          X4NAME
  GVCS12CR       FUNGEN           PSIG02          VCS12ON        TABG4R          TABG4S
@ IOPT           GAIN              A1              A2              A3              A4
  0              %fvcs12c%        0.              0.              0.              0.
@
S----- MASS FLOW RATE OF VCS INJECTION INTO COLD LEG OF LOOP 1/3 (INTACT)
@ YNAME          CONTYPE          X1NAME          X2NAME          X3NAME          X4NAME
  GVCS13CR       FUNGEN           PSIG02          VCS13ON        TABG4R          TABG4S
@ IOPT           GAIN              A1              A2              A3              A4
  0              %fvcs13c%        0.              0.              0.              0.
@
S----- TOTAL MASS FLOW RATE OF VCS INJECTION INTO COLD LEG OF LOOP 1 (INTACT)
@ YNAME          CONTYPE          X1NAME          X2NAME          X3NAME          X4NAME
  GVCS1CR        ADDER            GVCS11CR       GVCS12CR       GVCS13CR       -
@ IOPT           GAIN              A1              A2              A3              A4
  0              1.              0.33333333    0.33333333    0.33333333    0.
@
S----- MASS FLOW RATE OF VCS INJECTION INTO COLD LEG OF LOOP 2 (BROKEN)
@ YNAME          CONTYPE          X1NAME          X2NAME          X3NAME          X4NAME
  GVCS2CR       FUNGEN           PSIG02          VCS2ON         TABG4R          TABG4S
@ IOPT           GAIN              A1              A2              A3              A4
  0              %fvcs2c%        0.              0.              0.              0.
@

```

Figure A.15: Input for the GCSM signals used for the reflooding simulation, part VII

Bibliography

- [1] Dr. H. Lauer. Curriculum on nuclear power. *Technical University of Darmstadt*, 2010.
- [2] A. Ziegler and J. Heithoff. *Lehrbuch der Reaktortechnik: Band 3: Kernkraftwerkstechnik*. Springer, 1985. ISBN 978-3540154730.
- [3] T. Hollands. Presentation on Core Modeling. ATHLET-CD Users Meeting, Garching, 2014.
- [4] U. Hesse et al. *Methodenentwicklung zum Hochabbbrand einschließlich Burnup Credit*. Gesellschaft für Reaktorsicherheit GRS, 2009. GRS-A-3491, p. 57.
- [5] Japan Meteorological Agency (JMA). Earthquakes and Tsunamis - Disaster prevention and mitigation efforts. <http://www.jma.go.jp/jma/kishou/books/jishintsunami/jishintsunami.pdf>, March 2013.
- [6] Tokyo Electric Power Company, Inc. The Development of and Lessons from the Fukushima Daiichi Nuclear Accident, 1st edition. <http://www.tepco.co.jp/en/decommission/accident/images/outline01.pdf>, March 2013.
- [7] Tokyo Electric Power Company, Inc. Fukushima Nuclear Accident Analysis Report. http://www.tepco.co.jp/en/press/corpcom/release/betu12_e/images/120620e0104.pdf, June 2012.
- [8] L. L. Humphries, R. K. Cole, D. L. Louie, V. G. Figueroa, and M. F. Young. *MELCOR Computer Code Manuals Vol. 1: Primer and Users' Guide*. Sandia National Laboratories, version 2.1.6840 edition, 2015.
- [9] L. L. Humphries, R. K. Cole, D. L. Louie, V. G. Figueroa, and M. F. Young. *MELCOR Computer Code Manuals Vol. 2: Reference Manual*. Sandia National Laboratories, version 2.1.6840 edition, 2015.
- [10] L. L. Humphries, D. L. Louie, V. G. Figueroa, M. F. Young, S. Weber, K. Ross, J. Phillips, and R. J. Jun. *MELCOR Computer Code Manuals Vol. 3: MELCOR Assessment Problems*. Sandia National Laboratories, version 2.1.7347 edition, 2015.
- [11] P. Chatelard and N. Reinke. *Overview of the integral code ASTEC V2.0*. IRSN/DPAM and GRS mbH, rapport technique dpam/semca-2009-149 / technische notiz grs astec 09/02 edition, 2009. http://www.grs.de/sites/default/files/pdf/Overview_ASTEC.pdf.

Bibliography

- [12] Gesellschaft für Reaktorsicherheit GRS. *Deutsche Risikostudie Kernkraftwerke Phase B*. Verlag TÜV Rheinland, 1990. ISBN 3-88585-809-6.
- [13] U.S. Nuclear Regulatory Commission. Reactor safety study - an assessment of accident risks in u.s. commercial power plants. Technical report, WASH 1400 (NUREG 75/014), October 1975.
- [14] Gesellschaft für Reaktorsicherheit (GRS) mbH. *Deutsche risikostudie kernkraftwerke phase b - eine zusammenfassende darstellung*. Technical report, GRS-72, Juni 1989.
- [15] Institut de Radioprotection et de Sûreté Nucléaire IRSN D. Jacquemain. *Nuclear Power Reactor Core Melt Accidents - Current State of Knowledge*. edp sciences, 2015. ISBN 978-2-7598-1835-8.
- [16] OECD NEA. Progress made in the last fifteen years through analyses of the TMI-2 accident performed in member countries. Technical report, NEA/CSNI/R(2005)1, 2005.
- [17] OECD NEA. Ability of current advanced codes to predict core degradation, melt progression and reflooding. Benchmark exercise on an alternative TMI-2 accident scenario. Technical report, NEA/CSNI/R(2009)3.
- [18] B. R. Sehgal. *Nuclear Safety in Light Water Reactors - Severe Accident Phenomenology*. Elsevier, 2012. ISBN 978-0-12-388446-6.
- [19] G. Pohlner, A. Trometer, M. Buck, F. Schäfer, P. Tusheva, T. Hollands, V. Di Marcello, U. Imke, V. Sanchez, X. Cheng, F. Kretschmar, P. Dietrich, and R. Gehr. *Störfallmaßnahmen zur milderung der folgen von reaktorunfällen mit schweren kernschäden*. Technical Report IKE 2-163, Institut für Kernenergetik und Energiesysteme (IKE), Universität Stuttgart, 2014.
- [20] W. Hering and C. Homann. OECD Benchmark Exercise on the TMI-2 Plant: Analysis of an Alternative Severe Accident Scenario. *International Conference Nuclear Energy for New Europe*, Bled, Slovenia, September 5-8, 2005.
- [21] H. Austregesilo, C. Bals, A. Hora, G. Lerchl, P. Romstedt, P. Schöffel, D. von der Cron, and F. Weyermann. *ATHLET Mod 3.0 Cycle A - Models and Methods*. Gesellschaft für Anlagen- und Reaktorsicherheit (GRS) mbH, vol 4, rev. 3 edition, September 2012.
- [22] *ATHLET Mod 3.0 Cycle A - Input Data Description*. Gesellschaft für Anlagen- und Reaktorsicherheit (GRS) mbH, vol 1, rev. 6b edition, September 2012.
- [23] J. Venker. *Development and Validation of Models for Simulation of Supercritical Carbon Dioxide Brayton Cycles and Application to Self-Propelling Heat Removal Systems in Boiling Water Reactors*. Phd-thesis, University of Stuttgart, 2015.
- [24] G. Lerchl, H. Austregesilo, P. Schöffel, D. von der Cron, and F. Weyermann. *ATHLET Mod 3.0 Cycle A - User's Manual*. Gesellschaft für Anlagen- und Reaktorsicherheit (GRS) mbH, vol 1, rev. 6 edition, September 2012.

- [25] P. Hofmann, H. Uetsuka, A. N. Wilhelm, and E. A. Garcia. Dissolution of UO₂ by molten zirkaloy and its modeling. *Int. Symposium on Severe Accidents in Nuclear Power Plants*, Sorrento, Italy, March 1988.
- [26] K. T. Kim and D. R. Olander. Dissolution of uranium oxide by molten zirkaloy (convection controlled reaction). *Journal of Nuclear Materials*, Vol. 154, pp. 102 (1988).
- [27] H. Austregesilo, C. Bals, T. Hollands, C. Köllein, W. Luther, J.-D. Schubert, K. Trambauer, and S. Weber. *ATHLET-CD Mod 3.0 Cycle A - User's Manual*. Gesellschaft für Anlagen- und Reaktorsicherheit (GRS) mbH, vol. 1 edition, July 2013.
- [28] J. Kronenberg. Simulation des Kernschmelzens in Leichtwasserreaktoren. *Dissertation, Institut für Kernenergetik und Energiesysteme, Universität Stuttgart, IKE 2-142* (2001).
- [29] J. D. Gabor, L. Baker, Jr., J. C. Cassulo, D. J. Erskine, and J. G. Warner. Heat transfer to curved surfaces from heat generating pools. *Joint ASME/AIChE 18th National Heat Transfer Conference, San Diego, California*, August 6-8, 1979.
- [30] C. Müller and K. Schaaf. *Der Simulationsmodul AIDA*. Gesellschaft für Anlagen- und Reaktorsicherheit (GRS) mbH, GRS - A - 2933 edition, May 2001.
- [31] M. Buck. *Modelling of the Late Phase of Core Degradation in Light Water Reactors*. Phd-thesis, University of Stuttgart, 2007. IKE 2 - 153.
- [32] P. Hoffmann, S. J. L. Hagen, V. Noack, G. Schanz, and L. K. Sepold. Chemical-Physical Behavior of Light Water Reactor Core Components Tested Under Severe Reactor Accident Conditions in the CORA Facility. *Nuclear Technology*, 118 - 3: 200-224, 1997.
- [33] L. K. Sepold, P. Hoffmann, W. Leiling, A. Miassoedov, D. Piel, L. Schmidt, and M. Steinbrück. Reflooding experiments with LWR-type fuel rod simulators in the QUENCH facility. *Nuclear Engineering and Design*, 204 (1-3):205 – 220, 2001.
- [34] W. Erdmann. Nachrechnung des Bündel-Quench-Versuches CORA-13 mit dem Rechenprogramm ATHLET-CD. Technical report, TN-ERD-1/00, RS 1100, 2000.
- [35] J. Bestele. Nachrechnung des Bündel-Quench-Versuches CORA-13 mit ATHLET-CD. Technical report, TN-BES-94-3, 1994.
- [36] J. Bestele, J.-D. Schuber, and K. Trambauer. Posttest Calculation of Bundle Quench Test CORA-13 with ATHLET-CD. *International Conference on New Trends in Nuclear System Thermalhydraulics, Pisa, Italy*, 1994.
- [37] M. Firnhaber, K. Trambauer, S. Hagen, and P. Hofmann. International Standard Problem No. 31: CORA-13 Experiment on Severe Fuel Damage. Technical report, NEA/CSNI/R(93)17, GRS-106, KfK 5287, 1993.
- [38] W. Erdmann. Nachrechnung des Versuches CORA-17 mit dem Rechenprogramm ATHLET-CD. Technical report, TN-ERD-3/99, RS 1100, 1999.

Bibliography

- [39] T. Hollands et al. Nachrechnung des Siedewasserreaktorversuchs CORA-28 mit ATHLET-CD 2.1A und Bewertung der SWR-Modellbasis. Technical report, 2007.
- [40] J. Bestele. Nachrechnung des Experiments CORA-28 mit ATHLET-CD. Technical report, TN-BES-96-2, 1996.
- [41] J. Bestele. Nachrechnung des Experiments CORA-33 mit ATHLET-CD. Technical report, TN-BES-96-1, 1996.
- [42] J. Bestele. Nachrechnung des Versuches CORA-W1 mit dem Programm ATHLET-CD. Technical report, 1994.
- [43] W. Erdmann. Nachrechnung des Versuches CORA-W2 mit dem Rechenprogramm ATHLET-CD. Technical report, TN-ERD-3/98, RS 1100, 1998.
- [44] M. Firnhaber, L. Yegorova, U. Brockmeier, S. Hagen, P. Hofmann, and K. Trambauer. International Standard Problem 36: CORA-W2 Experiment on Severe Fuel Damage for a Russian Type PWR. Technical report, OCDE/GD(96)19, GRS-120, 1996.
- [45] K. Müller, G. Bleher, J. Kronenberg, and A. Schatz. KESS-III: Ergebnisse des Internationalen Standardproblems Nr. 36: CORA-W2 Experiment. Technical report, IKE 2 - 125, 1995.
- [46] J. Bestele. Nachrechnung des Versuches CORA-W2 mit dem Programm ATHLET-CD. Technical report, TN-BES-94-2, 1994.
- [47] W. Erdmann. Nachrechnung des Bündel-Quench-Versuches QUENCH-01 mit dem Rechenprogramm ATHLET-CD. Technical report, TN-ERD-2/00, RS 1100, 2000.
- [48] W. Erdmann. Nachrechnung des Bündel-Quench-Versuches QUENCH-06 mit ATHLET-CD und Vergleich mit der Vorausrechnung (ISP 45). Technical report, TN-ERD-2/01, RS 1100, 2001.
- [49] W. Erdmann. International Standard Problem No. 45: QUENCH-06 Test, Calculations with ATHLET-CD. Technical report, TN-ERD-1/01, RS 1100, 2001.
- [50] Ch. Bals, K. Trambauer, and H. Austregesilo. Zr/Air Oxidation Model in ATHLET-CD and First Verification against QUENCH-10. *11. International Quench Workshop, Karlsruhe*, 2005.
- [51] W. Erdmann. New Calculations of the SARNET Benchmark Experiment QUENCH-11 with ATHLET-CD. *Benchmark Quench-11 Final Workshop, Forschungszentrum Karlsruhe*, 2007.
- [52] T. Hollands, T. Drath, H.-J. Wagner, and M. K. Koch. RUB-LEE results of the SARNET Code Benchmark QUENCH-11 Using ATHLET-CD. *Benchmark Quench-11 Final Workshop, Forschungszentrum Karlsruhe*, 2007.
- [53] S. M. Jensen and D. W. Akers. Post-irradiation examination results from the LP-FP-2 center fuel module. Technical report, Report EGG-M-90152, 1990.

- [54] C. Nalezny. Summary of Nuclear Regulatory Commission's LOFT Program Research Findings. Technical report, NUREG/CR-3005 - EGG-2231, 1985.
- [55] J. Bestele. Nachrechnung des Experiments LOFT-FP2. Technical report, TN-BES-94-4, 1994.
- [56] B. Clément, N. Hanniet-Girault, G. Repetto, D. Jacquemain, A. V. Jones, M. P. Kissane, and M. P. von der Hardt. LWR severe accident simulation: synthesis of the results and interpretation of the first Phebus FP experiment FPT0. *Nuclear Engineering and Design*, 226 (1):5 – 82, 2003.
- [57] M. Schwarz, G. Hache, and P. von der Hardt. PHEBUS PF: a severe accident research programme for current and advanced light water reactors. *Nuclear Engineering and Design*, 187:47 – 69, 1999.
- [58] J. Bestele. PHEBUS-FPT0: Parameter study on the bundle thermal behavior with ATHLET-CD. Technical report, TN-BES-95-2, 1995.
- [59] J. Bestele. Post test calculation of the experiment PHEBUS-FPT0 including fission product release and transport. Technical report, TN-BES-95-1, 1995.
- [60] K.-D. Hocke and A. Schatz. PHEBUS-Experiment FPT-0: Analysen zur Bündelaufheizung für das Referenzszenario und erste Versuchsnachrechnungen. Technical report, IKE 2 - 132, 1995.
- [61] W. Erdmann. International Standard Problem No. 46: Phébus FPT1, Calculation with ATHLET-CD. Technical report, TN-ERD-1/02, RS 1100, 2002.
- [62] J.-D. Schubert. Nachrechnung des Phebus-FPT1-Versuches mit dem Rechenprogramm ATHLET-CD. Technical report, TN-SHU-1/00, RS 1100, 2000.
- [63] J. Bestele. Posttest Calculation of the Experiment PHEBUS-FPT1. Technical report, TN-BES-97-1, 1997.
- [64] P. Kruse, T. Hollands, H.-J. Wagner, and M. K. Koch. Simulation des In-Pile-Versuchs PHEBUS FPT-4 mit ATHLET-CD 2.1A. Technical report, 2008.
- [65] W. Erdmann and M. Sonnenkalb. Nachrechnung des Experiments Phebus SFD B9+ mit dem Rechenprogramm ATHLET-CD. Technical report, TN-ERD-2/99, RS 1100, 1999.
- [66] OECD-CSNI International Standard Problem No. 28. Post Test Calculations for PHEBUS SFD Test B9+ with ATHLET-SA. Technical report, GRS-A-1801, 1991.
- [67] W. Erdmann. Nachrechnung des Versuches PBF SFD 1-1 mit dem Rechenprogramm ATHLET-CD. Technical report, TN-ERD-1/98, RS 1100, 1998.
- [68] M. Maltschewski and K. Trambauer. Nachrechnung des Versuches PBF SFD 1-1 mit dem Rechenprogramm ATHLET-SA. Technical report, GRS-A-1878, 1992.
- [69] W. Erdmann. Nachrechnung des Versuches PBF SFD 1-4 mit dem Rechenprogramm ATHLET-CD. Technical report, TN-ERD-2/98, RS 1100, 1998.

Bibliography

- [70] A. Ball and K. Trambauer. Nachrechnungen zum AIC Test der PHEBUS-SFD Versuche mit ATHLET-SA. Technical report, GRS-A-1675, 1990.
- [71] Ch. Bals. Nachrechnung des Bündelversuchs CODEX AIT-1 mit dem Rechenprogramm ATHLET-CD. Technical report, Technische Notiz TN-MIS-07/1, 2007.
- [72] K. Trambauer. Nachrechnung der Halden Experimente IFA650 Test 2 und 3 mit ATHLET-CD zur Validierung des Brennstabmodells. Technical report, TN-TRB-05-2, RS 1155, 2005.
- [73] K. Trambauer. Halden test IFA-650.3: Prediction with ATHLET-CD. Technical report, TN-TRB-05-1, 2005.
- [74] J. Bestele and K. Trambauer. Nachrechnung des Versuchs NRU-FLHT-2 mit dem Programm ATHLET-CD. Technical report, GRS-A-2038, 1993.
- [75] J. Bestele. Nachrechnung des Unfalles in Block 2 des Kraftwerkes Three-Mile-Island mit ATHLET-CD. Technical report, TN-BES-97-2, 1997.
- [76] J. V. Cathcart, R. E. Pawel, R. A. McKee, R. E. Druscel, G. J. Yurek, J. J. Cambell, and S. H. Jury. Zirconium metal-water oxidation kinetics iv. reaction rate studies". *ORNL/NUREG-17*, Aug. 1977.
- [77] V. F. Urbanic and [T. R. Heidrick. High-temperature oxidation of zircaloy-2 and zircaloy-4 in steam. *J. Nucl. Mater.* 75, pages 251–261, 1978.
- [78] V. F. Urbanic. Oxidation of zirconium alloys in steam at 1000 to 1850 °C. *Zirconium in the Nuclear Industry, ASTM STP 633, A. L. Lowe, Jr. and G. W. Parry, Eds., American Society for Testing and Materials,*, pages 168–181, 1977.
- [79] G. Schanz. *Recommendations and Supporting Information on the Choice of Zirconium Oxidation Models in Severe Accident Codes*. Institut für Materialforschung, Forschungszentrum Karlsruhe GmbH, 2003. FZKA 6827.
- [80] P. Tusheva, F. Schäfer, Y. Kozmenkov, S. Kliem, T. Hollands, A. Trometer, and M. Buck. WASA-BOSS: ATHLET-CD model for severe accident analysis for a generic KONVOI reactor. *AMNT 2015: Best Paper, atw Vol. 60, Issue 7*, 2015.
- [81] KSB. Product catalogue for nuclear power stations. <https://shop.ksb.com/>, June 2016.
- [82] A. Trometer, M. Strätz, M. Buck, and J. Starflinger. Parametric study on a KONVOI MB-LOCA scenario for the determination of coolability parameters. *Proceeding of the 46th Annual Meeting on Nuclear Technology (AMNT)*, May 5 - 7, 2015, Berlin, Germany.
- [83] W. Hering, Ch. Homann, and J. Stuckert, editors. *Integration of New Experiments into the Reflood Map*, volume ICAPP-2015, 3.5. - 6.5.2015, Nice, France.
- [84] A. Trometer, A. Hartmann, and J. Starflinger. Investigation on cooling possibilities of a degraded core in an mbloca scenario for a german pwr with athlet-cd. *Nuclear Engineering and Design*, 2017. submitted for publication.

Acknowledgement

First of all, I would like to thank my dissertation supervisor Prof. Dr.-Ing. Jörg Starflinger for giving me the opportunity to work on this project. My time at his institute was exceptional and has taught me a lot about myself. Prof. Dr.-Ing. Stefan Weihe, second corrector to my thesis and committee member, I want to thank for taking on this task and giving valuable advice on the final presentation. Prof. Dr.-Ing. Dr. h.c. Dr. h.c. Prof. E.h. Michael M. Resch I have to thank for taking the time to be chairman of the committee.

I want to express my gratitude to the aforementioned as well as Ms. Vencia (IKE), Ms. Kleinbauer (MPA), Ms. Emre (HLRS) and Ms. Pedrollo (Faculty 4) for their support in the organisation of my thesis defense.

The German Federal Ministry of Education and Research (BMBF) I want to thank for funding the WASA-BOSS project, which gave me the once-in-a-lifetime chance to work with the leading nuclear research institutions on important issues in the nuclear field. My colleagues in this project I would like to thank for numerous inspiring talks and all the fun we had on the evenings of our project meetings.

A special thanks goes to Dr.-Ing. Michael Buck, who supervised my work in the frame of the WASA-BOSS project and supported me as best he could during the creation of this thesis.

For their support and sharing joys and sorrows, I want to thank my colleagues at IKE, especially the participants of the daily lunch table. I still remember my first time at the institute, when I met Jeanne and Ana who were supposed to convince me to take on this opportunity. They succeeded and I am happy that both are close friends to this day.

There are a number of people which have to be mentioned here for taking a special part in the finalisation of my thesis. I want to thank both Tilak and Christophe for providing welcome diversion whenever necessary, Marcel for his contribution to my work in terms of a case study, Stuart for proof-reading my thesis, Stefan for his advice on presentation layouts, Rebecca and Matthias for their confidence building letters, Julia for believing in me, Sebastian for keeping up with my frustration and Manuel for sending the penguin.

At last I must express my gratitude to my family, who has supported me throughout my life. This has never been an easy task, but no matter how difficult the situation became, my family has always remained at my side. I am proud of my parents, sibling and grandparents, and I hope we will always stick together the way we have done in the past.

Erklärung zur Dissertation

Hiermit erkläre ich, dass ich die beigefügte Dissertation selbstständig verfasst und keine anderen als die angegebenen Hilfsmittel genutzt habe. Alle wörtlich oder inhaltlich übernommenen Stellen habe ich als solche gekennzeichnet.

Ich versichere außerdem, dass ich die beigefügte Dissertation nur in diesem und keinem anderen Promotionsverfahren eingereicht habe und dass diesem Promotionsverfahren keine endgültig gescheiterten Promotionsverfahren vorausgegangen sind.

Ort, Datum

Unterschrift

Ailine J. Trometer
Pfadstraße 15
71069 Sindelfingen

Institut für Kernenergetik und
Energiesysteme

Universität Stuttgart

Pfaffenwaldring 31

D-70569 Stuttgart

